Exergoeconomic Analysis and Optimization of Organic Rankine Cycles

By

Paolo Cuda

A Thesis Submitted in Partial Fulfillment

Of the Requirements for the Degree of

Master of Applied Science

In

The Faculty of Engineering and Applied Science

Mechanical Engineering Program

University of Ontario Institute of Technology

March 2012

Abstract

Heat sources such as biomass, industrial waste heat and solar thermal provide the potential to produce renewable environmentally low impact electricity. Using these resources efficiently within economic constraints is important for viability of these systems. This thesis explores a regenerative organic Rankine cycle for use in low temperature heat sources. A Bitzer model scroll expander is used for the prime mover for the system. This expander has a reliable model in which thermodynamic analysis can be done. Various working fluids are explored to investigate which one will provide the most power output and efficiency within system constraints. Using optimization, each fluid is tested within physical constraints for optimal operating conditions using system exergy efficiency as the objective function. An exergoeconomic analysis is performed to predict the cost rate of electricity of the system and is compared to current contract rates from the Ontario Power Authority. Dimethyl ether shows promising results with a system exergy efficiency of 11.76% and system energy efficiency of 2.84% at a source temperature of 120°C. The degree of superheat and pressure ratio are used as the independent variables in the optimization. Highest isentropic efficiency for the expander is 29.22%, showing large potential for improvement. Electricity cost rates for the system assuming 20 year life are 0.132 $/kWh to 0.197 $/kWh depending on the fuel input cost for dimethyl ether. At the current state the system shows merit with large potential for improvement in the expander.

Acknowledgement

There have been many people who have helped and influenced me get where I am today, and without them things would be much different.

Professor Ibrahim Dincer's supervision has been very valuable for me throughout my graduate years. Dr. Calin Zamfirescu has been helpful with the expander modeling and general EES knowledge. Pouria Ahmadi has also helped with general optimization techniques and exergoeconomic knowledge.

My father has been extraordinary and patient throughout my university years by supporting me whenever needed. Without his hard work and sacrifice this would not be possible. To my sister for providing her support as well as my friends and family.

To all the fellow students on the 5th floor of the ACE building who've made the year enjoyable.

Table of Contents

Abstract ii
Acknowledgement iii
List of Figures vi
List of Tables ix
Nomenclature x
Chapter 1: Introduction 1
1.1 Motivation and Objectives 4
Chapter 2: Literature Review 6
Chapter 3: Background 13
3.1 General Heat Engine Cycles 13
3.2 Organic Rankine Cycles 14
3.2.1 Regenerative Organic Rankine Cycles 15
3.2.2 Combined Heat and Power Organic Rankine Cycles 15
3.2.3 Super Critical Organic Rankine Cycles 18
3.2.4 Working Fluids 19
3.3 Expander Types 22
3.3.1 Gerotors Expanders 23
3.3.2 Screw Expanders 23
3.3.3 Scroll Expanders 24
3.4 Optimization Methods 25
Chapter 4: System Description 31
4.1 Bitzer Expander 32
Chapter 5: Analysis 34
5.1 Expander Analysis 34
5.2 Working Fluid Selection 37
5.3 Thermodynamic Analysis 44
5.3.1 Expander Model 44
5.3.2 Thermodynamic Model 48
5.4 Exergoeconomic Analysis 52
5.5 System Optimization 56

Chapter 6: Results and Discussion 59
6.1 Identifying Proper Optimization Conditions 59
6.2 Parametric Study of the System 60
6.2 Optimization of the System 75
6.3 Exergy Analysis and Destruction 87
6.4 Exergoeconomic Analysis 94
Chapter 7: Conclusions and Recommendations 99
7.1 Conclusions 99
7.2 Recommendations 100
References 102
Appendix 106
EES example code for R134a 106

List of Figures

Figure 1.1: Diagram of a basic organic Rankine cycle 3

Figure 2.1: Solar thermal organic Rankine cycle modified from (Wang et al., 2010) 9
Figure 2.2: Eneftech scroll expander geometry modified from (Eneftech Innovation SA, 2011) 11

Figure 3.1: T-s diagram of R227ea 16
Figure 3.2: System diagram for a cogeneration organic Rankine cycle 17
Figure 3.3: T-s diagram of R227ea showing potential heat available for cogeneration applications 17
Figure 3.4: T-s diagram of a supercritical organic Rankine cycle using R227ea 18
Figure 3.5: Practical and unpractical conditions for isentropic and dry working fluids 21
Figure 3.6: Screw expander modified from (ElectraTherm Inc, 2011) 24

Figure 4.1: Diagram of system used in the analysis 32

Figure 5.1: Illustrative example of the scroll geometry modified from (Tarique, 2011) 35
Figure 5.2: Temperature-entropy diagram for R134a 38
Figure 5.3: Temperature-entropy diagram for water 39
Figure 5.4: Temperature-entropy diagram for R227ea 40
Figure 5.5; Temperature-entropy diagram for R245fa 41
Figure 5.6: Temperature-entropy diagram for toluene 41
Figure 5.7: Temperature-entropy diagram for iso-butane 42
Figure 5.8: Temperature-entropy diagram for acetone 42
Figure 5.9: Temperature-entropy diagram for iso-pentane 43
Figure 5.10: Temperature-entropy diagram for n-pentane 43
Figure 5.11: Temperature-entropy diagram for dimethyl ether 44
Figure 5.12: Scroll expander thermodynamic model diagram 45
Figure 5.13: Possible leakages in a scroll expander modified from (Wang, et al., 2005) 46

Figure 6.1: Isentropic efficiency vs. pressure ratio for R227ea 59
Figure 6.2: Electrical power output for R134a 61
Figure 6.3: System exergy efficiency for R134a 61
Figure 6.4: Expander isentropic efficiency for R134a 62
Figure 6.5: Electrical power output for water 63

Figure 6.6: System exergy efficiency for water 63
Figure 6.7: Expander isentropic efficiency for water 64
Figure 6.8: Electrical power output for R227ea 65
Figure 6.9: System exergy efficiency for R227ea 65
Figure 6.10: Expander isentropic efficiency for R227ea 66
Figure 6.11: Electrical power output for R245fa 67
Figure 6.12: System exergy efficiency for R245fa 67
Figure 6.13: Expander isentropic efficiency for R245fa 68
Figure 6.14: Electrical power output for iso-butane 69
Figure 6.15: System exergy efficiency for iso-butane 69
Figure 6.16: Expander isentropci efficiency for iso-butane 70
Figure 6.17: Electrical power output for iso-pentane 70
Figure 6.18: System exergy efficiency for iso-pentane 71
Figure 6.19: Expander isentropic efficiency for iso-pentane 71
Figure 6.20: Electrical power output for dimethyl ether 72
Figure 6.21: System exergy efficiency for dimethyl ether 73
Figure 6.22: Expander isentropic efficiency for dimethyl ether 73
Figure 6.23: Optimized values of pressure ratio and degree of superheat for all working fluids 75
Figure 6.24: System exergy efficiency for various working fluids 77
Figure 6.25: System energy efficiency for various working fluids 78
Figure 6.26: Expander isentropic efficiency for various working fluids 79
Figure 6.27: Electricity cost rate for various working fluids 80
Figure 6.28: Electrical output for various working fluids 81
Figure 6.29: T-s diagram for dimethyl ether at optimal operating conditions 82
Figure 6.30: T-s diagram for toluene at optimal operating conditions 82
Figure 6.31: RPM for various working fluids at optimized conditions 83
Figure 6.32: Pressure difference between Input and output of expander at optimized conditions 84
Figure 6.33: Output torque for various working fluids at optimized conditions 85
Figure 6.34: Heat input for various working fluids at optimized conditions 86
Figure 6.35: Exergy destruction of each component for R134a at optimized conditions 87
Figure 6.36: Exergy destruction of each component for water at optimized conditions 88
Figure 6.37: Exergy destruction of each component for R227ea at optimized conditions 89
Figure 6.38: Exergy destruction of each component for R245fa at optimized conditions 89
Figure 6.39: Exergy destruction of each component for toluene at optimized conditions 90
Figure 6.40: Exergy destruction of each component for iso-butane at optimized conditions 90
Figure 6.41: Exergy destruction of each component for acetone at optimized conditions 91

Figure 6.42: Exergy destruction of each component for iso-pentane at optimized conditions 91
Figure 6.43: Exergy destruction of each component for n-pentane at optimized conditions 92
Figure 6.44: Exergy destruction of each component for dimethyl ether at optimized conditions..... 93
Figure 6.45: Electricity cost rate and electric power output with varying superheat at optimal pressure ratio and three different fuel costs (dimethyl ether)..... 95
Figure 6.46: Electricity cost rate and electrical power output with varying superheat at optimal pressure ratio and three different fuel costs (water)..... 96
Figure 6.47: Optimized values of electricity rate for dimethyl ether and iso-butane..... 97

List of Tables

Table 1.1: Solid wood waste and pulping liquor used for energy production (kilotonnes and equivalent terajoules) 3

Table 3.1: Practical limits for preselected organic working fluids 20

Table 5.1: Selected parameters for each working fluid 39
Table 5.2: Parameters for the thermodynamic model of the Bitzer expander 48
Table 5.3: Costing values and equations for the various parts in the system 54
Table 5.4: Upper and lower bounds for the important variables involved in the optimization 57

Table 6.1: Percent change of system exergy efficiency between iso-butane and respective working fluids 76

Nomenclature

A_f	Amortization factor
BVR	Built in volume ratio of the expander
$\boldsymbol{d}$	Direction vector
c	Exergy cost, \$/kWh
$\dot{C}$	Exergy cost rate, \$/h
ex	Specific exergy, kJ/kg
$\dot{Ex}$	Exergy rate, kW
g	Gradient vector
h	Height of scrolls, m or specific enthalpy kJ/kg
$\boldsymbol{H}$	Hessian Matrix
i	Interest rate, %
ICC	Initial capital cost, \$
K_p	Pressure torque coefficient
K_ω	Angular velocity torque coefficient
$\dot{m}$	Total mass flow rate, kg/s
$\dot{m}_{exp}$	Expander mass flow rate, kg/s
$\dot{m}_{leak}$	Leakage mass flow rate, kg/s
m_{pocket}	Mass of Pocket, kg/rev
n	Number of years
OM	Operating and maintenance cost, \$
$OM\%$	Percentage of operating and maintenance of initial capital cost
ORC	Organic Rankine cycle
ΔP	Difference in pressure, kPa

P	Pressure, kPa
q	Specific heat input or output, kJ/kg
$\dot{Q}$	Heat rate, kW
r_b	Basic Radius of the circle, m
r_o	Orbiting radius of rotating scroll, m
RPS	Revolutions per second
T	Temperature, ˚C
t	Time, s
TCC	Total capital cost, $
v	Specific volume, m^3/kg
V_{ed}	Volume of discharge, m^3
V_{ee}	Volume of expansion pocket, m^3
V_{ei}	Expander inlet pocket volume m^3
$\dot{W}$	Rate of work or Power, kW
$\dot{Z}$	Operating rate for component, $/h

Greek Letters

δ	Change in the independent variables
ζ	Expander leakage coefficient
η	Efficiency
θ	Rotation angle, rad
Π	Isochoric pressure building coefficient
τ	Torque, Nm
φ	Polar angle, rad
φ_0	Initial angle of the involute, rad
φ_{i0}	Initial angle of inner involute, rad

φ_{o0} Initial angle of outer involute, rad

ω Angular velocity, rad/s

Subscripts

o Reference state

acc Acceleration of fluid

b Boiler

cond Condenser

d Destroyed

e Expander or electric

elec Electric

exp Expander

in Input

out Output

pf Pressure forces

pump Pump

regen Regenerator

s Isentropic

sv Saturated vapour

th Thermal

x Component x

Chapter 1: Introduction

The importance of energy in the world has become higher as we have developed new technologies which help make our lives easier and more productive. Energy is needed everywhere from transportation to housing and plays a fundamental role in how the world is today. Currently, much of the world's energy is derived from fossil fuels which are an unsustainable resource. A small amount of provinces rely on low impact sources such as nuclear and hydro (Ontario and Quebec for example). As it becomes harder to exploit oil and gas deposits in the world, the price of energy is increasing. Coupled with increasing demand due to increased technology implementation and population, sustainable alternatives are becoming more important as time goes on. According to the International Energy Agency energy, coal accounts for nearly half of the increase in global energy use over the past decade. The bulk of this growth is due to the power sector in emerging economies (International Energy Agency, 2011). This has adverse effects on the environment due to increased CO_2 and other harmful emissions.

Sustainable energy sources play a large role in replacing current fossil fuel energy sources. Apart from hydroelectric production, wind and solar technologies are gaining wide acceptance. Capacity for wind and solar is increasing, especially in Ontario where government subsidies such as the Feed-in-Tariff program help promote investment in sustainable energy projects by paying higher rates for electricity production.

While solar photovoltaic and wind energy are gaining ground through government subsidies, there are many other forms of sustainable energy which can provide a replacement to conventional fossil fuels with low environmental impact. Low temperature

heat sources such as solar thermal, biomass, industrial waste heat and landfill gas have the potential to produce useable energy with low impact to the environment. To take advantage of these energy sources, heat engine cycles need to be explored to see which provides the most efficient performance within economic constraints. One such heat engine cycle which shows promising potential to be efficient in producing energy from these low temperature heat sources is the organic Rankine cycle. Similar to the Rankine cycle currently in use in large thermal power stations, the cycle uses a different working fluid other than water which works better for the temperatures involved in this application. The advantage of using an organic Rankine cycle over solar photovoltaic or wind turbine power generation is that there is control over when power is available. Whereas, solar and wind power are dependent on weather conditions unless there is some energy storage system installed. This adds cost and complexity to the system which makes it unviable and currently there is little implementation of energy storage for wind and solar. Using an organic Rankine cycle (shown in Figure 1.1) solves many of these problems especially when using renewable energy sources such as biomass, landfill gas and other biogas sources. An example of available energy from biomass is given in Table 1.1 where wood waste and pulp liquor are used for energy production. The results show the amount of kilotonnes and equivalent terajoules consumed to produce energy from this source in Canada.

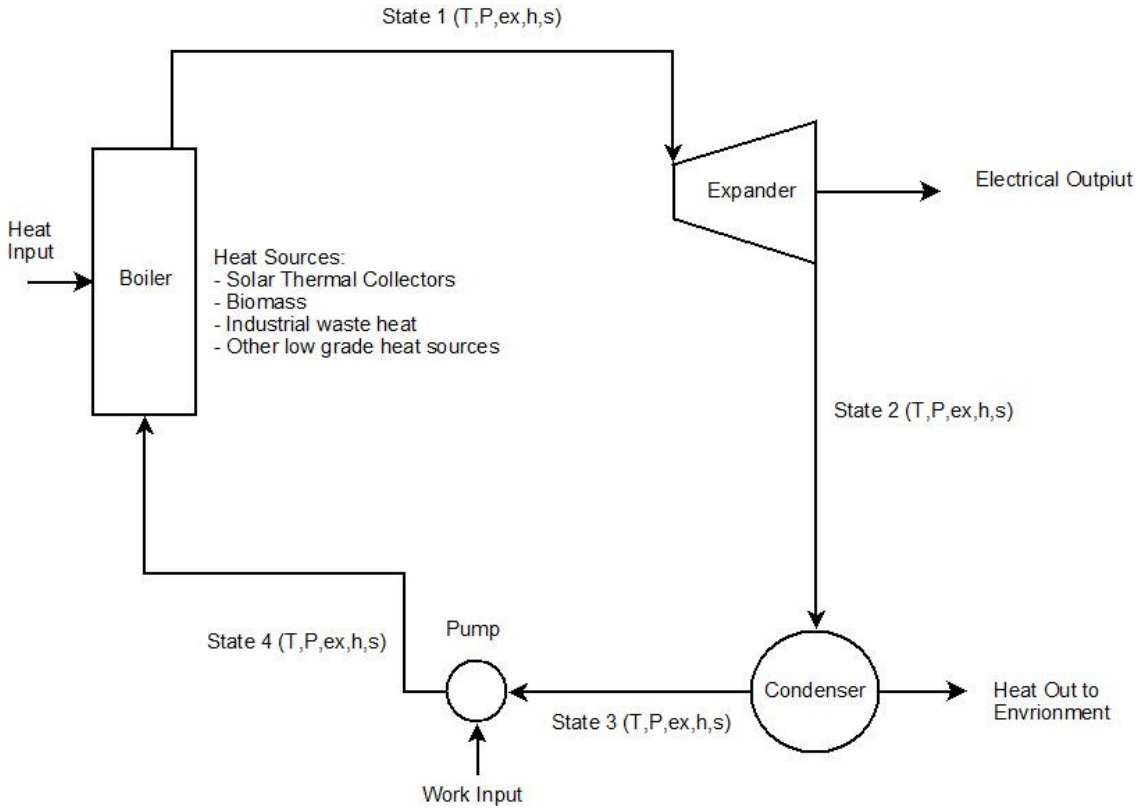

Figure 1.1: Diagram of a basic organic Rankine cycle

Table 1.1: Solid wood waste and pulping liquor used for energy production (kilotonnes and equivalent terajoules)

Fuel type	Units	2003	2004	2005	2006	2007	2008	2009	2010
Solid wood waste	Kilotonnes	13213	15782	16346	16528	15534	14630	13688	13221
Solid wood waste	Terajoules	237837	284066	294229	297502	279619	263346	246377	237984
Spent pulping liquor	Kilotonnes	20258	23828	22857	20729	20618	17490	16980	16906
Spent pulping liquor	Terajoules	283606	333590	320000	290203	288657	244857	237720	236678

Source: (Statistics Canada, 2011)

There is great potential to tap into renewable energy sources such as biomass that may otherwise just go to waste. As seen from Table 1.1 significant energy is available to use for production of electricity and heat in just this biomass source alone. Other biomass sources, industrial waste heat, landfill gas and solar thermal are all available for use with

an organic Rankine cycle system. Using these sources instead of mining for new fossil fuel sources could potentially reduce CO_2 emissions significantly. The importance of exploring and analysing an organic Rankine cycle system which can use these sources efficiently is high. If greenhouse gas emissions are to be reduced, then these energy sources need to be used appropriately. Proposing efficient and economically viable methods such as an organic Rankine cycle system are important for wide acceptance.

1.1 Motivation and Objectives

The goal of this thesis is to optimize the use of low grade heat while working within economic and physical constraints. Specifically, using the organic Rankine cycle to produce electricity at a small to medium scale in much the same way a Rankine cycle does in a large scale.

Previous investigations have concentrated on modeling and building organic Rankine cycle systems using the scroll expander to generate shaft work. There are two experiments performed where the performance of a scroll expander evaluated in a system (Tarique, 2011 and Oralli, 2010). The goal is to use a suitable model for the scroll expander developed by the previous projects and design an organic Rankine cycle system. Energy and exergy analysis as well as computerized optimization are used to find optimal operating parameters. Optimization is also used to test different working fluids to find ideal conditions for maximum efficiency and power output within certain constraints. Finally, an exergoeconomic analysis is performed on the system to determine costs to produce electricity using different working fluids and input costs. Optimization is applied

to the exergoeconomic analysis to determine optimal parameters for each working fluid within certain cost constraints.

The specific objectives of this thesis are listed below:

- To use exergy and energy analysis for each component in the organic Rankine cycle system to evaluate performance
- To perform a parametric study of the system using various parameters to observe behaviour of the efficiency (energy and exergy), and use the study for comparison against optimization results.
- To select different working fluids which are appropriate for the application considered
- To identify a working fluid which provides the best performance through energy and exergy analyses in conjunction with the optimization and exergoeconomic techniques.
- To evaluate energy and exergy efficiencies of the system as well as the exergy destruction of each component to identify areas of improvement
- To conduct an exergoeconomic analysis on the system to evaluate the cost rate of electricity and the effect of different input costs
- To perform an optimization analysis using a direct search optimization technique to find optimal efficiencies and optimal exergoeconomic parameters.

Chapter 2: Literature Review

Exploring academic literature shows several researchers which have experimented with positive displacement machines for power generation applications. The earliest research found is by Badr et al. (1985) who experiment with multi-vane expanders for use in low grade low power output applications. Mathematical and computer models are developed to predict and improve the performance of the expander. The models are verified by comparing them to an experimental organic Rankine cycle. The isentropic efficiency of the expander ranges from 45 to 55% in this experiment (Badr et al., 1985). Bong et al. (1990) introduce a thermodynamic model for a screw expander. The thermodynamic model predicts isentropic efficiencies of 60-85% while taking into account leakage and frictional losses (Bong et al., 1990). Kaushik et al. (1994) integrate an organic Rankine cycle with a vapour compression cycle in a thermodynamic study for solar cooling. No specific expander is analyzed, although a parametric study is performed to evaluate the performance. The analysis shows that increasing the inlet temperature from 90-110°C increases the system efficiency by 25% (Kaushik et al., 1994). Yamamoto et al. (2001) explore an ORC with an axial turbine using fluid HCFC-123. Isentropic efficiency ranges from 35% to 50% compared to the same system using water with isentropic efficiencies of 40% to 35% (Yamamoto et al., 2001).

Working fluid selection by Maizza et al. (2001) explores various organic fluids for ORC systems. R123 and R124 show good system performance for source temperatures of 80˚C-100°C and condenser temperatures of 35˚C to 60°C (Maizza et al., 2001). Liu et al. (2004) explore various working fluids such as R123 using first and second law parametric studies (Liu et al., 2004). Siloxane based working fluids explored by Fernandez et al. (2011) show a

thermal efficiency of 22% at 165˚C-170°C source temperatures (Fernandez et al., 2011). Exergy based fluid selection done by Herberle and Bruggemann (2010) compares a combined heat and power ORC system and regenerative ORC system preferring R227ea and isopentane as working fluids (Heberle et al., 2010).

Optimization of organic Rankine cycles is performed throughout literature. Wei et al. (2007) propose a system using R245fa and perform a parametric optimization to maximize energy and exergy efficiency of the system. Bruno et al. (2008) apply parametric optimization techniques to a solar ORC used for reverse osmosis desalination. Thermal efficiency is optimized for the system, and then used for comparison in two geographical scenarios (Bruno et al., 2008). Sun and Li (2011) use the ROSENB optimization algorithm to maximize either thermal efficiency or net power generation. Heat source temperature and ambient dry bulb temperature show a near quadratic relationship with respect to thermal efficiency (Sun et al., 2011). Roy and Misra (2012) using parametric optimization compare R123 and R134a. First and second law efficiency is used to optimize the system resulting in optimum conditions in the range of 165°C – 250°C and 2.7 MPa for R123 (Roy et al., 2012).

Jie et al. (2010) perform analysis on a regenerative ORC in a solar thermal setting. A thermal efficiency of 8.6% is realized with solar radiation of 750 W/m^2 using a regenerative system, while 4.9% is realized without regeneration (Jie et al., 2010). Mago et al. (2008) explore a regenerative organic Rankine cycle using dry fluids. R245fa, R123 and iso-butane show improved performance using regeneration over non-regeneration. Lower heat input and no superheat is needed for a system which uses regeneration (Mago et al.,

2008). Kosmadakis et al. (2011) propose a combined concentrated solar photovoltaic and solar thermal system (CPV/T) for increased power generation. Thermal efficiency of the system is 10.52% with the CPV/T and 6.56% with concentrated solar photovoltaic only. Electricity rates are 0.113 €/kWh (0.146$/kWh in 2012) for CPV/T and 0.147€/kWh (0.190 $/kWh in 2012) for CPV only (Kosmadakis et al., 2011).

Quoilin et al. (2010) study a scroll expander using HCFC-123 as the working fluid. In this experiment a scroll compressor is converted to an expander. Heat sources include two hot air streams and a piston diaphragm pump to circulate the working fluid in the system. A condenser is cooled with water and various measuring instruments are distributed throughout the system to measure temperature, pressure and flow rate. 39 steady sate points are taken and the results show a maximum cycle efficiency of 7.4% and a maximum isentropic efficiency of 68%. Rotation speed varied in steps from 1771 RPM, 2296 RPM and 2660 RPM. The working fluid mass flow rates ranged from 45 g/s to 86 g/s and maximum shaft power was 1800 W. Average source temperature was 163.2 ˚C while average condenser temperature was 15.0 ˚C (Quoilin et al., 2010).

Other systems based on organic Rankine cycles (ORC) but use different expanders have been experimented with. A complete system developed by Wang et al. (2010), as shown in Figure 2.1, studies a solar ORC using a rolling piston expander. The working fluid is R245fa and the system is able to achieve a power output of 1.73 kW with 45.2% expander isentropic efficiency. System efficiency is around 4.2% with vacuum tube solar collectors, producing heat at a temperature of 110˚C. The efficiency does not take into account the

energy needed to power the circulation pump, and if that is taken into account the efficiency is around 1%.

Other experimental studies are performed with organic Rankine cycles using conventional turbines. A study by Pei et al. (2011) use a custom designed turbo expander and R123 as the working fluid. Inlet temperatures averaged 100˚C and the system achieved efficiencies of 6.8%. Isentropic efficiency for the turbine was 65% (Pei et al., 2011).

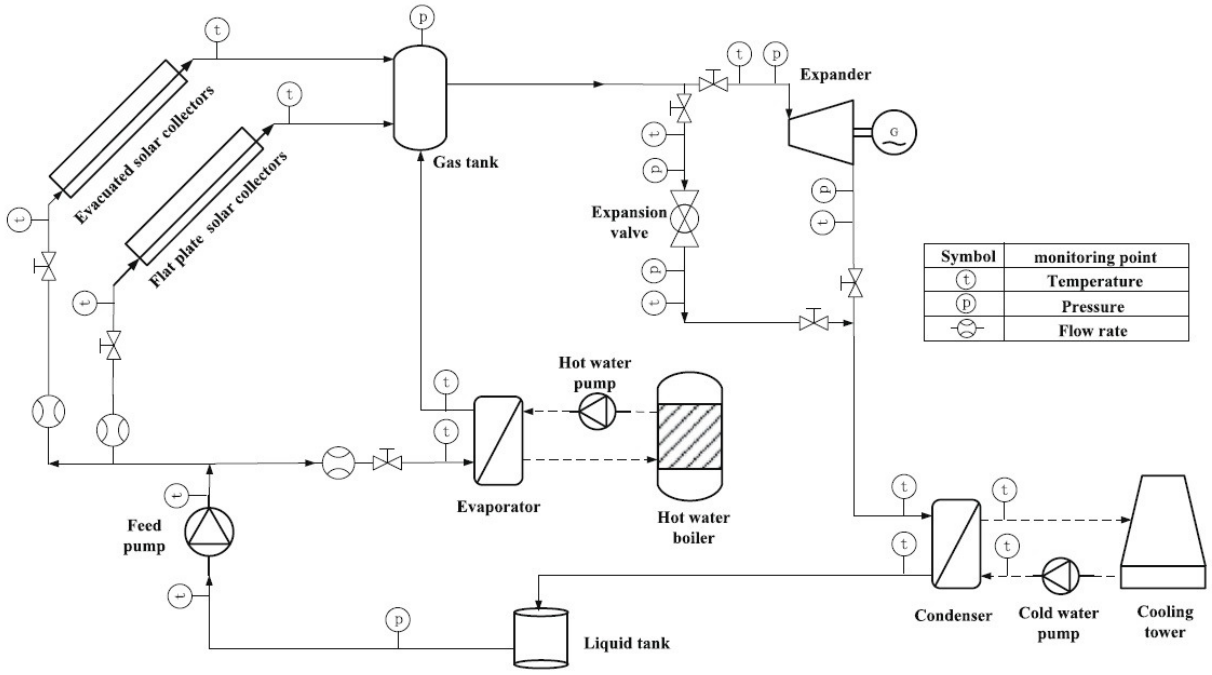

Figure 2.1: Solar thermal organic Rankine cycle modified from (Wang et al., 2010)

Another experimental application for an organic Rankine cycle is combining the system with a reverse osmosis desalination system for clean water production. One study by Manolakos et al. (2007) uses a scroll expander converted from a compressor to be integrated into a desalination/ORC system. R134a is used for the working fluid and when tested, the expander reached an efficiency of 65% while the ORC system had a maximum

efficiency of 4% (Manolakos et al., 2007). On average current work on organic Rankine cycle expanders is producing isentropic efficiencies of 45 to 70%. Due to the low source temperatures, losses need to be reduced to make these types of systems viable. While 70% maximum isentropic efficiency is a good start for experimentation, there is large room for improvement with the expander. This improves system efficiencies from the current 4% to 6.5% to higher percentages which make a strong case for organic Rankine cycle systems.

Commercial applications of organic Rankine cycle systems exist and have just recently begun marketing and sales of complete systems. Many of these systems are designed and marketed in a co-generation configuration to maximize fuel input use and system efficiency. Typically these systems range from 5 kW to 50 kW of electrical output with input temperatures from 80˚C to 120˚C. Electratherm Inc. in the USA uses a screw expander for their 50 kW ORC system. The system is designed to be attached to waste heat sources, biomass or solar thermal applications to produce electricity only. Many case studies are done with the ORC system, from biogas, geothermal from oil wells, solar thermal and waste heat from large internal combustion engines (ElectraTherm Inc, 2011).

Eneftech in Switzerland has developed a scroll expander (Figure 2.2) ORC with combined heat and power capabilities. Power ranges from 5 kW to 30 kW. Input heat required is 125˚C to 150˚C. One application is the heat recovery of hot oil from an industrial source, producing 22 kW of electricity. Another innovative application of Eneftech's system being used in practical applications is at a swimming pool facility. Heat from a district heating source produces electricity while heating up the swimming pool. 150˚C heat from the district heating loop produces 15 kW of electricity while the remaining

heat after expansion heats up the swimming pool which acts as the cold sink (condenser) for the unit (Eneftech Innovation SA, 2011).

Figure 2.2: Eneftech scroll expander geometry modified from (Eneftech Innovation SA, 2011)

Thermoeconomic optimization and evaluation is performed on organic Rankine cycle systems in literature. An analysis carried out by Quoilin et al (2011) compares different working fluids such as R245fa, n-butane and n-pentane. Thermodynamic efficiency, economics and profitability are the objective functions evaluated. N-butane produces an economical optimum of 2136€/kW (2787$/kW in 2012) at an efficiency of 4.47%. Maximum thermodynamic efficiency for n-butane in the system is 5.22%. One of the things the study takes into account is the component sizing and the associated cost when changing temperatures and other parameters in the system. One parameter, evaporating temperature, is used to show the effect of change on the component costs as it increases. Overall component costs for the system go down; the biggest change is the cost of the

expander which goes down considerably with increased temperature. The pump cost increases due to the increased fluid pressure difference needed (Quoilin et al., 2011).

The literature survey has demonstrated that there is much improvement possible for expander and system efficiency. Even while these systems require further investigation there are companies which implemented this technology successfully for a wide range of applications. Further investigation is beneficial to improve these systems to promote wider adoption in the market place.

Chapter 3: Background

3.1 General Heat Engine Cycles

Heat engine systems typically produce electricity. The basic thermodynamic principle involves two sinks, a high temperature heat source and a low temperature heat sink. In between these two sinks a heat engine converts a portion of the heat flow into shaft work which is used to produce electricity. Typically, in large scale systems high temperature heat sources from, coal, natural gas, fuel oil, and nuclear power a heat cycle known as a Rankine Cycle.

In the Rankine Cycle a fluid, typically water, is circulated and heated up to superheated, high pressure vapour. This superheated vapour is then run through a turbine which expands and lowers the pressure and temperature of the fluid while extracting work from it. Typically a force is put on the blades by the change in fluid pressure which produces torque. The exiting fluid is cooled down to a saturated liquid which is pumped into the heat source to heat and vaporize the fluid. Many improvements to this cycle to increase efficiency and reduce losses have been implemented over time. Turbines have improved in efficiency to convert more energy from the fluid. Other improvements such as combining a Rankine cycle with a gas turbine cycle also are implemented to improve overall efficiency.

Other heat cycles which convert heat into shaft work are the Kalina cycle and Stirling cycle. The Kalina cycle is a variation of the Rankine cycle described above and the Sterling cycle is based on an ideal model called the Carnot cycle. The Carnot cycle is the ideal model which is used for comparison against all heat cycles (Cengel et al., 2008).

The Stirling cycle is considered to be similar to the Carnot cycle except that the isentropic processes in the Carnot cycle are replaced by constant volume processes in the Stirling cycle. The constant volume processes are when regeneration occurs in the cycle. In the first constant volume process some energy is stored from the working fluid in a regenerator. After heat is rejected into the cold sink that stored heat is returned to the working fluid at constant volume. While this is an idealized cycle, the actual sterling engine does not behave exactly like the cycle is designed. Regeneration is still part of the cycle to help improve efficiency of the engine.

The Kalina cycle uses a mixture of two fluids usually ammonia and water to convert thermal energy into shaft work. The advantage is that more heat is extracted from the source by adjusting the boiling point of the mixture. The boiling point is adjusted by changing the pressure of the ammonia water mixture in the boiler. The Kalina cycle is usually found in industrial waste heat applications where the waste temperature can change frequently depending on plant output (Cengel et al., 2008).

3.2 Organic Rankine Cycles

One area which is beginning to use a variation of the Rankine cycle is low temperature heat sources such as solar, biomass and industrial waste heat. This cycle is similar to a normal Rankine cycle except that the working fluid is usually something other than water. Fluids other than water are used are due to the temperatures and pressures that this low temperature cycle run on. As in the typical Rankine cycle, in the organic version, the main components are a boiler, turbine (or expander), condenser, and pump. The working fluid is heated in the boiler to a super-heated vapour, where it is expanded in

the turbine. Once passing through the turbine the fluid is cooled in the condenser to a saturated liquid. A pump then increases the pressure back to the working pressure and circulates it back to the boiler. There are several configurations for an organic Rankine cycle. The configuration described above is similar to a conventional Rankine cycle in terms of the components needed for operation. Other typical configurations which exist are regenerative organic Rankine cycle, combined heat and power organic Rankine cycle and supercritical Rankine Cycle.

3.2.1 Regenerative Organic Rankine Cycles

Depending on the type of the fluid used, the state after expansion may still be a superheated vapour. This is the case with isentropic and dry fluids (fluids which are still a superheated vapour after expansion), which have a saturated vapour line on a T-s diagram that is vertical or negative entropy sloped. Figure 3.1 shows the T-s diagram for R227ea which is considered to be a "dry fluid". Dry fluids exhibit behavior which allows them to still be superheated at the exit of the expander. With these fluids there is an opportunity to use the heat at the turbine outlet for heating applications if the temperature is sufficient or to use a regenerator and reintroduce the heat into the fluid stream. Generally it is desirable to use a regenerator to maximize efficiency of electric production if it is the prime use for the system. If the temperature of the heat is sufficient and is useable within a short distance, then building or process heating is possible as well.

3.2.2 Combined Heat and Power Organic Rankine Cycles

This cycle is the same as the basic organic Rankine cycle except there is a heat exchanger after the expander to take advantage of the remaining heat that still may be at a

high enough temperature for practical use. The configuration for a cogeneration system is shown in Figure 3.2 with the heat exchanger representing the external heating loop. Figure 3.3 shows the T-s diagram of R227ea undergoing expansion and the changing temperatures during the process. Outlet temperature for the expander under ideal expansion is 92.8 ˚C and the condenser temperature is 31.7˚C. This is using the Bitzer expander at optimal conditions and would be similar for other scroll expanders with fixed built in volume ratio. If a heat exchanger is placed between the outlet of the expander and the inlet condenser, there is potential to further increase the overall system efficiency.

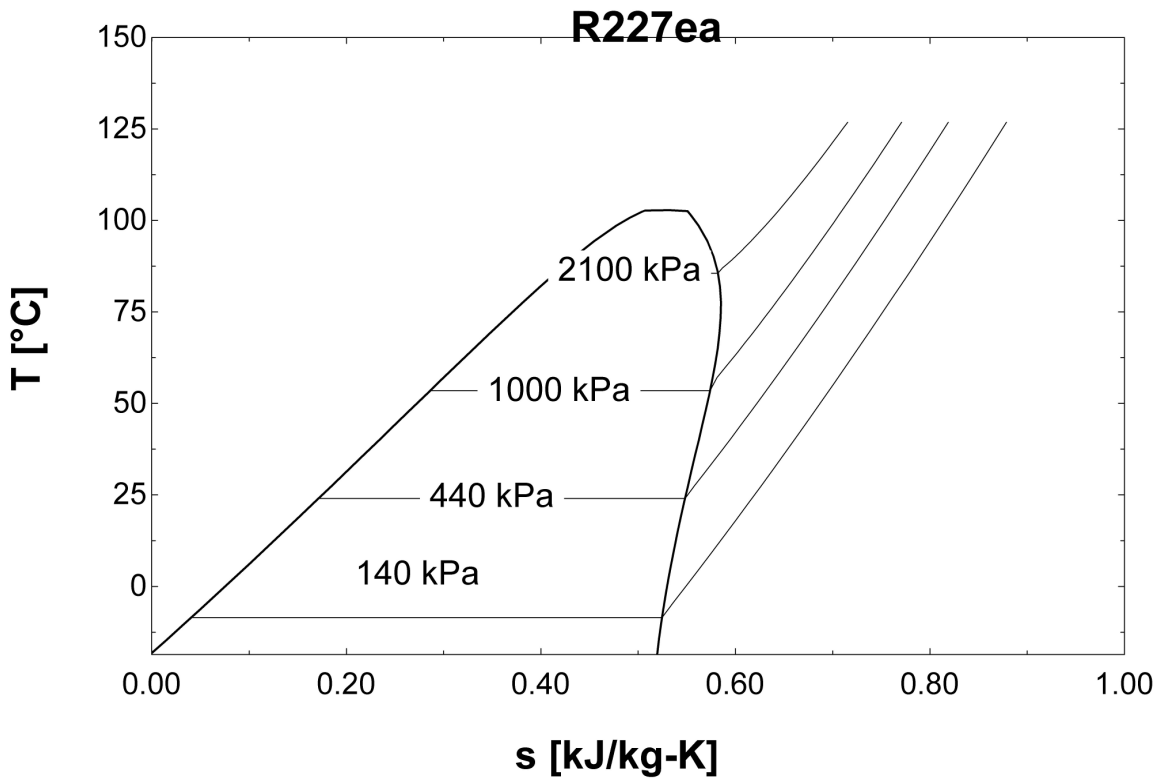

Figure 3.1: T-s diagram of R227ea

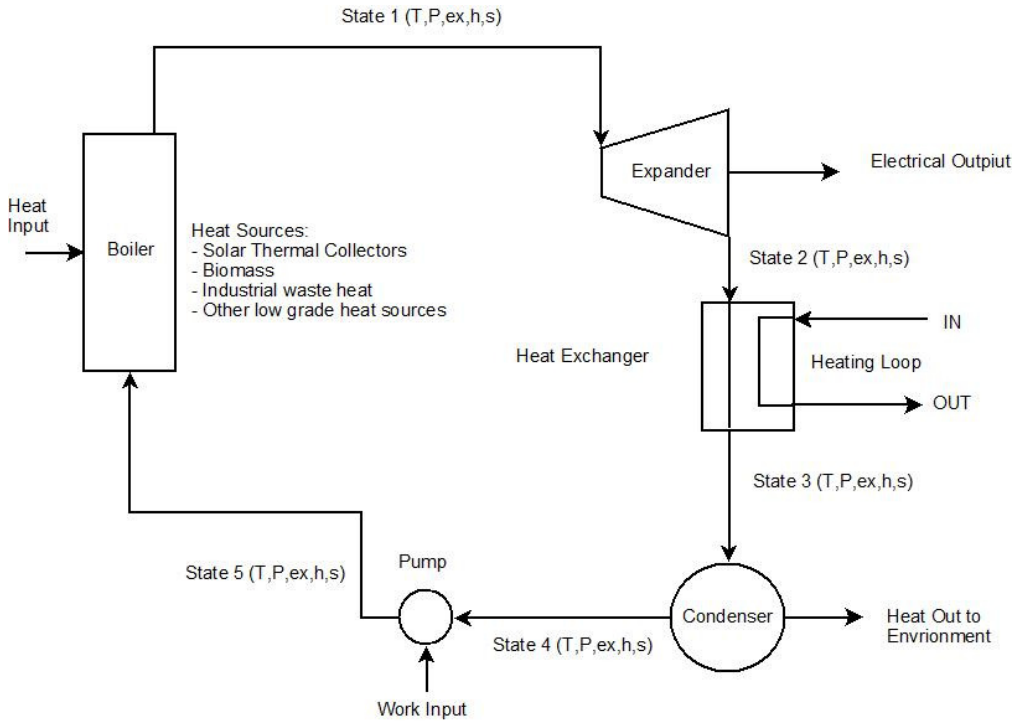

Figure 3.2: System diagram for a cogeneration organic Rankine cycle

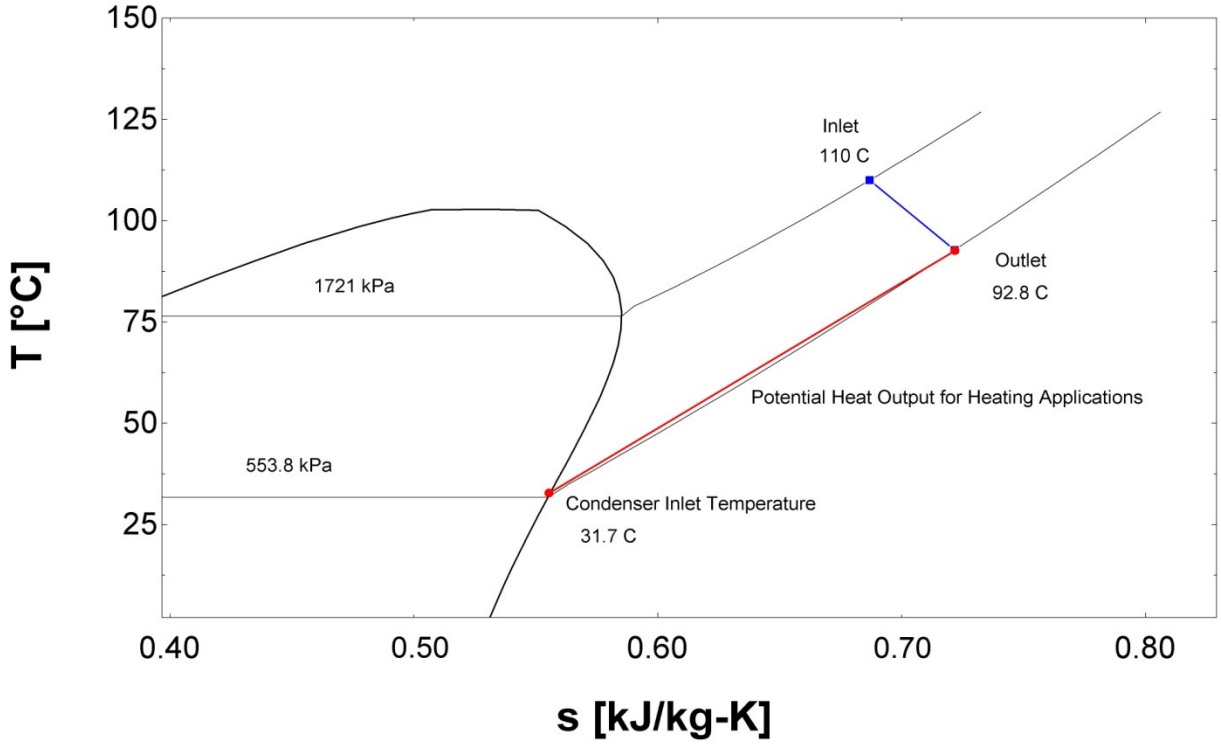

Figure 3.3: T-s diagram of R227ea showing potential heat available for cogeneration applications

3.2.3 Super Critical Organic Rankine Cycles

The super critical organic Rankine cycle shown in Figure 3.4 operates at the critical point of the fluid to avoid entering the mixture phase of the fluid which helps reduce losses in the boiler. When matching the heat source temperature profile with the profile of the working fluid in the boiler, the pinch point is eliminated thus reducing losses during heat exchange.

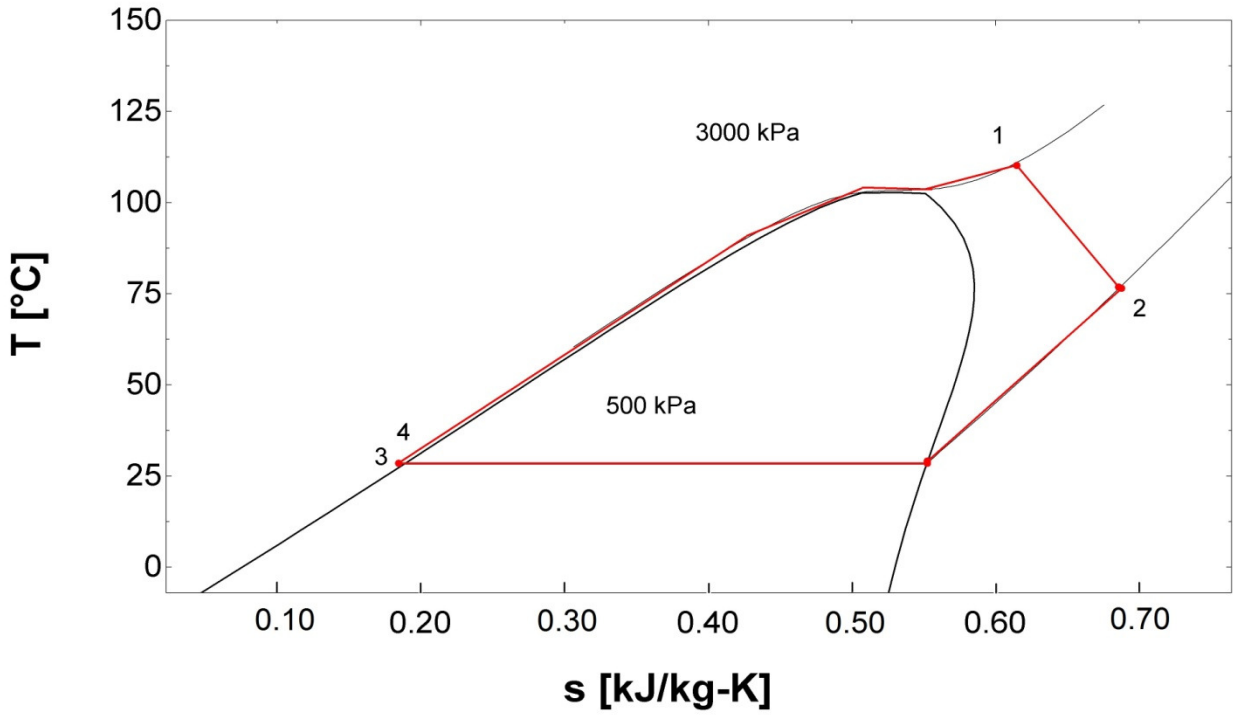

Figure 3.4: T-s diagram of a supercritical organic Rankine cycle using R227ea

3.2.4 Working Fluids

Many working fluids are explored in literature with various techniques for selection. Global warming potential, ozone depletion potential and critical temperature are some of the characteristics proposed for selection (Tchanche et al., 2009). Preliminary selection of a working fluid for the Organic Rankine Cycle (ORC) starts with identifying fluids which are high in ozone depletion and in global warming potential (GWP). Particularly, fluids that contain chlorine atoms such as CFC's and HCFC's are not appropriate. Global warming potential can be identified from property tables for each of these fluids from respective manufacturers or literature. Low global warming potential is preferred to reduce environmental effects in the case of a leak. Another characteristic to look for in a working fluid is the slope of the temperature-entropy curve, particularly on the super-heated side. Fluids are categorized based on this curve as, isentropic, dry or wet. Isentropic and dry are the most desirable for ORC systems, because these fluids are still superheated after isentropic expansion in a turbine (or expander). This eliminates and problems with liquid forming at the turbine outlet, which can potentially reduce service life significantly (Rayegan et al., 2011). Wet fluids exhibit this behaviour when running through the turbine since they enter a mixture zone when going from higher to lower pressures. Fluids should also be chosen based on the expected source and condenser temperatures. Usually condenser temperatures should not be lower than 25°C as this is the average value chosen for external environment temperature. Table 3.1 shows the practical limits of the various organic working fluids available which satisfy the above preliminary requirements. Once a preliminary study has been performed, a fluid that will work within pressure and temperature ratings of the expander should be investigated.

Table 3.1: Practical limits for preselected organic working fluids

Working Fluid	Maximum Practical Pressure (kPa)	Max Practical Temperature (˚C)	Minimum Pressure (kPa)	Minimum Temperature (˚C)
Acetone	3379	213	30.7	25
Benzene	4067	274	12.7	25
Butane	3013	138	234.7	25
Butene	2808	125	297.2	25
C4F10	2057	107	268.3	25
C5F12	1803	141	84.7	25
Cis-Butene	3035	142	213.7	25
Cyclohexane	3655	272	13	25
Decane	1896	337	5.1	85
Dodecane	1723	281	5.1	121
E134	2747	125	212.8	25
Heptane	2410	258	6.1	25
Hexane	2680	226	20.2	25
Isobutane	2890	121	350.5	25
Isobutene	2877	125	305	25
Isohexane	2682	216	282.2	25
Isopentane	2887	177	91.8	25
Neopentane	2788	152	171.4	25
Nonane	2059	314	5	65
Octane	2200	287	5	44
Pentane	2865	186	68.3	25
R218	1899	57	867.5	25
R-227ea	2352	91	455.2	25
R236ea	2955	132	205.9	25
R236fa	2288	108	272.4	25
R245fa	2951	158	100.8	25
R245ca	2817	140	149.4	25
R365mfc	2712	177	53.4	25
RC318	2314	106	312.5	25
Toluene	3576	307	5.1	31
Trans-butene	2906	136	234.1	25
R413A	1839	59	720.2	25
R423A	2966	90	598	25
R426A	1562	55	687.8	25

Source: (Rayegan et al., 2011)

The temperature and pressure limits are chosen based on the slope on the saturated line on the temperature-entropy graph for each fluid. Also limits are below any decomposition temperatures for each of the fluids. To avoid entering a mixture zone during the pressure drop through the expander a point where the slope of the saturated vapour

line is infinite is needed. Figure 3.5 illustrates the points for R227ea which are appropriate and not appropriate for maximum limits. Point A would not be appropriate because the fluid would enter a mixture zone when dropping in pressure in the expander potentially shortening the life of the expander. Point B would be more appropriate since there is no chance that the fluid will enter the mixture zone during operation in the expander. This case is appropriate when there is little to no super heat added to the fluid. Raising the temperature of the fluid at a specific pressure to the superheated region would solve this problem.

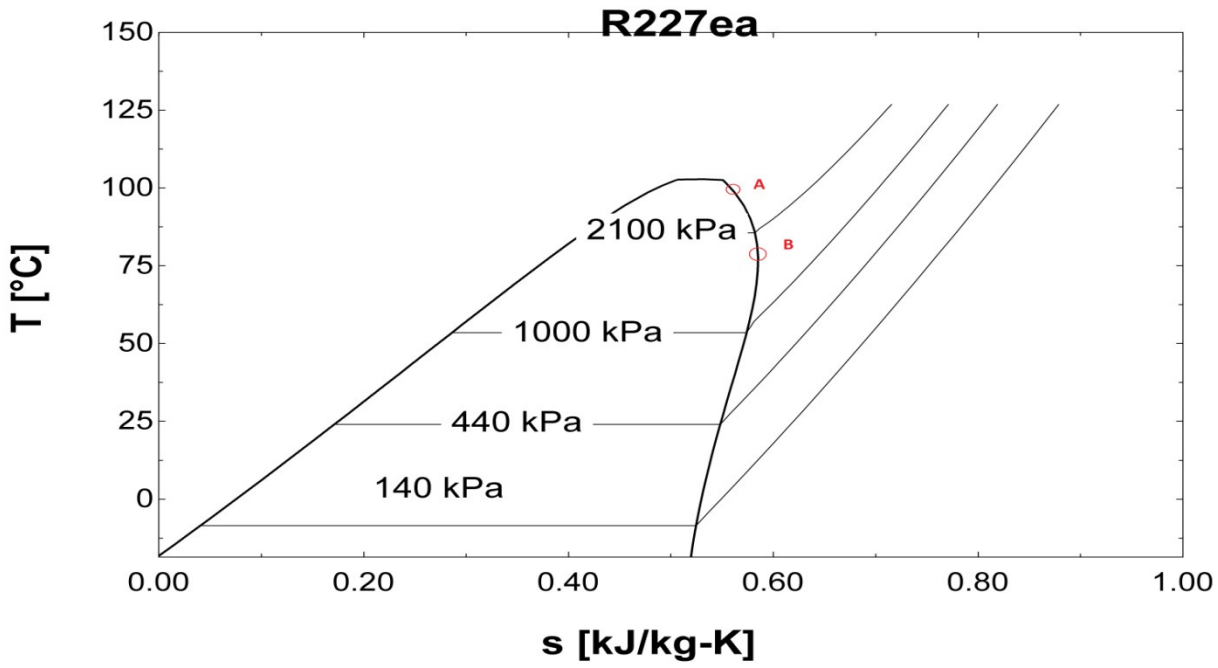

Figure 3.5: Practical and unpractical conditions for isentropic and dry working fluids

Once these practical limits are evaluated, a fluid is chosen based on the expected upper temperatures. If the inlet saturation temperature of the expander causes the pressure to be higher than the critical pressure of the fluid, that fluid is avoided. This is due to the fact that the software used cannot easily determine properties above critical

pressures where two phase conditions may exist. Also the main focus of this thesis is to study regenerative organic Rankine cycles.

3.3 Expander Types

Many turbines and expanders are proposed and researched for use in organic Rankine cycles. Some of these include: conventional axial turbines, screw expanders, scroll expanders, vane expanders and other positive displacement machines. Turbines can be categorized into two types, impulse and reaction. Impulse turbines use fixed nozzles to increase the velocity of the fluid which then impacts the blades and thus producing a torque. The change in fluid kinetic energy is the main conversion of energy in the turbine. The fluid pressure does not drop when entering the moving blades, and only drops when moving across the fixed nozzle. Reaction turbines produce a torque by reacting to the change in pressure of the fluid across the blades of the turbine. Newton's third law is applicable to reaction turbines, where for every action there is an equal and opposite reaction. Turbines have been used in organic Rankine cycles, and most require high rotation speeds and custom manufacturing. This is due to the fact that there are no practical uses for small scale (<100 kW) turbines in commercial operation. One case by Gang et al. (2011) involved designing and manufacturing a radial-axial turbine for use with R123 working fluid. The turbine is designed for a rotation speed of 60,000 RPM and 3.3 kilowatt output. Inlet temperature is around 100˚C and mass flow rate is 0.083 kg/s. Average isentropic efficiency for this turbine is 0.65 and average system efficiency was 6.8% at 1kW shaft power output (Gang et al., 2011).

3.3.1 Gerotors Expanders

Positive displacement machines converted to expanders for organic Rankine cycle applications have produced many studies dedicated to the subject. Gerotors have been investigated for use in organic Rankine cycles. A gerotor consists of an inner gear with N teeth and an outer ring gear with N+1 teeth. As the machine turns fluid pockets are expanded when the gears un-mesh from each other. One test of a gerotor by Mathias et al. (2009) yielded a max isentropic efficiency of 85% (Mathias et al., 2009). Other than this particular study, there are limited studies which deal with the gerotor expander. Further studies could produce other results which may or may not qualify this particular expander for further study.

3.3.2 Screw Expanders

Screw expanders (Figure 3.6) are comprised of a pair of meshing helical rotors which rotate when a fluid acts against them. Fluid volume decreases as it becomes trapped between the meshing screws and increases as the screws turn in the appropriate direction. A study by Wang et al. (2011) uses a screw compressor which is converted for use as an expander. It is run on a test bench to strictly test expander performance and not as part of a system. Average isentropic efficiencies of 0.59 are achieved (Wang et al., 2011). Commercial applications of screw expanders are available in the range of 20-50kW with installation costs of 1500-2000 $/kWh$_e$. Electricity can be generated at 0.03 to 0.04 $/kWh if 3 year payback period is used (Qiu et al., 2011).

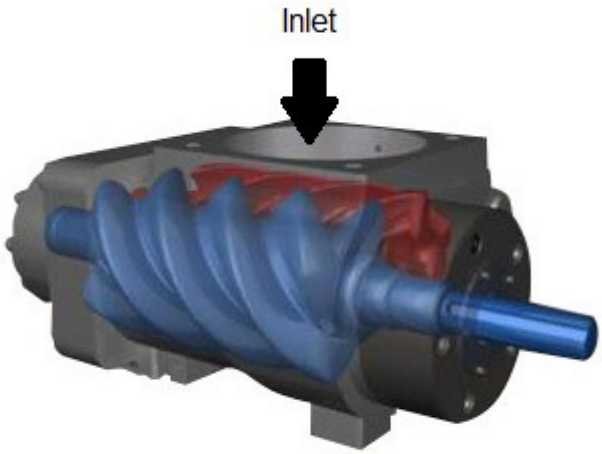

Figure 3.6: Screw expander modified from (ElectraTherm Inc, 2011)

3.3.3 Scroll Expanders

Scroll expanders are another type of positive displacement machine with a unique geometry. First patented by Leon Creux in 1905, commercially viable machines did not come out until proper tolerances could be achieved with machine tools. Scroll machines depend on tight tolerances to reduce leakages which can hinder performance. The geometry of the scroll is usually an involute of a circle. This produces a shape which resembles a spiral. An example of an involute of a circle in practice is a tether ball attached to a pole. When you wrap the string around the pole the ball gets closer to the pole while tracing out a spiral as it turns to wind around the pole. In practice two of these spiral shaped disks (scrolls) with spirals at height x are put together. One of these scrolls is fixed in place, while the other is free to move. The moving scroll orbits the fixed scroll while always keeping contact with each other to produce pockets of fluid which can either be compressed or expanded. The scroll machine is commonly used as a compressor for

refrigeration with many large manufacturers producing compressors for various sizes, from residential to commercial. This gives great flexibility when testing needs to be done for expander operation as there is a large market for used or low cost scroll expanders. Compared to axial turbines and helical screws, manufacturing of a scroll machine is comparatively simpler due to the 2D geometry. In compressor operation the fluid enters from the outer edge of the scroll and is moved towards the center of the scroll compressor. This forces the gas to decrease in volume and thus raising its pressure. When used as an expander the fluid enters in the center and moves to the outer edge of the machine. This causes the fluid to drop in pressure since the volume of the fluid pocket increases in size while it pushes against the scrolls producing torque. Several studies have been performed with scroll expanders. One by Quoilin et al. (2010) produced isentropic efficiencies of 0.42 to 0.68 depending on operating conditions using R123 as the working fluid. Commercial applications of scroll expander exist for cogeneration configurations. Eneftech produces a unit with electrical outputs of 5 kW to 30 kW with thermal capacities of 45 to 255 kW (Eneftech Innovation SA, 2011).

3.4 Optimization Methods

The basic structure of an optimization problem includes design variables, design parameters and design functions. Design variables are the variables that will change as the problem is optimized. These are usually variables which identify a particular design, for example, length, width, height, temperature, etc. Design parameters are usually constants that do not change when an optimization is performed such as material properties or source and sink temperatures. Design functions are made up of two kinds of functions, the objective function and constraint functions. The constraint functions are further divided

into two types of functions called equality and inequality constraints. The objective function is the function which is used to maximize or minimize the problem. An example would be to minimize the mass of a structural beam or maximize the efficiency of the system. The constraint functions are used to constrain the objective function. For example if the objective function is to minimize mass of a soda can, a constraint function would be set so that the diameter cannot be greater than the height of the can. This is an example of an inequality constraint. An equality constraint would constrain the volume of the can to exactly 500 mL. Depending on the problem there would be constraint bounds on certain variables so they do not exceed certain limits. Once all functions, variables and bounds are determined for the problem, an algorithm or method is needed to optimize the problem.

There are many optimization methods for different situations and goals. Optimization has applications in fields such as engineering to economics even to instruments. Most real life problems have several solutions or infinitely many solutions. If more than one solution exists for a problem optimization can be achieved by finding the best solution within the criteria given. There are many general approaches to optimization such as, analytical methods, graphical methods, experimental methods, and numerical methods (Antoniou et al., 2007).

Analytical methods involve using calculus to find the minimum or maximum of a function by finding the values of the independent variables which cause the derivative of the function to become zero. While simple and useful for cases where there are two or three independent variables, it cannot be applied problems with more than these variables.

Graphical methods plot the function on a graph and can be used when there are one to two independent variables. When plotting on a graph (when f(x) is dependent on only one variable) within a specific range the maxima and minima of a function become apparent easily. When dealing with two independent variables (x1, x2) a contour plot is made where the variables are set on the x and y axes and the function evaluated for various values of x1 and x2. An optimum set of variables is chosen based on the criteria of finding the maximum or minimum.

Experimental methods involve changing certain variables one by one and recording the system performance. With this method there are limitations, such that changing one variable interacts with another leading to unreliable results and difficulties achieving optimization of the system.

The most important approach to optimization used in this thesis is based on numerical methods. Numerical methods use iterative steps to progressively get closer to an improved solution starting with an initial guess. This method completes when changes in the independent variables from iteration to iteration become insignificant.

Numerical methods can solve highly complex problems and are programmed into a computer to be solved. This makes the approach adaptable to many situations and thus is very popular for all kinds of problems. In general optimization problems involve an objective function which is dependent on x_n number of independent variables. There can be a certain number of constraints, mainly equality constraints and inequality constraints. An example of an equality constraint is the area of a space needs to be exactly 300 square meters. An inequality constraint can be that the length has be less than or equal to 2 times

the width. Another important constraint is a side constraint or bound. This sets the range for which the independent variables are to be evaluated within.

The program used to perform the optimization for the system is EES. EES has a min/max function built in the program which uses numerical optimization methods to minimize or maximize a function based on 1 to x number of variables. The two methods available are the direct search method and the variable metric method.

The direct search method is also called a conjugate-direction method; specifically EES uses Powell's Method for direct search optimization. The basic premise of this method is to search for the optimum value using one independent variable while holding the others constant. Once the optimum value is found for that variable the process is repeated for the next set of variables. The advantage of this method is that it is useful when functions are not easily differentiable, which may be the case for the thermodynamic functions involved for this project. Also this method is ideal for when the optimum value may be on one of the bounds which is entirely possible with Rankine cycle systems.

The algorithm of Powell's Method is given as follows (Antoniou et al., 2007):

Step 1

Input $x_{00} = [x_{01}\ x_{02} \ldots x_{0n}]^T$ and initialize the tolerance ε.

Set

$$\mathbf{d}_{01} = [x_{01}\ 0 \ldots 0]^T$$

$$\mathbf{d}_{02} = [0\ x_{02}\ \ldots 0]^T$$

$\mathbf{d}_{0n} = [0\ 0\ \ldots\ x_{0n}]^T$

Step 2

For $i = 1$ to n:

Find α_{ki}, the value of α that minimizes $f(x_{k(i-1)} + \alpha\mathbf{d}_{ki})$

Set $x_{ki} = x_{k(i-1)} + \alpha_{ki}\mathbf{d}_{ki}$

Step 3

Generate a new direction

$\mathbf{d}_{k(n+1)} = x_{kn} - x_{k0}$

Find $\alpha_{k(n+1)}$, the value of α that minimizes $f(x_{k0} + \alpha\mathbf{d}_{k(n+1)})$

Set

$X_{k(n+1)} = x_{k0} + \alpha_{k(n+1)}\mathbf{d}_{k(n+1)}$

Calculate $f_{k(n+1)} = f(x_{k(n+1)})$

Step 4

If $|| \alpha_{k(n+1)}\mathbf{d}_{k(n+1)}|| < \varepsilon$, output $x^* = x_{k(n+1)}$ $f(x^*) = f_{k(n+1),}$ and stop.

Step 5

Update directions by setting

$\mathbf{d}_{(k+1)1} = \mathbf{d}_{k2}$

$\mathbf{d}_{(k+1)2} = \mathbf{d}_{k3}$

$\mathbf{d}_{(k+1)n} = \mathbf{d}_{k(n+1)}$

set $x_{(k+1)0} = x_{k(n+1)}$, $k = k+1$, and repeat from step 2.

In step 1 the vectors $\mathbf{d}$ are a set of coordinate directions. In step 2 f(x) is minimized along the path $x_{k0}, x_{k1}, \ldots x_{kn}$. In step 3 f(x) is minimized in the new conjugate direction. The advantage with this method is that derivatives do not have to be evaluated. X^* is the optimized value of the independent variable. n is the number of independent variables involved in the search. With this method an initial guess x_{00} is assumed and a set of directions $\mathbf{d}_{0n}$ are assumed. A series of line searches is performed for each iteration. In the first iteration f(x) is minimized sequentially in directions $\mathbf{d}_{01}, \mathbf{d}_{02}, \ldots \mathbf{d}_{0n}$, starting from point x_{00} yielding points $x_{01}, x_{02}, \ldots x_{0n}$. The new direction is generated as $\mathbf{d}_{0(n+1)} = x_{0n} - x_0)$ and f(x) is minimized in this direction to yield a new point $x_{0(n+1)}$.

The variable metric method is also known as the quasi Newton method. The original Newton method uses gradients and derivates to find the optimized value of a function. It does this by using the Taylor series to fit a function on the objective function. This involves developing a Hessian matrix (of second derivatives) and making small changes to the independent variables until a convergence criterion is met. The Hessian matrix ($\boldsymbol{H}$) is a square matrix of second order partial derivatives of a function. A gradient vector (g), which is a vector of first derivatives of the Taylor function, is also necessary with the Newton methods. The optimum change in the independent variables is:

$$\delta = -\boldsymbol{H}^{-1}\mathrm{g}$$

It is critical in the Newton algorithm to find the optimum value of the objective function. The quasi Newton method modifies what was described above. The basic principle is that the direction of search is based off an n × n matrix which is similar to the inverse Hessian matrix. As iterations are performed, the n × n matrix becomes closer to the inverse Hessian matrix. One of the disadvantages of the Hessian matrix is that it requires partial second derivates which may not be possible for all functions. The quasi-Newton method avoids these problems by eliminating the need to evaluate second derivates.

Chapter 4: System Description

The system which an analysis is done is a regenerative organic Rankine cycle. In this system there is a boiler, expander, regenerator, condenser and pump. The regenerator transfers some of the useable heat exiting from the expander to the fluid stream before it enters the boiler. The reason this is necessary for the system is that when using an isentropic or dry fluid, the state of the fluid exiting the expander is always going to be superheated. Depending on the fluid and the pressure ratio of the expander, the temperature is much higher than the fluid stream after the pump. Therefore, there is a potential to return (or regenerate) some of that heat back into the system instead of dumping it to the atmosphere in the condenser. This helps increase cycle efficiency, since less heat input is needed to heat up the fluid to the expander input state.

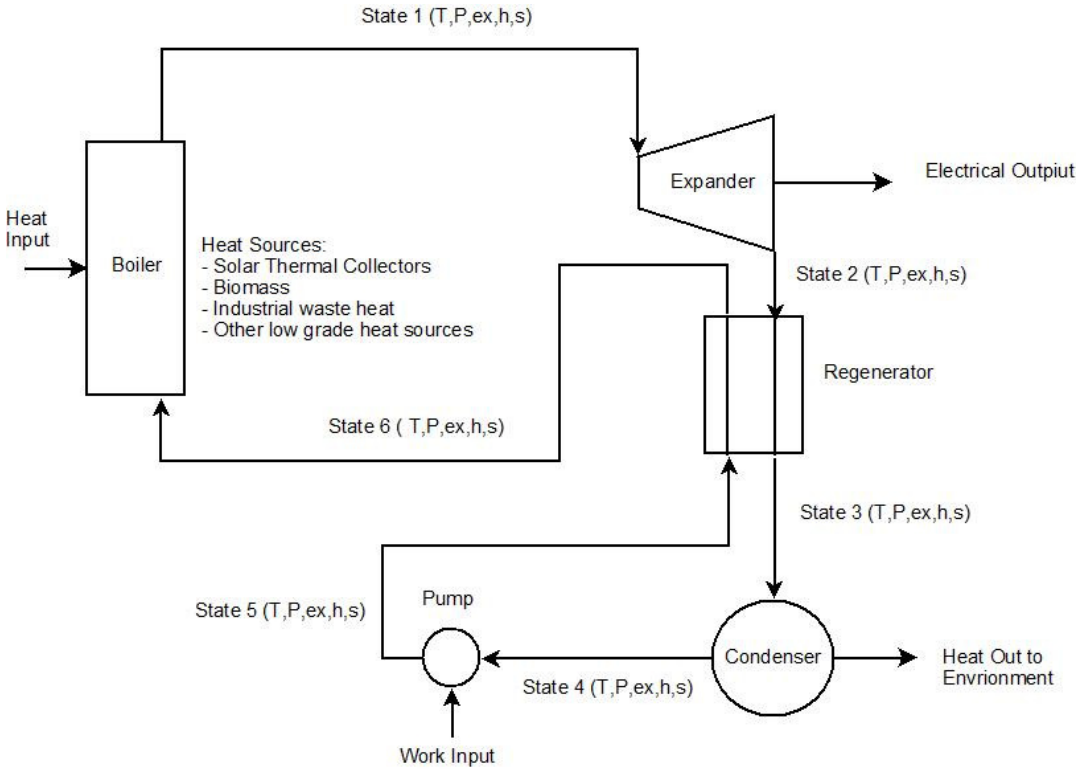

Figure 4.1: Diagram of system used in the analysis

4.1 Bitzer Expander

The expander in the system shown in Figure 4.1 is based on an actual model by Bitzer. Originally designed for compressor duty, the Bitzer ECH209Y-02G is designed for use in the transportation industry. Specifically the compressor is designed to be used for air conditioning systems in buses. The compressor has a built in 26 V DC permanent magnet motor, which makes it ideal to test voltage and current output easily. Other compressors usually come with an induction non-synchronous motor which cannot produce power on its own without some outside current to produce an initial magnetic field. In the current state the Bitzer compressor has been turned into an expander by removing the check valve at the outlet. It has been built into a system that uses a hot air loop as a heat source and a compressor to circulate the working fluid. This system was

configured by Shaikh in 2011 and uses R134a as a working fluid. Before Shaikh (2011), Tarique (2011) obtained the compressor and configured it for expander duty. It was tested solely for expander performance as part of a comparison with other expanders. While the expander is small for practical uses it provides a good medium to experiment and understand the operation of scroll expanders. The expander is rated at 1500W input for compressor duty, and is expected to produce less during expander operation. This is due to losses internally, such as friction and leakages.

Figure 4.1 shows the system used in analysis and assumptions are outlined below:

- The efficiency of the generator is considered to be constant at 80%.
- The inlet temperature to the expander is constant at 110˚C.
- The isentropic efficiency of the pump is considered to be constant at 70%.
- The environment temperature and pressure are set to 25˚C and 101.325 kPa.
- All heat losses from the turbine, piping and pump are considered to be negligible.
- The regenerator has an effectiveness of 0.8.
- The temperature at state 3 is 5˚C higher than the temperature at state 4.
- The source temperature is 120˚C.
- The system is considered to be at steady state operation.

Chapter 5: Analysis

In this section the analysis is explained in detail beginning with the expander model and moving on to the thermodynamic model. The optimization procedure and exergoeconomic analysis are also explained in detail. The main goals for the analysis are to optimize the system for different working fluids and using the optimized results to perform an exergoeconomic analysis on the system.

5.1 Expander Analysis

Thermodynamic analysis consists of applying a suitable model which will predict expander behaviour accurately. This is important because when dealing positive displacement machines converted to expanders it is simply not appropriate to assign a value for isentropic efficiency arbitrarily. Some accuracy is needed in order to properly assess the viability of the system. Previous work has been done to model a scroll expander by Tarique (2011), Shaikh (2011), and Oralli (2010). Particularly, Tarique (2011) proposed a method which fit well with the thermodynamic goals of this project.

In positive displacement machines the volume of the chamber which expands the fluid changes as the machines turns. Knowing the volume as the expander turns is important to predict how much energy is converted to useful work. The geometry of the scroll expander is called an involute of a circle. This looks like a spiral shape and is indicated in Figure 5.1.

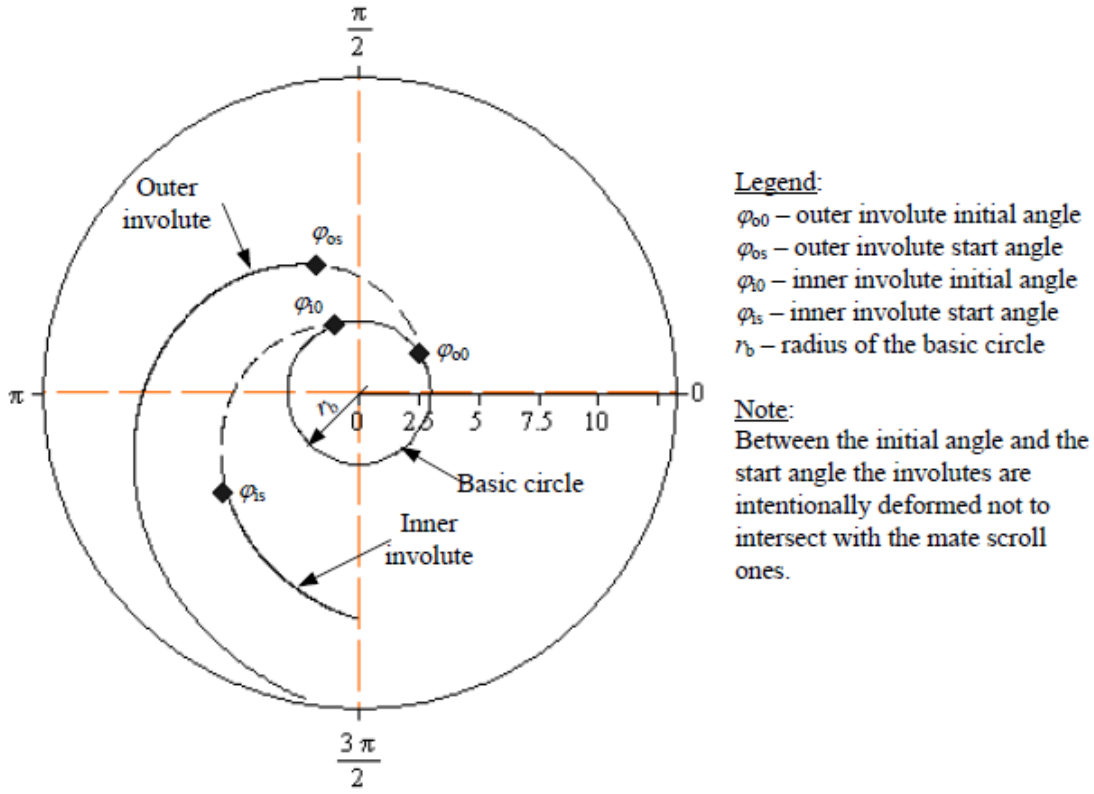

Figure 5.1: Illustrative example of the scroll geometry modified from (Tarique, 2011)

The fluid enters the centre of the expander and as the scrolls turn the volume increases thus expanding the fluid and extracting work. During rotation there are three different pockets which are of importance. The intake pocket where the fluid enters at high pressure, the expanded-crescent at intermediate pressure and discharge at exit pressure. The involute of a circle can be modeled in Cartesian coordinates or polar coordinates. In polar coordinates the equation is given as

$$r = r_b * \sqrt{1 + (\varphi - \varphi_0)^2} \qquad (5.1)$$

where $\varphi_0$is the initial angle of the involute, φ is the polar angle, r is the polar radius. The angle of $\varphi_0$can refer to inner or outer involutes, depending on the case. The rolling angle is

the ending angle of the involute and it affects the built in volume ratio of the expander. During the inlet condition the fluid enters in the centre of the scroll expander where there is a space between the two mated scrolls. The pocket size increases as the scroll orbits and after a certain angle the intake process ends and the initial pocket is divided into two small pockets. This process is modeled by the equation below.

$$V_{ei}(\theta) = hr_b r_o \theta * (\theta - \varphi_{i0} - \varphi_{o0} + 3\pi) \tag{5.2}$$

This is valid for angles ranging from $0 \leq \theta < 2\pi$.

The expander's expansion volume is given by the equation below which is valid for angles between $2\pi \leq \theta \leq \varphi_e - 2\pi$.

$$V_{ee}(\theta) = 2\pi hr_b r_0 (2\theta - (\varphi_{i0} - \varphi_{o0} - \pi)) \tag{5.3}$$

The last relation for modeling the volumes during orbiting is the discharge process. This happens during orbiting angles of $\varphi_e - 2\pi \leq \theta < \varphi_e$ and is shown below.

$$V_{ed}(\theta, \varphi_e) = hr_b r_0((2\varphi_e - 2\theta)\varphi_e - (\varphi_e - \theta)^2 - (\varphi_e - \theta)(\varphi_{i0} + \varphi_{o0} + \pi) + 2(1 - \cos(\varphi_e - \theta)) - 2(\varphi_e - \pi)\sin(\varphi_e - \theta) - \frac{\pi}{4}\sin\big(2(\varphi_e - \theta)\big)) \tag{5.4}$$

The built in volume ratio of the expander is the ratio of the expansion volume at the end of expansion over the value of the expansion volume at the beginning of the expansion process. Equations 5.1-5.4 are used in the relation of the ratio which is shown below:

$$BVR = \frac{V_{ee}(\varphi_e - 2\pi)}{V_{ei}(2\pi)} = \frac{2\varphi_e - \varphi_{i0} + \varphi_{o0} - 3\pi}{5\pi - \varphi_{i0} + \varphi_{o0}} \tag{5.5}$$

The built in volume ratio (BVR) is very important in modeling the scroll expander since it decides what the volume of the fluid will be at the end of the expansion process. This ultimately decides optimal pressure ratio and the amount of work that can be extracted from the superheated fluid. The built in volume ratio is part of the analysis that makes up the complete modeling of the scroll machine; other considerations are internal leakage and friction losses. These volume relations also play a role in determining the amount of torque and work that the scroll expander will output. Later sub sections on the expander thermodynamic modeling derive parameters from these volume relations.

5.2 Working Fluid Selection

Several different working fluids were chosen for the analysis to study the behaviour of the system with each one. Table 5.1 outlines the appropriate working fluids consolidated using the preliminary selection techniques. Not all working fluids are tested due to the number of restrictions. The first restriction is that the critical pressure and temperature of some of the working fluids is too low to be used with the degree of superheat and inlet temperatures involved. R32 has a critical temperature of 78.4˚C which means that in order to use it, the superheat needs to be high. When expanded optimally at a pressure ratio of 3.62, the condensation temperature was below 25˚C. Therefore the fluid would never properly run in the program made in EES. Fluids are chosen based on having critical temperatures above 90˚C. Another issue is that the properties of R236fa are not correct in EES, producing results which do not make sense. This is due to the equations of state being programmed incorrectly into EES producing enthalpy values which do not correspond to other parameters in the state equations. When comparing enthalpy values to the actual property tables from the manufacturer this issue becomes apparent. The last restriction is

that some fluids do not have properties in EES, and thus cannot be analysed. The final list of fluids is given below:

- R134a
- Water
- R227ea
- R245fa
- Toluene
- Iso-Butane
- Acetone
- Iso-Pentane
- N-Pentane
- Dimethyl Ether

Water is chosen for the sake of experimenting to see what the results would be if this particular fluid is used. Even though water is not typically used for organic Rankine cycles, due to the low pressures needed for the cycle to run, it is still possible to investigate its performance. Water typically has a higher density than most of these fluids and therefore the mass flow rate would be less than the other fluids. This would benefit the system by requiring less pumping work to circulate it through the system. Important properties for each of the fluids and the respective T-s diagrams are shown below (Table 5.1). The temperature-entropy diagrams help identify whether the fluid will be a dry vapour or wet vapour after expansion (Figures 5.2 – 5.11).

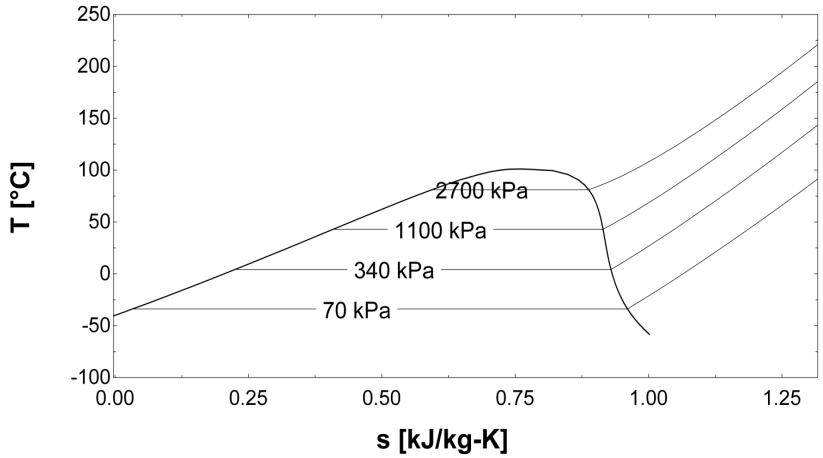

Figure 5.2: Temperature-entropy diagram for R134a

Table 5.1: Selected parameters for each working fluid

Fluid	Global Warming Potential 100 Year	Ozone Depletion Potential	Critical Temperature ˚C	Critical Pressure kPa	Density at Room Temperature 25˚C 1ATM	Heat of Vaporization at 1 ATM
R134a	1430	0	101	4059	4.258	217
Water	N/A	0	374	22064	997.1	2257
R227ea	3220	0	102.8	2999	7.148	131.7
R245fa	1030	0	154	3651	5.718	196
Toluene	2-6	0	318.6	4126	862.2	361.3
Iso-Butane	3.3	0	134.7	3640	2.44	165.5
Acetone	2-6	0	235	4700	784.7	501.3
Iso-Pentane	2-6	0	187.2	3370	614.5	342.5
N- Pentane	2-6	0	196.5	3364	620.8	358
Dimethyl Ether	2-6	0	127.2	5367	1.918	465.5

Source: (Intergovernmental Panel on Climate Change, 2007)

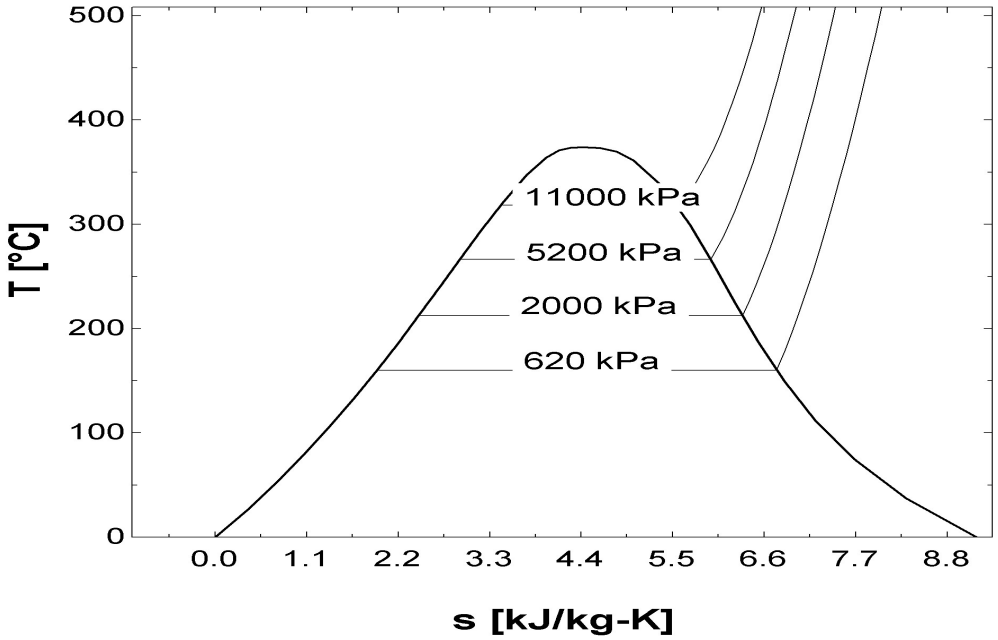

Figure 5.3: Temperature-entropy diagram for water

Water is considered a wet fluid since after expansion the fluid will be a mixture of liquid and vapour instead of a superheated vapour. Low isentropic efficiency expanders may not enter a mixture zone, although the potential exists when the isentropic efficiency increases. This has the potential to shorten the life of the expander due to water droplets striking internal parts and damaging the scrolls.

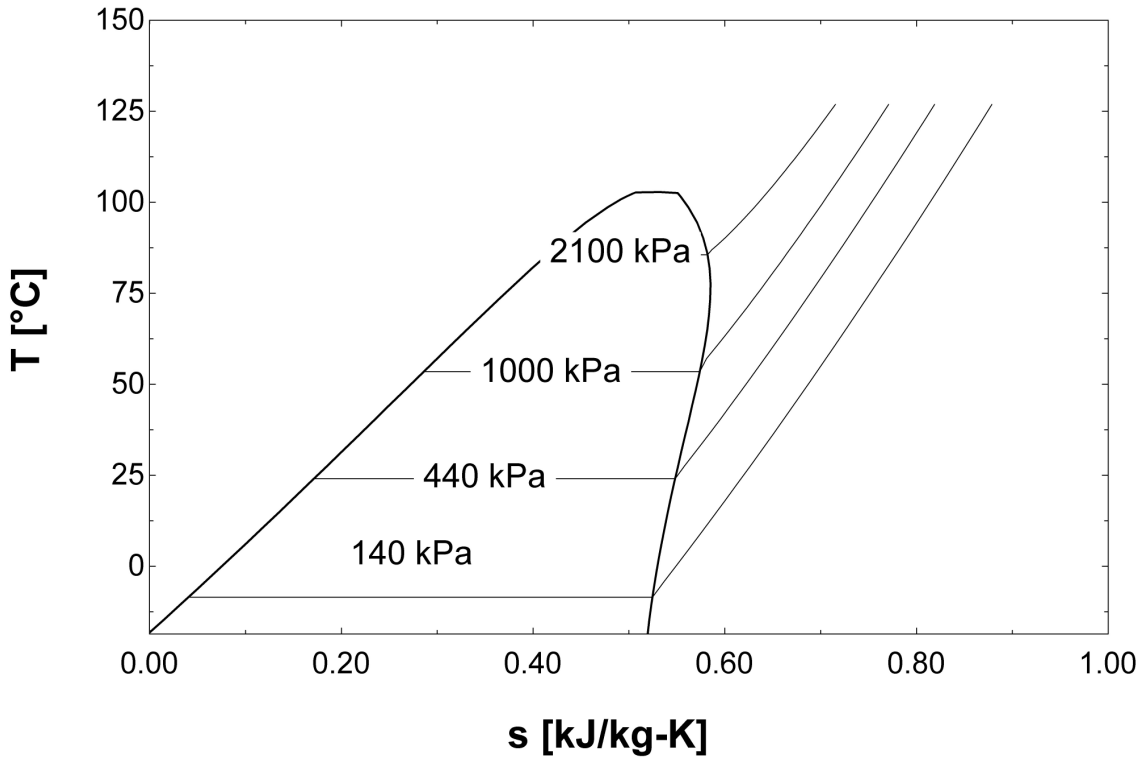

Figure 5.4: Temperature-entropy diagram for R227ea

R227ea is considered to be a dry fluid since the fluid after expansion will not be a mixture regardless of isentropic efficiency of the expander. This reduces the potential for damage to the expander and is preferred since there are many uses for the superheated fluid after expansion.

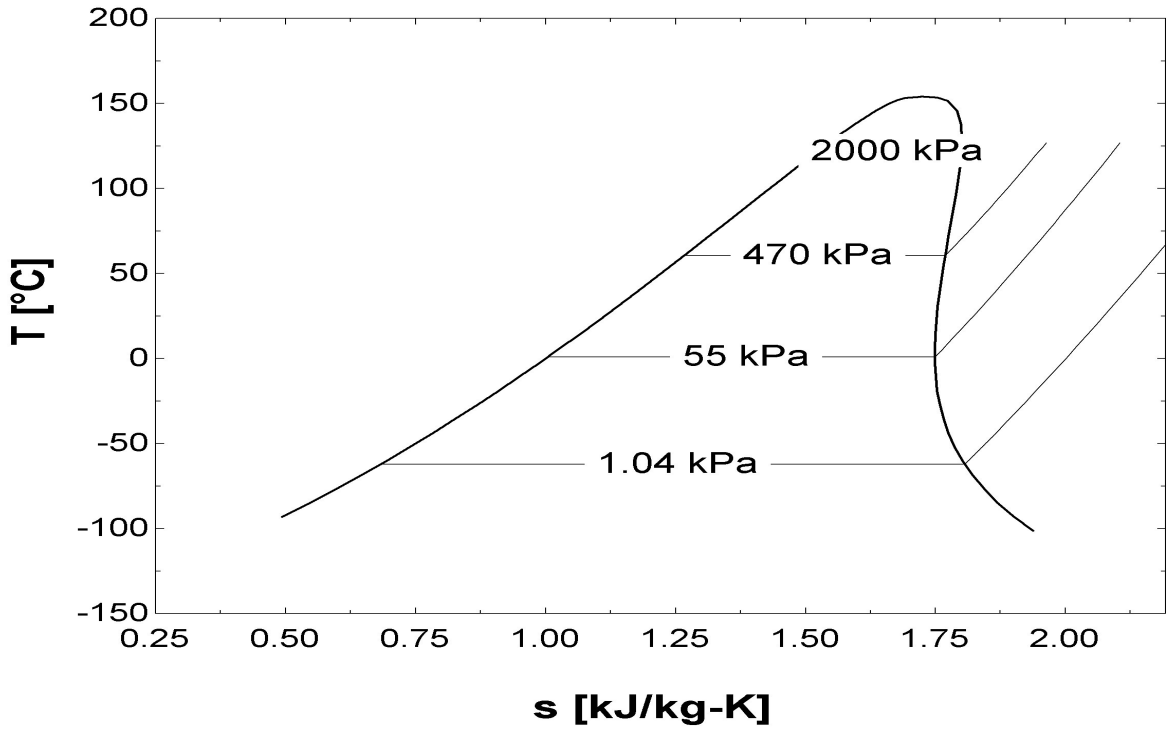

Figure 5.5; Temperature-entropy diagram for R245fa

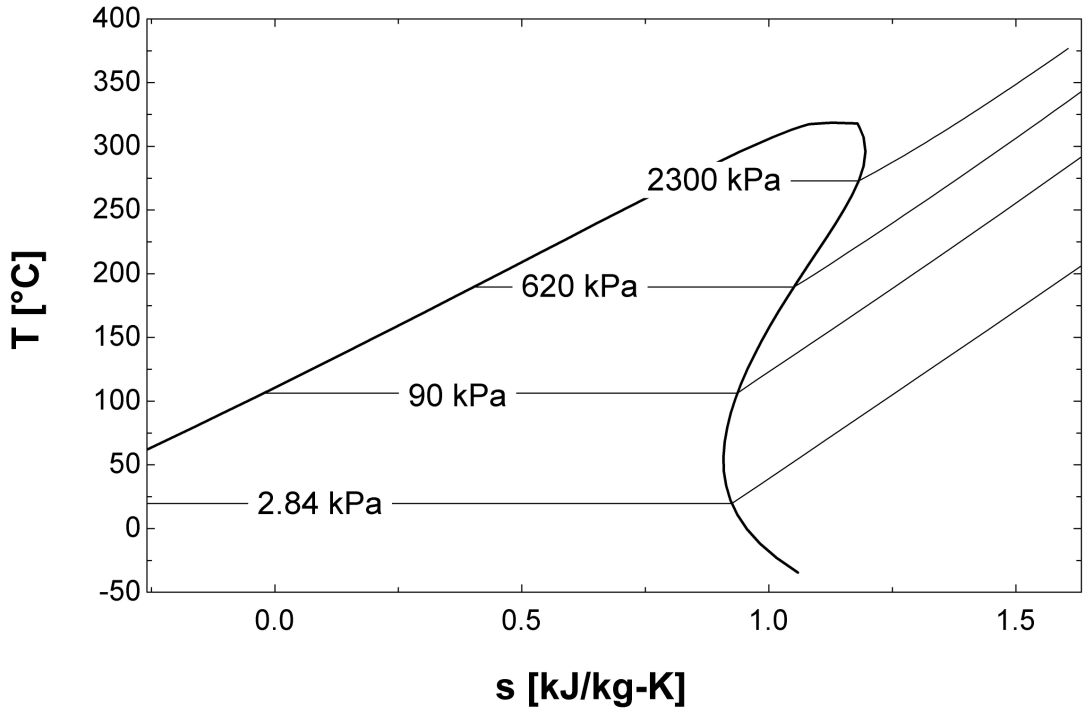

Figure 5.6: Temperature-entropy diagram for toluene

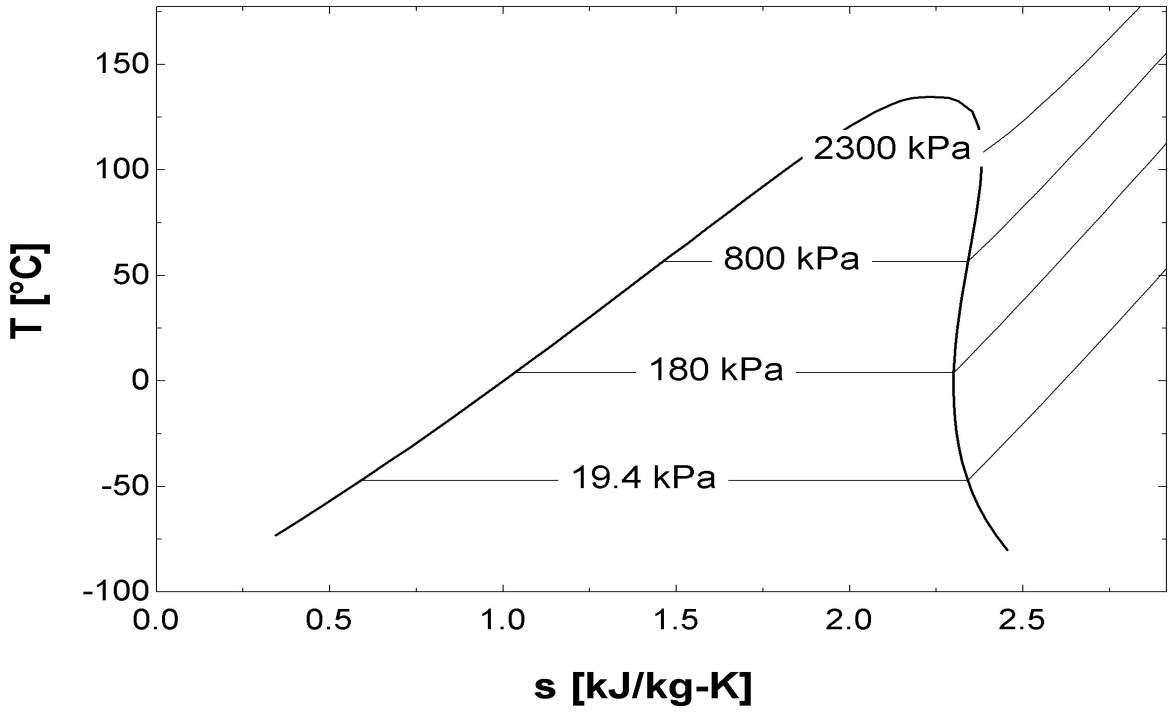

Figure 5.7: Temperature-entropy diagram for iso-butane

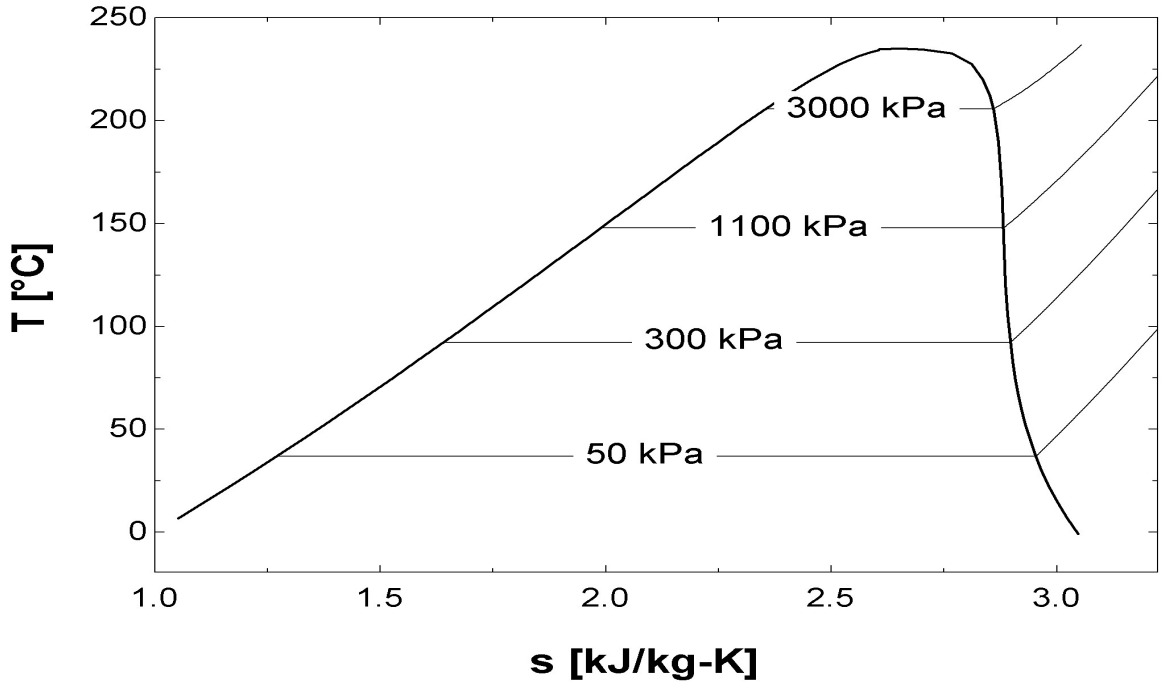

Figure 5.8: Temperature-entropy diagram for acetone

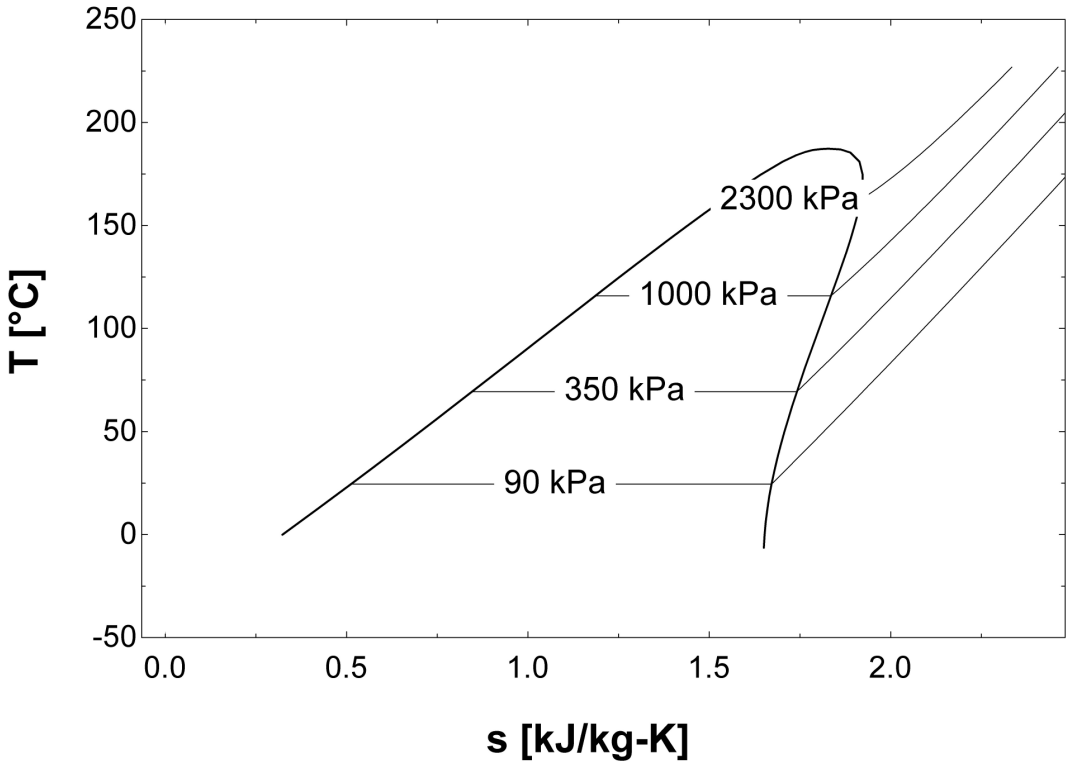

Figure 5.9: Temperature-entropy diagram for iso-pentane

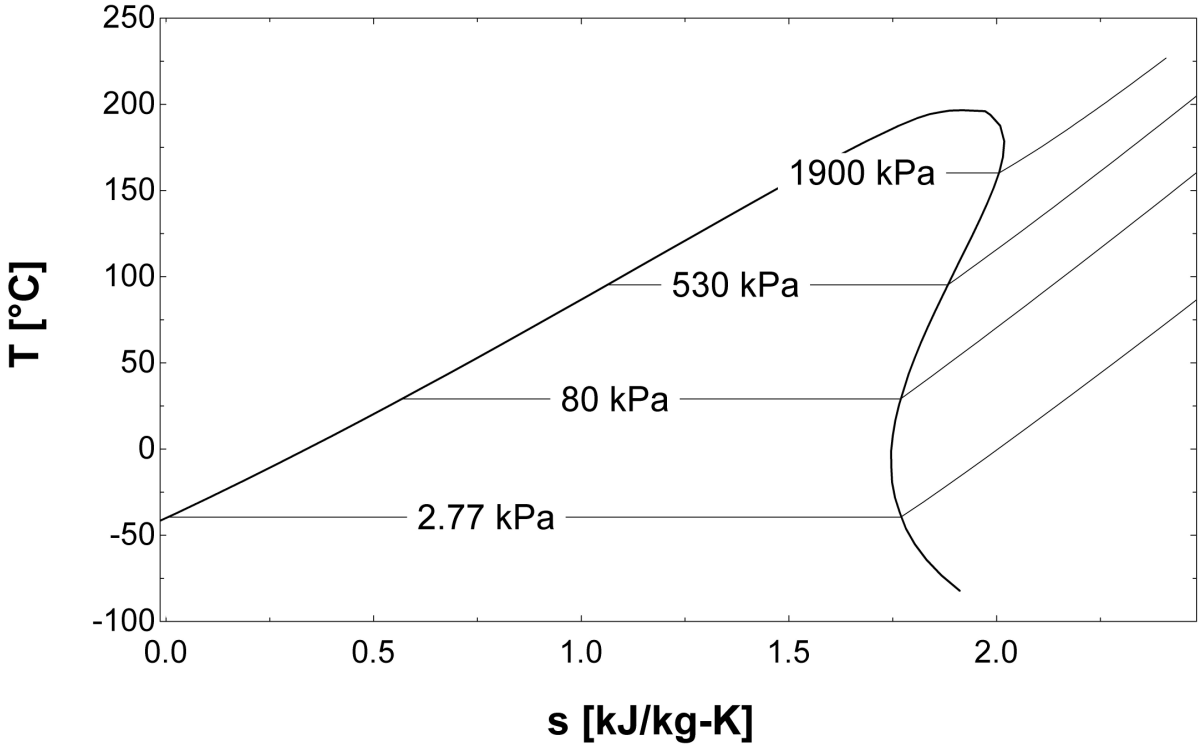

Figure 5.10: Temperature-entropy diagram for n-pentane

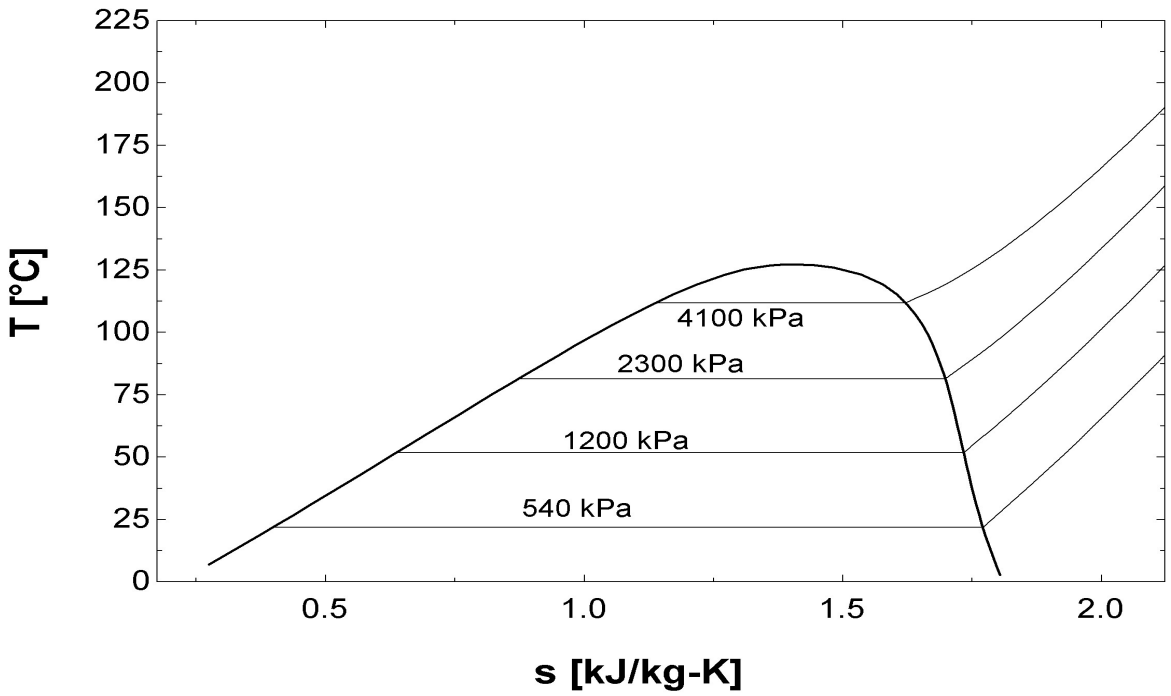

Figure 5.11: Temperature-entropy diagram for dimethyl ether

R227ea, R245fa, iso-pentane, n-pentane, iso-butane, and toluene show isentropic and dry behaviour. Other fluids such as R134a and dimethyl ether have the potential to enter a mixture zone, but are very unlikely to when expanded since expansion is never isentropic. The temperature-entropy charts help identify and understand fluid behavior during expansion to identify appropriate fluids for the organic Rankine cycle.

5.3 Thermodynamic Analysis

5.3.1 Expander Model

Oralli (2010) and Tarique (2011) define a model which can be applied to the scroll expander to define the expansion process, the dissipation losses and the leakage losses. Figure 5.12 is the system diagram of the model proposed by Tarique (2011). The model begins with an isentropic expansion which is limited by the built in volume ratio. The next

step is a constant volume pressure rise which is calculated from a constant specific for the expander. The constant, is used to calculate the enthalpy of the fluid at the exit of this process. It takes into account internal frictional losses and other irreversibility's which cause non-isentropic operation. The last step is either a constant volume pressure rise or a constant enthalpy pressure drop depending on the pressure ratio and the fluid. Finally the fluid mixes with the fluid which has leaked internally to form state 2.

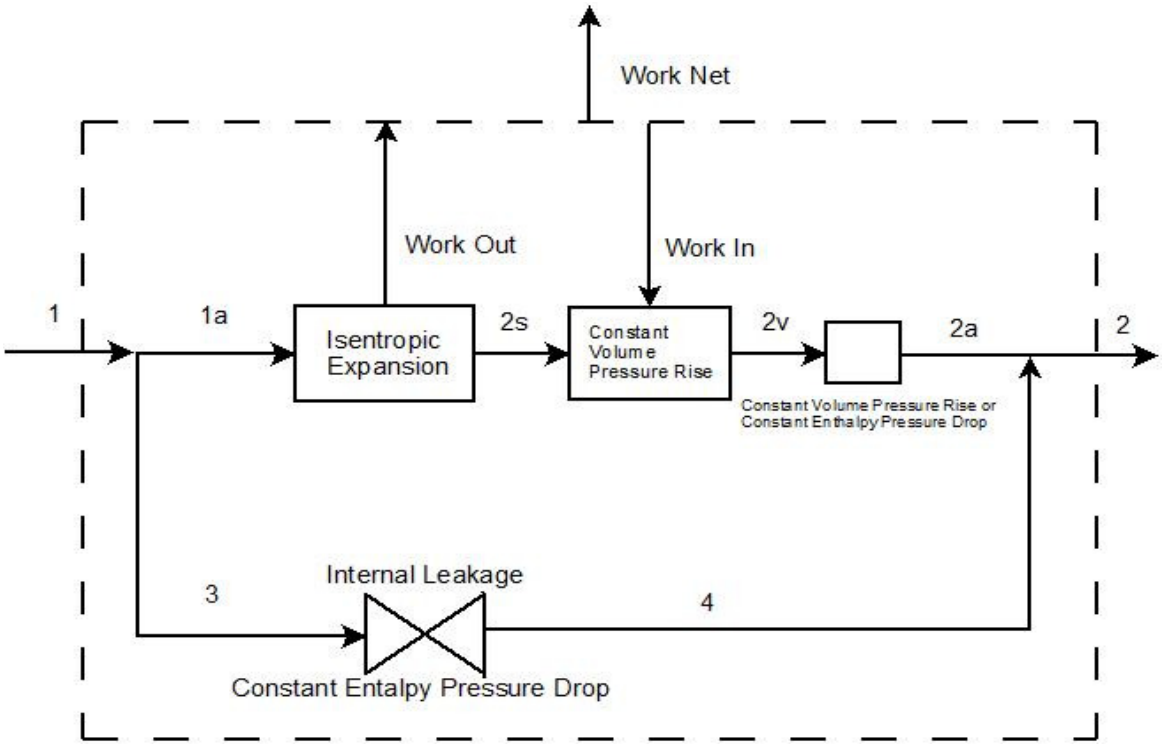

Figure 5.12: Scroll expander thermodynamic model diagram

The internal leakages in a scroll expander are important to take into consideration since manufacturing of the scrolls cannot be done perfectly as to have zero gaps with all mating surfaces. The main leakages in a scroll expander are flank leakages and radial leakages which are shown in Figure 5.13. The leakages between mating scrolls are

considered flank leakages, and the leakage at the end of the scrolls is considered the radial one.

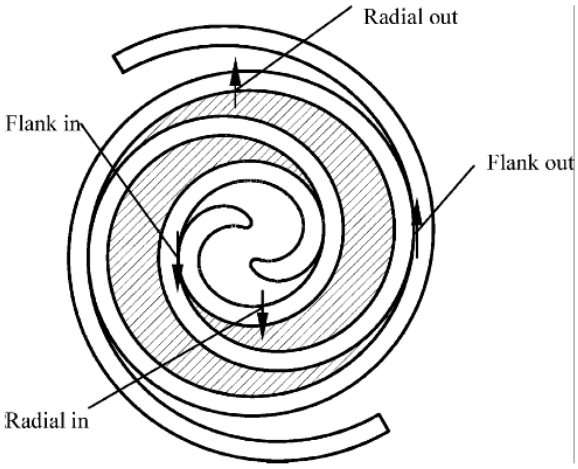

Figure 5.13: Possible leakages in a scroll expander modified from (Wang, et al., 2005)

To simplify all the leakages involved Oralli et al. (2011) proposes a leakage coefficient ζ which estimates the amount of leakage in an expander (Oralli et al., 2011). The equation below is where the coefficient is used to calculate leakage mass flow rate.

$$\dot{m}_{leak} = \zeta \times \sqrt{\frac{P_1}{v_1} - \frac{P_4}{v_4}} \tag{5.6}$$

Once the leak flow rate is calculated a relation is used to calculate the mass flow rate through the expander which is shown below (Oralli et al., 2011).

$$\frac{\dot{m}_{exp}}{\dot{m}_{leak}} = 2 \times \left(\frac{h_1 - h_{2s}}{h_{2a} - h_{2s}}\right) \tag{5.7}$$

The next coefficient which is used to calculate the exit conditions at the constant volume pressure building section is called the “isochoric pressure building coefficient (Π)”. This is

used to calculate state 2v in Figure 5.12. The equation below defines the isochoric pressure building coefficient (Tarique, 2011).

$$\Pi = \frac{h_{2v} - h_{2s}}{h_1 - h_{2s}} \tag{5.8}$$

The next part of the model deals with relating pressure forces to angular velocity and torque. In order to calculate the torque and RPM that is expected from the scroll expander during operation an understanding of how the fluid interacts with the geometry is necessary. In expander operation the fluid enters the center of the scroll machine with zero radial velocity. As the fluid pocket pushes against the scrolls it begins to exert forces which produce a torque and thus the machine begins to rotate. There are two kinds of torques in play during the expander operation. The first is torque due to the differences in pressure of the fluid as it moves through the expander and second is the torque needed to accelerate the fluid in the scroll expander. The equation below is the toque-pressure drop coefficient (Tarique, 2011).

$$\tau_{pf} = K_p \times \Delta P \tag{5.9}$$

A similar coefficient can be defined for torque needed to accelerate a fluid pocket. K_ω is the angular velocity coefficient for fluid pocket acceleration. It is used to calculate torque needed to accelerate a mass of fluid in the scrolls and is represented below (Tarique, 2011).

$$\tau_{acc} = K_\omega \omega^2 m_{pocket} \tag{5.10}$$

where ω is the angular velocity and m_{pocket} is the mass of a fluid pocket in the scroll expander. These two torques are used to calculate the output torque of the expander represented below (Tarique, 2011).

$$\tau_{out} = \tau_{pf} - \tau_{acc} \tag{5.11}$$

Angular velocity is represented by

$$\omega = 2\pi \times RPS \tag{5.12}$$

where RPS is revolutions per second.

The coefficients used in the analysis for the Bitzer ECH209Y-02G are shown in Table 5.2.

Table 5.2: Parameters for the thermodynamic model of the Bitzer expander

Parameters for the Bitzer ECH209Y-02G Scroll Compressor	
BVR	3.5
Π	0.61
ζ	7.23×10^{-7}
K_ω	0.0593
K_p	4.3×10^{-6}

Source: (Tarique, 2011)

5.3.2 Thermodynamic Model

Once a suitable model is applied for the expander, a thermodynamic model for the system is necessary to calculate system performance with the selected expander. Each component in the system has mass, enthalpy, entropy, and exergy balance equations written for steady state operation. Beginning with the boiler, all necessary balance equations are shown below. The system is designed for many types of low temperature

heat sources such as solar or industrial heat. In this system the boiler output temperature (state 1) is assumed to be constant at 110˚C while the source temperature is assumed to be at 120˚C.

Energy balance for the boiler is

$$q_{inb} = h_1 - h_6 \tag{5.13}$$

The exergy balance for the boiler is

$$\dot{E}x_6 + \dot{E}x_{in} = \dot{E}x_1 + \dot{E}x_{db} \tag{5.14}$$

where $\dot{E}x_{in}$ is

$$\dot{E}x_{in} = \left[1 - \left(\frac{T_o+273}{T_s+273}\right)\right] \times \dot{Q}_{inb} \tag{5.15}$$

For the turbine isentropic efficiency is given as

$$\eta_s = \frac{h_1-h_2}{h_1-h_{2s}} \tag{5.16}$$

The work output for the turbine is given as

$$\dot{W}_{out} = \dot{m}_{exp}(h_1 - h_{2a}) \tag{5.17}$$

The work output is also calculated using

$$\dot{W}_{out} = \tau_{out} \times \omega \tag{5.18}$$

The exergy balance for the expander

$$\dot{E}x_1 = \dot{E}x_2 + \dot{W}_{out} + \dot{E}x_{dexp} \tag{5.19}$$

The specific work lost to friction and other losses (e subscript represents expander)

$$w_{loss} = h_{2ae} - h_{2se} \tag{5.20}$$

The regenerator is assumed to have an effectiveness of 0.8. This means that the amount of heat transferred is 80% of the possible energy transfer from states 2 to 3. It is defined as

$$\varepsilon_{regen} = \frac{q_{regen,out}}{q_{regen,in}} \tag{5.21}$$

where

$$q_{regen,out} = h_6 - h_5 \tag{5.22}$$

$$q_{regen,out} = h_2 - h_3 \tag{5.23}$$

State 3 is assumed to be 5˚C higher than the condenser saturation temperature. Using an effectiveness (ε_{regen}) of 0.8 state 6 is calculated from the equation above.

The exergy balance for the regenerator is

$$\dot{E}x_2 + \dot{E}x_5 = \dot{E}x_3 + \dot{E}x_6 + \dot{E}x_{dregen} \tag{5.24}$$

The condenser energy balance is given below

$$q_{out} = h_3 - h_4 \tag{5.25}$$

The exergy balance for the condenser

$$\dot{E}x_3 = \dot{E}x_4 + \dot{E}x_{qout} + \dot{E}x_{qout1} + \dot{E}x_{dcond} \tag{5.26}$$

where $\dot{E}x_{qout}$ is given by

$$\dot{E}x_{qout} = \left[1 - \left(\frac{T_o+273}{T_4+273}\right)\right] \times (\dot{Q}_{out} - \dot{Q}_{outsv}) \tag{5.27}$$

$$\dot{E}x_{qout} = \left[1 - \left(\frac{T_o+273}{T_{condavg}+273}\right)\right] \dot{Q}_{outsv} \tag{5.28}$$

where $T_{cond,avg}$ is given by

$$T_{cond,avg} = \frac{(T_3+T_4)}{2} \tag{5.29}$$

$\dot{Q}_{out,sv}$ and $\dot{Q}_{out}$ are given by

$$\dot{Q}_{out,sv} = \dot{m}(h_3 - h_{3sv}) \tag{5.30}$$

$$\dot{Q}_{out} = \dot{m}q_{out} \tag{5.31}$$

where h_{3sv} is the working fluid state when it is a saturated vapour.

The pump isentropic efficiency (η_{pump}) is taken to be 0.7, and state 5 is calculated using

$$h_5 = \left[(h_{5s} - h_4) \times \left(\frac{1}{\eta_{pump}}\right)\right] + h_4 \tag{5.32}$$

where h_{5s} is the ideal enthalpy if the pump is isentropic.

The exergy balance for the pump is written as

$$\dot{E}x_4 + \dot{W}_{in} = \dot{E}x_5 + \dot{E}x_{dpump} \tag{5.33}$$

where $\dot{W}_{in}$ is given by

$$\dot{W}_{in} = \dot{m}(h_5 - h_4) \tag{5.34}$$

The system efficiencies include energy and exergy efficiencies, with exergy efficiency being the objective function for optimization. Consideration is made for the energy efficiency of the generator which is set at 0.8. Energy (η_{th}) and exergy (η_{ex}) efficiency for the system are given as

$$\eta_{th} = \frac{\dot{W}_{elec}}{\dot{Q}_{in}} \tag{5.35}$$

$$\eta_{Ex} = \frac{\dot{W}_{elec}}{\dot{E}x_{in}} \tag{5.36}$$

where

$$\dot{W}_{net} = \frac{\dot{W}_{out}}{1000} - \dot{W}_{pump} \tag{5.37}$$

$$\dot{W}_{elec} = \dot{W}_{net} \times 0.8 \tag{5.38}$$

5.4 Exergoeconomic Analysis

The exergoeconomic analysis requires that a specific cost is put on the exergy streams in an exergy balance on a component. On top of putting costs on the exergy streams, capital and running costs are taken into account in order to get a complete cost analysis. Exergy cost for the streams in any cost rate balance is given as

$$\dot{C} = c \times \dot{E}x \tag{5.39}$$

where c is in \$/kWh and $\dot{E}x$ is given in kW. The capital and running costs for the components is given as $\dot{Z}$ with units as \$/h (dollars per hour).

Typical cost rate balance for a component is given below:

$$\sum \dot{C}_{in} + \dot{W} \times c_{e\,in} + \dot{Z} = \sum \dot{C}_{out} + \dot{W} \times c_{e\,out} \tag{5.40}$$

For this system a costing analysis is done to estimate the initial capital costs (ICC) and the operating and maintenance costs (OM). An amortization factor is used to amortize the cost of the sum of ICC and OM over 20 years at 5% interest rate. This is given in the equation below (Nafey et al., 2010).

$$A_f = \frac{i(i+1)^n}{(1+i)^{n-1}} \tag{5.41}$$

Total costs for each of the components in the system are needed in $/h in order to use them in cost rate balance equations. The initial capital cost and the operating and maintenance costs are added and amortized. The total costs are then divided by the number of hours in a year to get a cost in $/h. Operating and maintenance costs are assumed to be a percentage of the initial capital costs. The general equations are given in below

$$TCC_x = A_f(ICC_x + OM_x) \tag{5.42}$$

where OM_x is given below:

$$OM_x = ICC_x \times OM\% \tag{5.43}$$

Here OM% is the percentage of operating and maintenance costs associated with initial capital cost.

$$\dot{Z}_x = \frac{TCC_x}{t_x} \tag{5.44}$$

Table 5.3 outlines the costs for each of the components and the equations used to get the final capital and operating rate ($\dot{Z}_x$).

Table 5.3: Costing values and equations for the various parts in the system

Component	ICC ($)	OM% (% of ICC)	OM ($)	TCC ($/y)	$\dot{Z}_x$ ($/h)
Boiler	1200	15	$OM_b = OM\%_b \cdot ICC_b$	72.45	0.008271
Expander	1000	25	$OM_{exp} = ICC_{exp} \cdot OM\%$	65.63	0.01801
Regenerator	1500	15	$OM_{regen} = OM\%_{regen} \cdot ICC_{regen}$	90.56	0.01034
Condenser	1200	15	$OM_{cond} = OM\%_{cond} \cdot ICC_{cond}$	72.45	0.008271
Pump	300	25	$OM_p = OM\%_p \cdot ICC_p$	19.69	0.002247

The percentages for operating and maintenance costs are taken from Nafey et al., (2010). The costs for the components are sourced from various vendors. The current experimental system is built using a combination of donated parts, used parts and new parts. It is difficult to truly find actual costs for these parts as the expander is a compressor which is converted for this use. A good estimate on the cost of the compressor and the cost to convert it is estimated in the table above. This cost takes into the account of the size of the current expander. Capital and operating costs for a solar field are not taken into account as this was not the scope for the project. The analysis is designed so that this system can potentially be used with any "low temperature" heat source. This assumption is made for the initial optimization. Subsequent optimizations for electricity cost rate will introduce an exergy price on the heat input to the boiler.

The cost rate balances for each of the components are done to complete the exergoeconomic analysis. The cost of the pump and condenser are added to the total capital and operating rate for the expander since the exergy stream in these components have negligible value. The cost rate for the exergy leaving the expander is assumed to have 50%

value to the exergy entering the expander as this is lower temperature heat which is of less use. Exergy cost rates for the inlet and outlet of the condenser and pump are zero since these streams have little useable energy which is valuable. The cost rate balances for each of the involved components (boiler, expander and regenerator) are shown below.

State 1 exergy cost rate balance and boiler exergy cost rate balance are

$$\dot{E}x_1 = \dot{m} \times ex_1 \tag{5.45}$$

$$\dot{E}x_6 \times c_6 + \dot{Z}_b = \dot{E}x_1 \times c_1 \tag{5.46}$$

Expander exergy cost rate balance, state 2 exergy cost rate, and electricity cost rate equations are

$$c_2 = c_1 \times 0.5 \tag{5.47}$$

$$\dot{E}x_2 = \dot{m} \times ex_2 \tag{5.48}$$

$$\dot{E}x_1 \times c_1 + \dot{Z}_{exp} = \dot{W}_{elec} \times c_e + c_2 \times \dot{E}x_2 \tag{5.49}$$

$$\dot{C}_e = c_e \times \dot{W}_{elec} \tag{5.50}$$

Regenerator exergy cost rate balance and state 6 exergy cost rate are

$$\dot{E}x_6 = ex_6 \times \dot{m} \tag{5.51}$$

$$c_2 \times \dot{E}x_2 + \dot{Z}_{regen} = \dot{E}x_6 \times c_6 \tag{5.52}$$

5.5 System Optimization

Once all applicable equations and relations are set up in EES for the expander, thermodynamic, exergoeconomic modeling and optimization could begin. The objective function for the thermodynamic analysis is system exergy efficiency given in the equation below

$$\eta_{Ex} = \frac{\dot{W}_{elec}}{\dot{E}x_{in}} \tag{5.53}$$

where $\dot{E}x_{in}$ is given as

$$\dot{E}x_{in} = \left[1 - \left(\frac{T_o+273}{T_s+273}\right)\right] \times \dot{Q}_{inb} \tag{5.54}$$

Since source temperature is a function of the inlet temperature which is constant, the only factor which changes exergy input to the boiler is heat input. Heat input depends on how much energy is recovered through the regenerator which also depends on how much energy is extracted in the expander. The more energy extracted in the expander (thus being closer to the condenser temperature) the less energy available to transfer in the regenerator.

The objective function for the exergoeconomic analysis is electricity cost rate. In this case, the cost rate of electricity is minimized. The equation for cost rate of electricity is given below and is modified from the cost rate balance given in Eq. 5.49.

$$c_e = \frac{\dot{E}x_1 \times c_1 + \dot{Z}_{exp} - c_2 \times \dot{E}x_2}{\dot{W}_{elec}} \tag{5.55}$$

Two independent variables are chosen to be used in the optimization, these are amount of superheat (T_{sh}) and pressure ratio (PR). The amount of superheat is the temperature in degrees Celsius above the saturation temperature and the pressure ratio is expander is inlet pressure over outlet pressure. Since total inlet temperature is constant, when the amount of superheat changes the saturation temperature and pressure change appropriately. These particular variables are chosen because they have the largest effect on expander performance and efficiency as shown in (Tarique, 2011).

Bounds for certain variables are important in any optimization dealing with engineering problems since "optimal" values may be found in areas which are not possible. Bounds are needed for the two independent variables due to the fact that there are limits for the pressure ratio and the amount of superheat possible before physical and practical limits are reached. Table 5.4 shows various variables and their bounds that are of importance in the optimization.

Table 5.4: Upper and lower bounds for the important variables involved in the optimization

Variable		Lower Bound	Upper Bound
Independent Variables	PR	1.5	10
	T_{sh}	5	45
Critical Variables which Require Physical Limits	T_4	25	100
	RPM	0	4000

Here, T_4 is the condenser outlet temperature and is set so that it is not possible to go below 25°C since this is the environment temperature which it operates in. RPM is set so that it cannot go below 0 or over 4000 which is a practical limit for this particular

expander. Depending on the pressure ratio, if there is significant over expansion, additional work is necessary to increase fluid pressure. In some cases this would cause the expander to consume power and not produce power which would produce negative results for RPM. Therefore it is necessary to constrain this variable. The next section deals with the results from the optimization, thermodynamic and exergoeconomic analysis.

Chapter 6: Results and Discussion

6.1 Identifying Proper Optimization Conditions

The first results show what values of superheat and pressure ratio produce the highest system exergy efficiency. When running an optimization it is important to input guess values for the independent variables which are within close range to optimal values. For this case this entailed running a parametric study to see where the highest isentropic efficiency is achieved for a set superheat. Figure 6.1 is a parametric study using R227ea as the working fluid to see the effect of pressure ratio versus expander isentropic efficiency.

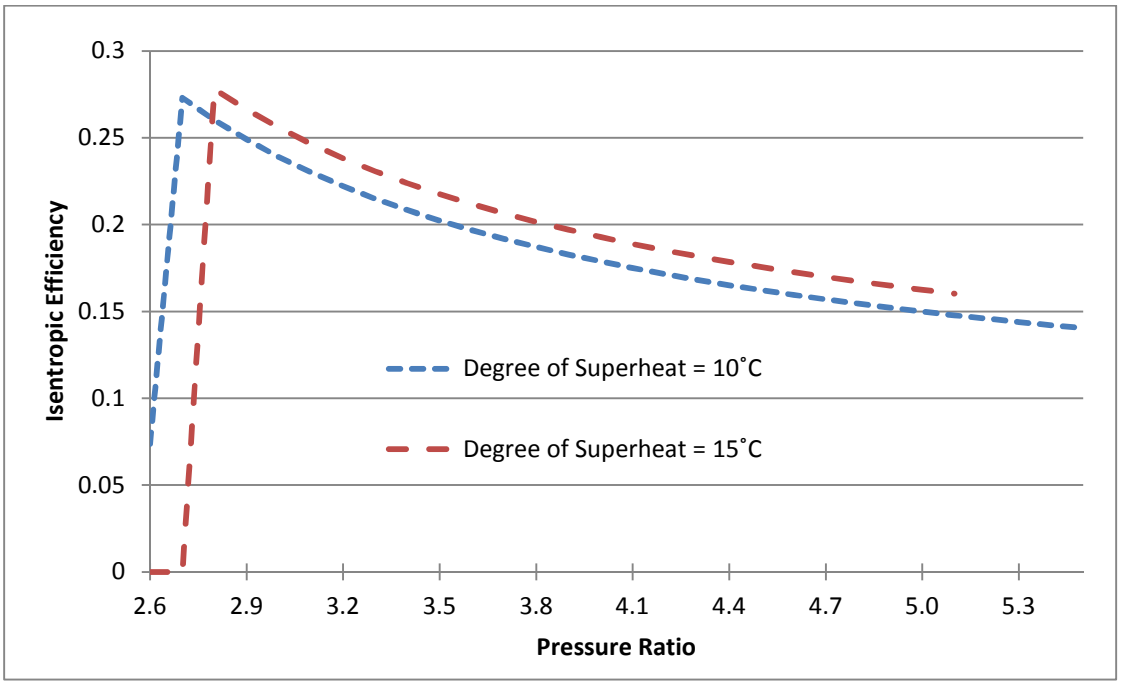

Figure 6.1: Isentropic efficiency vs. pressure ratio for R227ea

The peak isentropic efficiency occurs when expansion is performed optimally. This requires that the pressure of the fluid after the constant volume pressure building section is the same as the condenser or outlet pressure ($P_{2v} = P_{2a}$). If the pressure is too high and

throttling is needed, then it is considered to be under expanded. In the Figure this is the section from pressure ratio 2.7 to 5.8. If the outlet pressure is lower than the condenser pressure then additional work is needed to bring the fluid up to the appropriate pressure. This is over expansion and is represented from pressure ratio 2.5 to 2.7. The runs in Figure 6.1 have inlet temperature set at 110˚C and degree of superheat set at 10˚C and 15˚C over saturation temperature. For isentropic or dry fluids, as superheat is increased, exergy and isentropic efficiency increase. Wet fluids such as water behave differently, where lower superheat increases exergy efficiency but lowers isentropic efficiency. Regardless of how much superheat is used, optimal values are observed when expansion is optimal or slightly under expanded ($P_{2v} > P_{2a}$). Generally if an optimization is performed and these pressure values are equal or near each other then the results can be considered to be optimized.

6.2 Parametric Study of the System

A parametric study of the system is important to analyze how the system will perform while varying certain parameters. Each fluid is tested while varying the expander inlet temperature between 90˚C (or 95˚C depending on the fluid) and 110˚C. The degree of superheat is held constant at 15˚C. Three pressure ratios are used for comparison. The pressure ratios depend on the fluid characteristics and the physical constraints such as minimum condenser temperature. Power output, system exergy efficiency and isentropic efficiency are graphed for R134a, Water, R227ea, R245fa, iso-butane, iso-pentane and dimethyl ether (Figures 6.2-6.22).

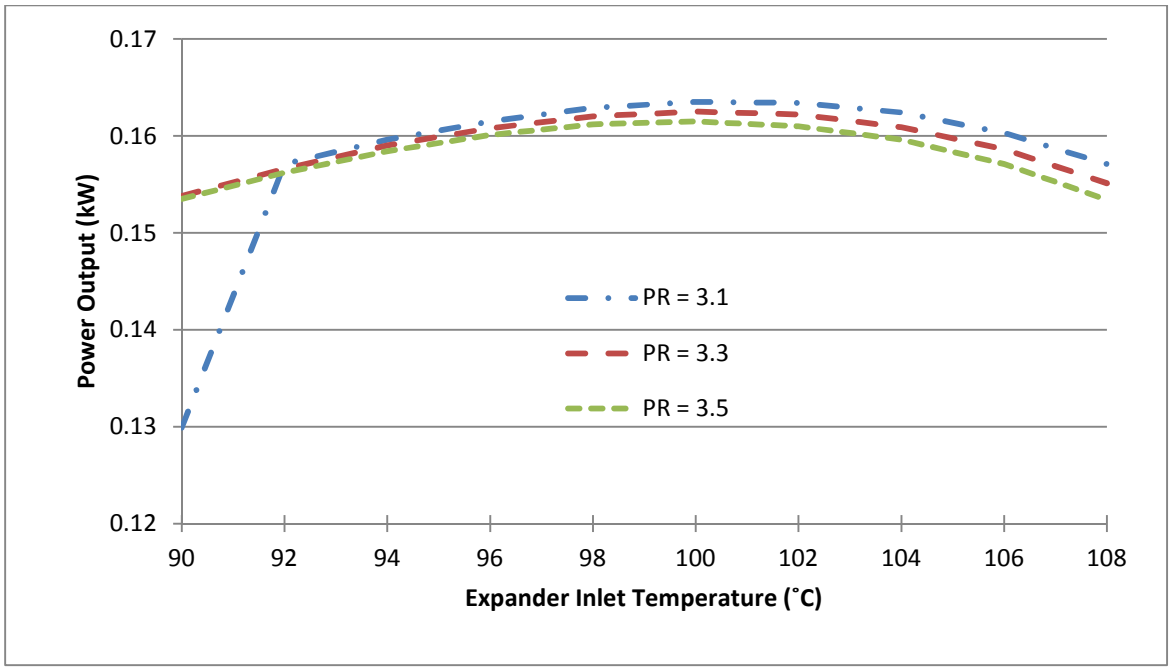

Figure 6.2: Electrical power output for R134a

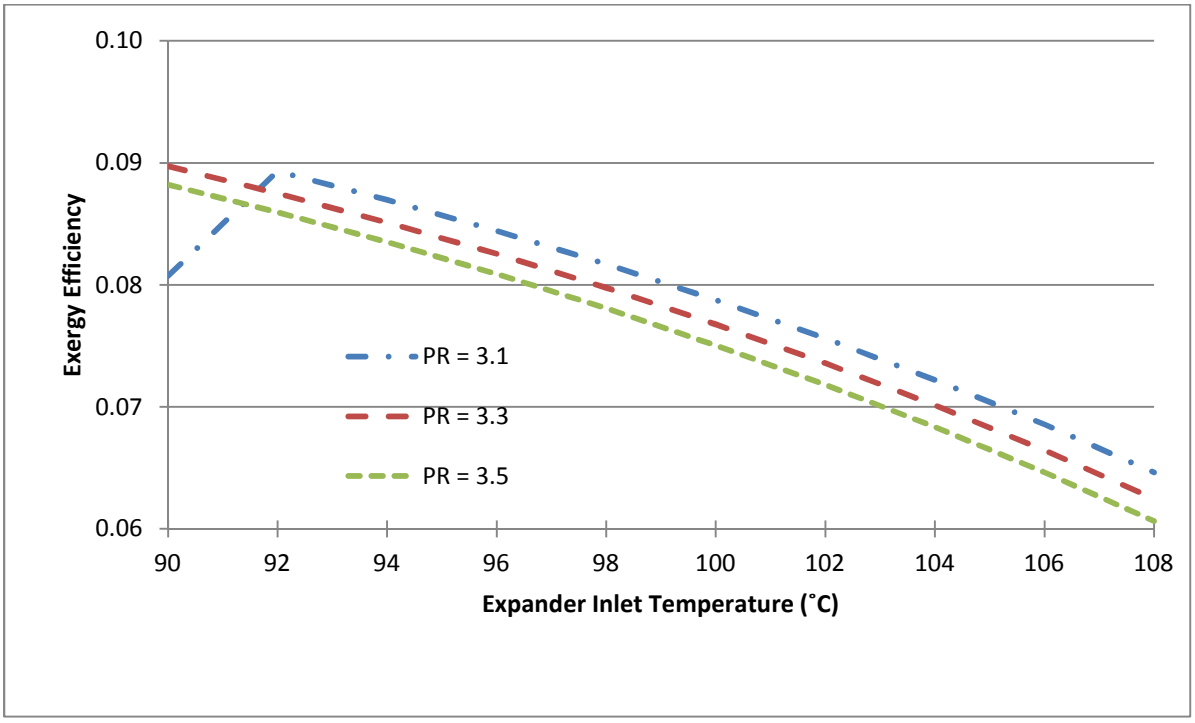

Figure 6.3: System exergy efficiency for R134a

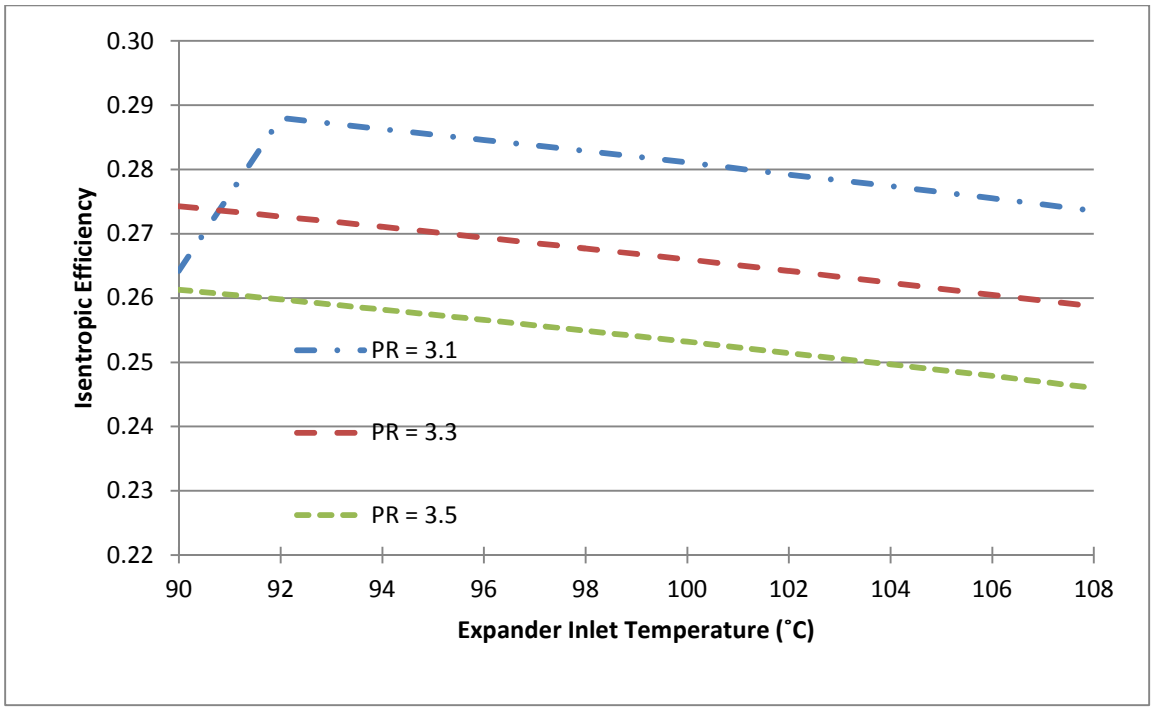

Figure 6.4: Expander isentropic efficiency for R134a

Figures 6.2 to 6.4 show how power output, exergy efficiency, and isentropic efficiency vary with various pressure ratios and inlet temperatures. A pressure ratio of 3.1 shows over expansion behavior at temperatures below 92˚C, as seen by the increasing sloped line. Since degree of superheat is constant, as the inlet temperature drops the pressure drops. Since the expander has a constant built in volume ratio, when the fluid is at lower pressures it will go below the condenser pressure during expansion in the expander. As the temperature increases the pressure increases to keep a constant degree of superheat. As the pressure difference between inlet and condenser increases, the pressure at the outlet of the expander is at or higher than the condenser pressure. This means that no additional work is needed to increase the pressure of the fluid at the end of expansion. This behavior is seen for pressure ratios of 3.3 and 3.5.

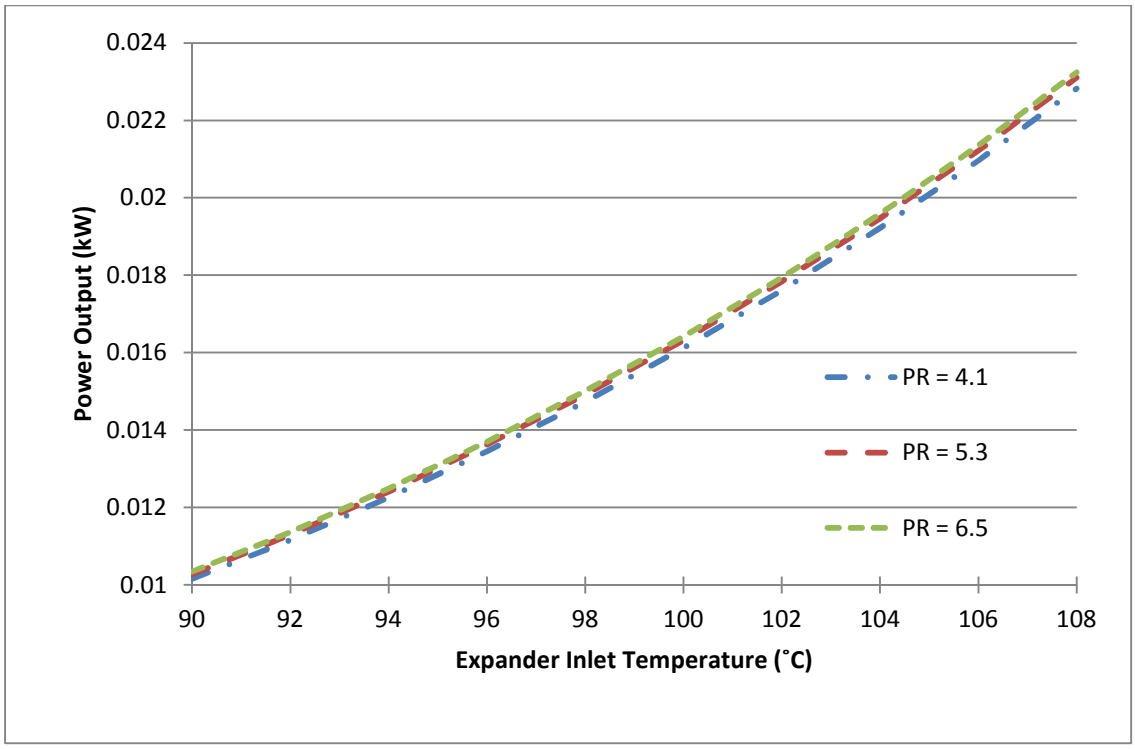

Figure 6.5: Electrical power output for water

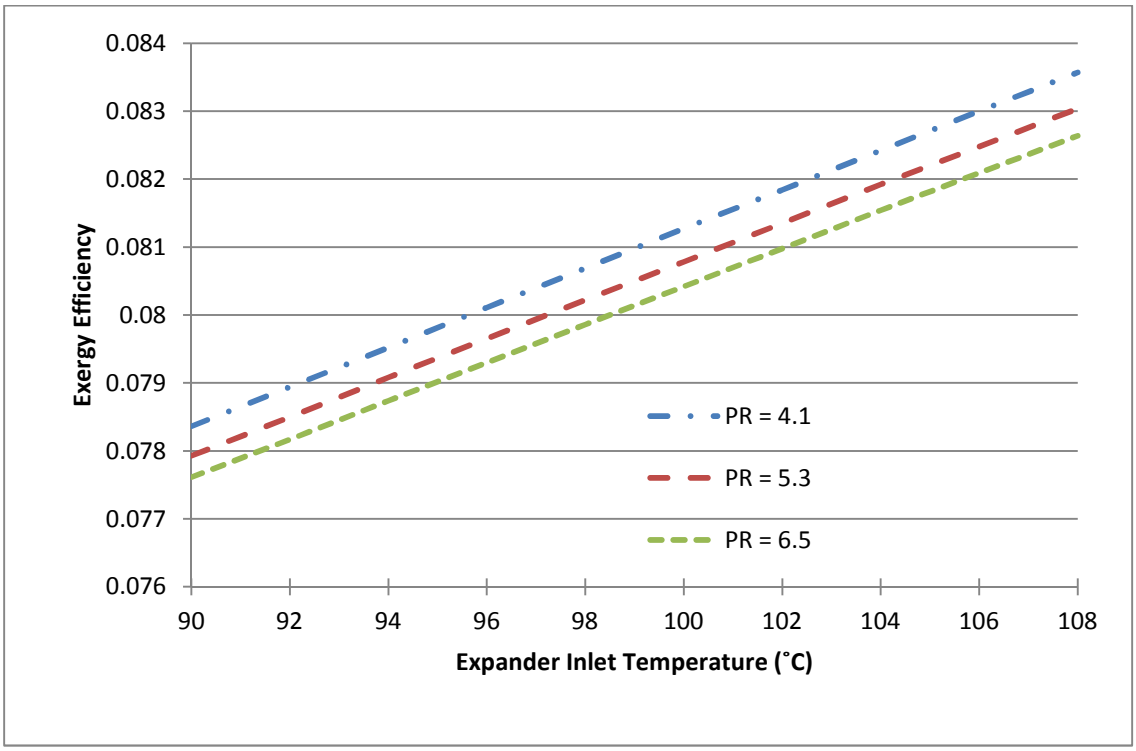

Figure 6.6: System exergy efficiency for water

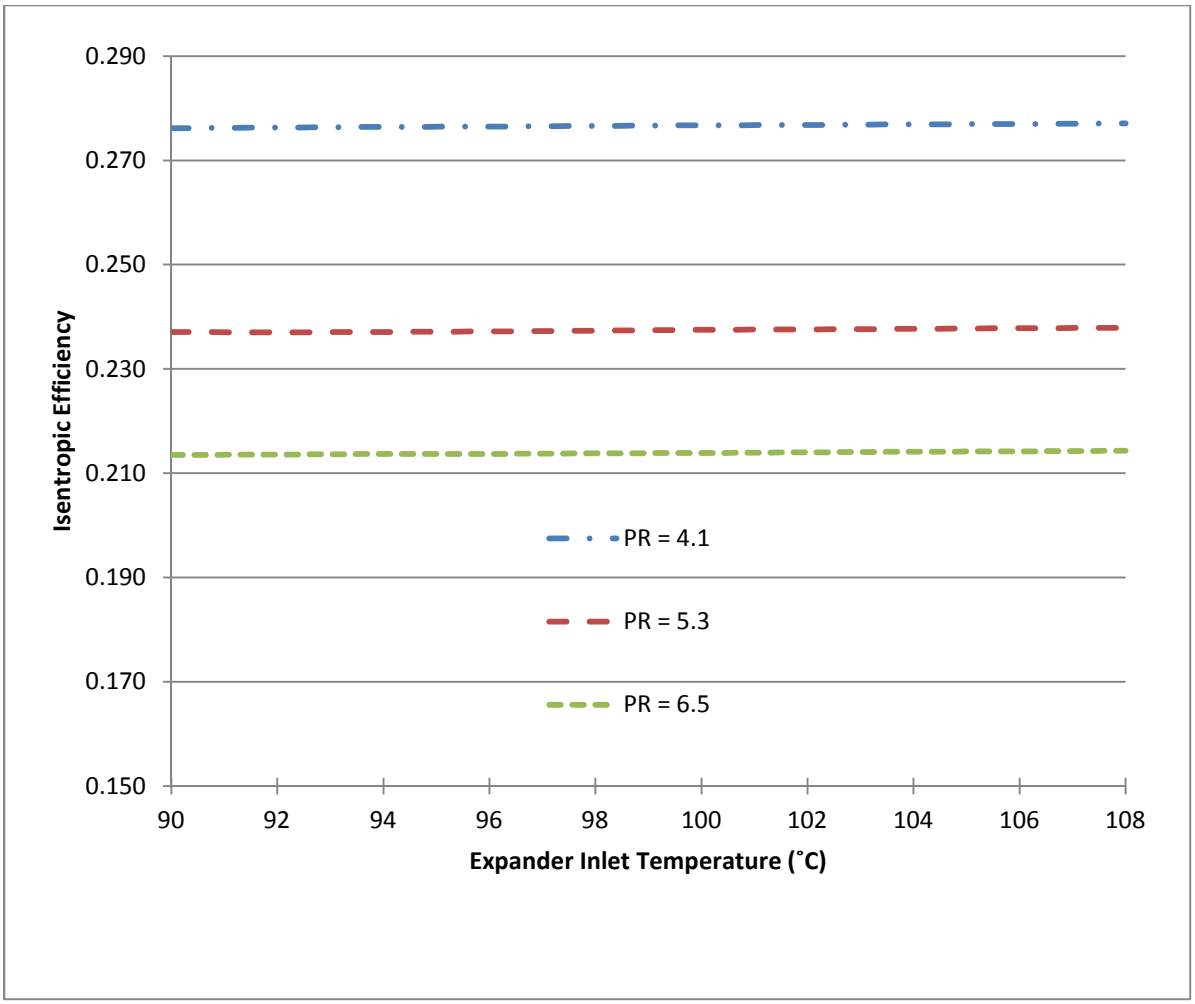

Figure 6.7: Expander isentropic efficiency for water

Figures 6.5 to 6.7 show increases in power output which results in increases in system exergy efficiency as the inlet temperature increases. Isentropic efficiency increases very slightly as temperature increases for all pressure ratios. Here pressure ratios are increased to 4.1, 5.3, and 6.5 due to the fact that water has more flexibility to stay within the constraints for minimum condenser temperature. At all conditions there is no over expansion, instead the expander is running in a under expansion condition where the pressure at the outlet has to be throttled to the condenser pressure.

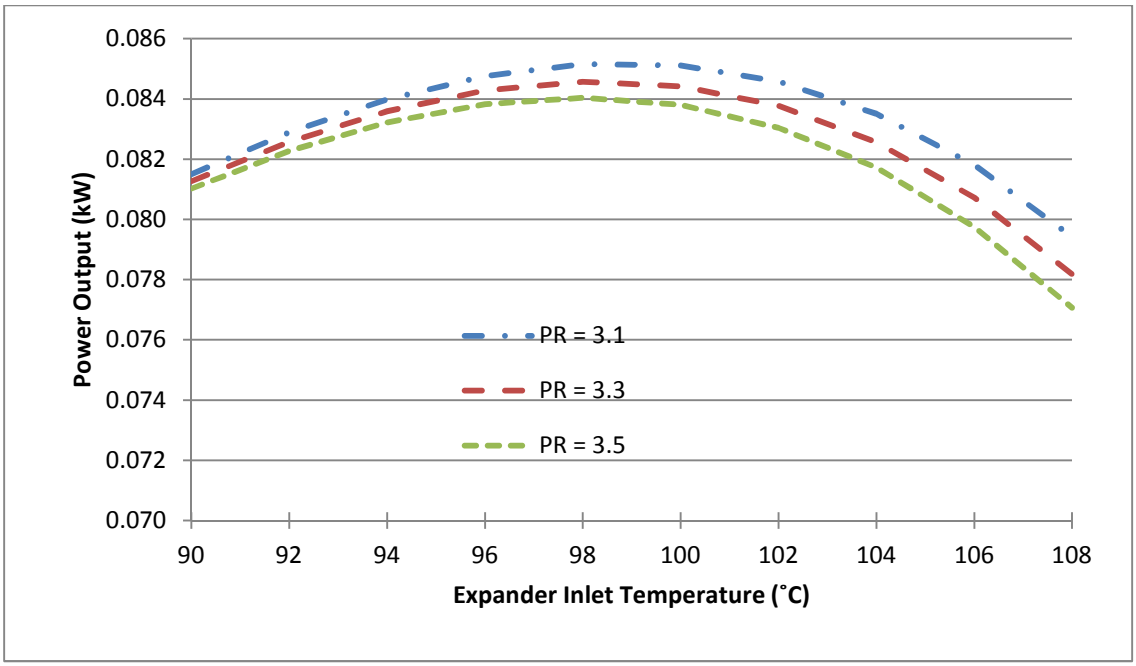

Figure 6.8: Electrical power output for R227ea

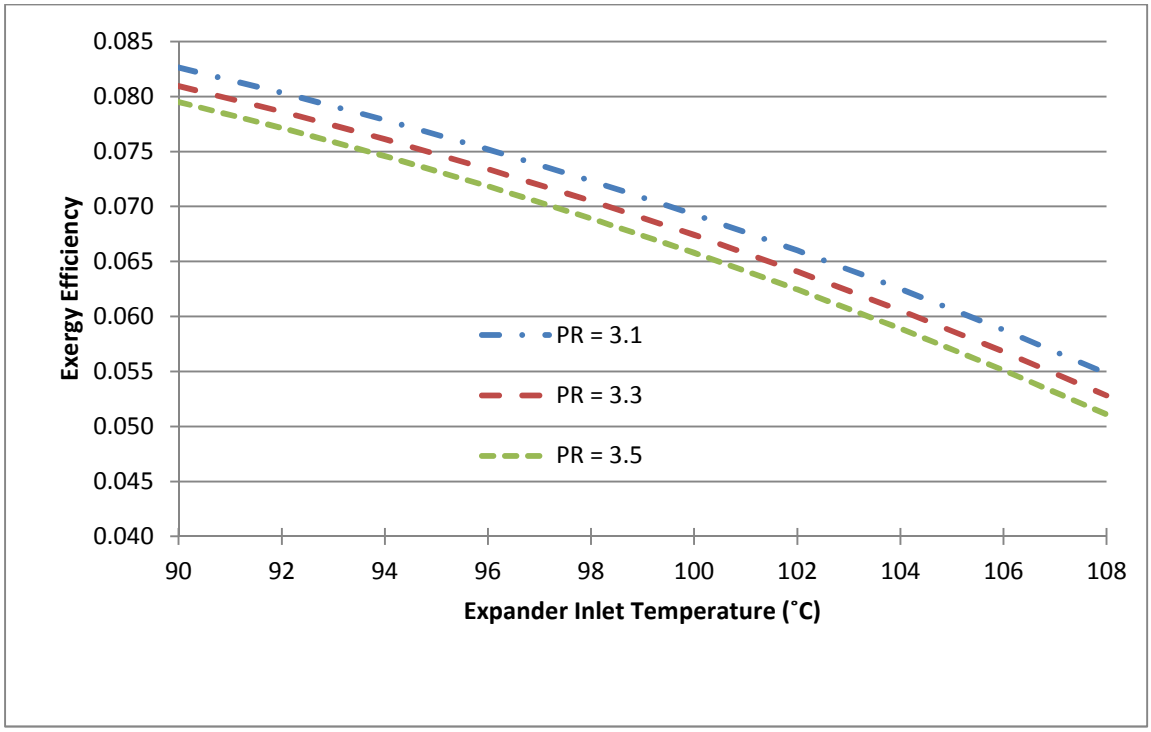

Figure 6.9: System exergy efficiency for R227ea

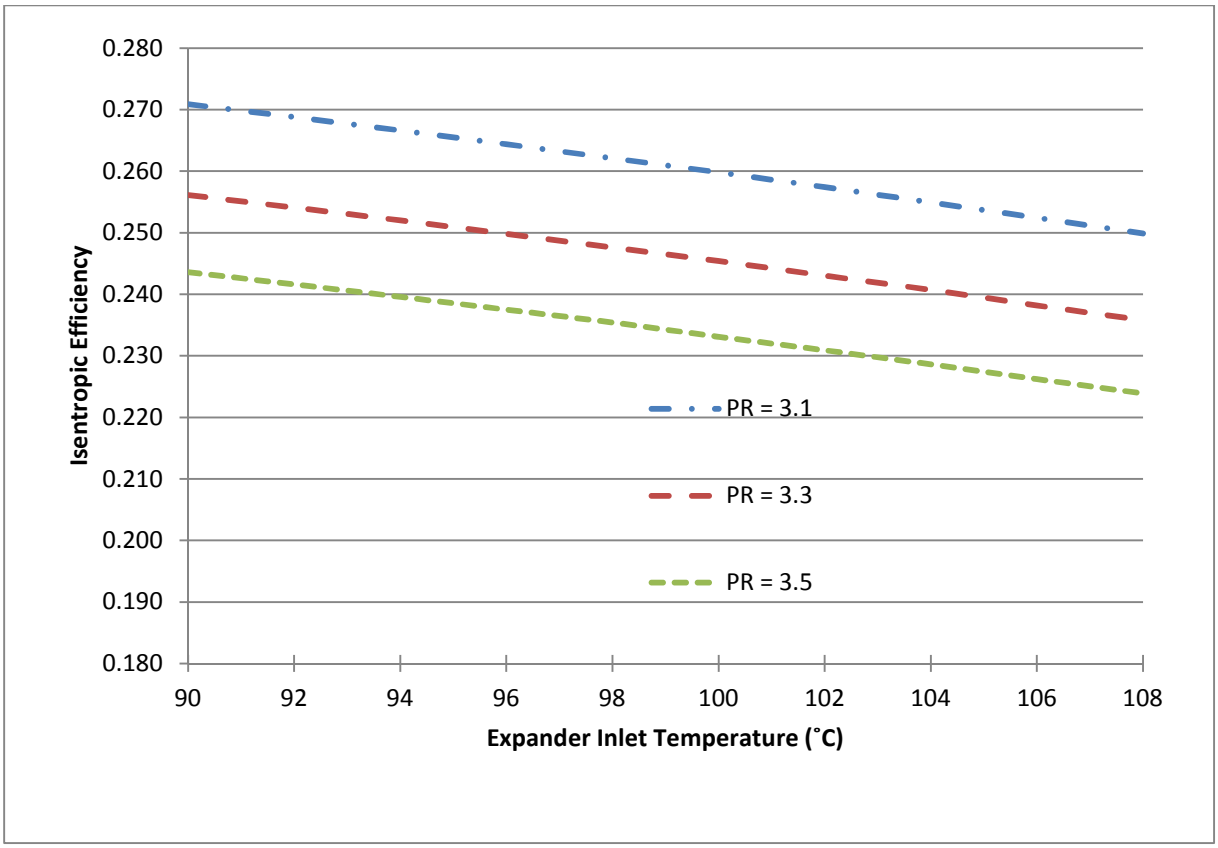

Figure 6.10: Expander isentropic efficiency for R227ea

Figures 6.8 to 6.10 show the results of the parametric study for R227ea. As inlet temperature is increased the power output reaches a peak around 98˚C. Exergy efficiency and isentropic efficiency all show decreasing trends as the temperature increases. For all pressure ratios the fluid is under expanded and therefore needs to be throttled to condenser pressure at the outlet. With increasing fluid temperature, the expansion moves farther away from the optimal expansion point resulting in decreasing exergy and isentropic efficiency. The power output increases due to the increase in temperature and pressure, although decreases once the losses from over expansion are greater than the gains from increased temperature.

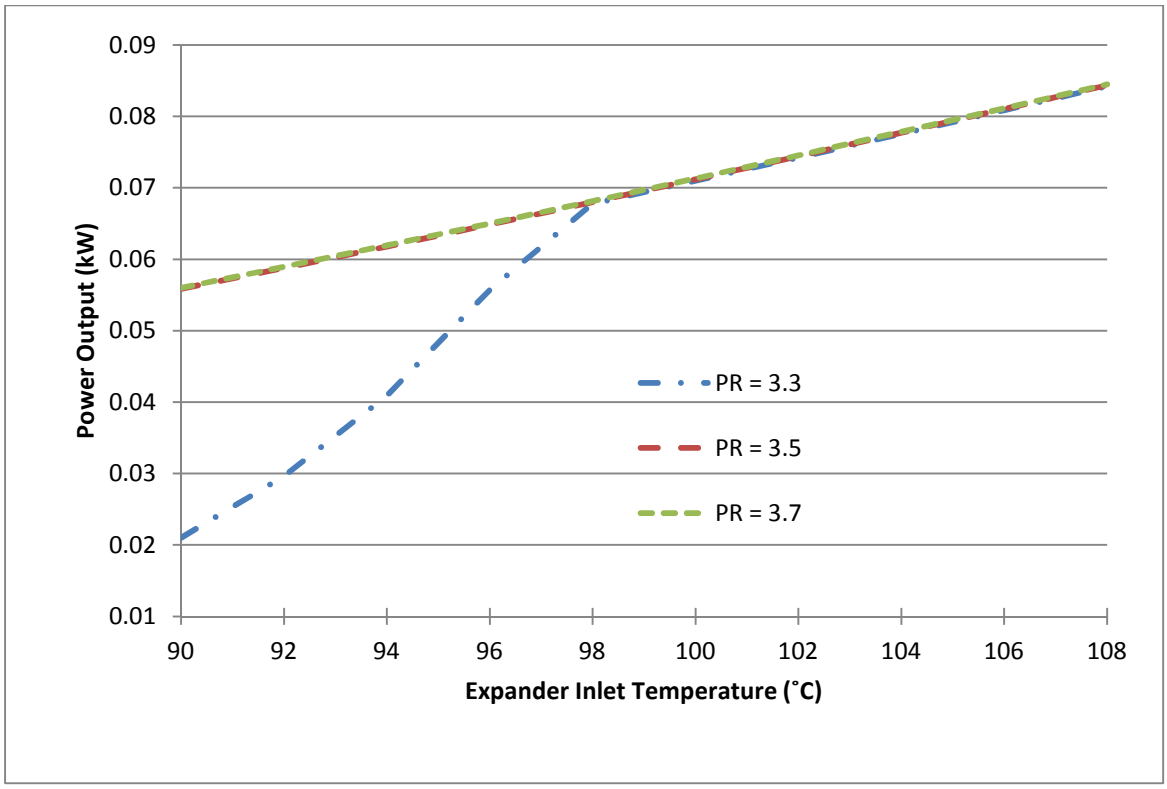

Figure 6.11: Electrical power output for R245fa

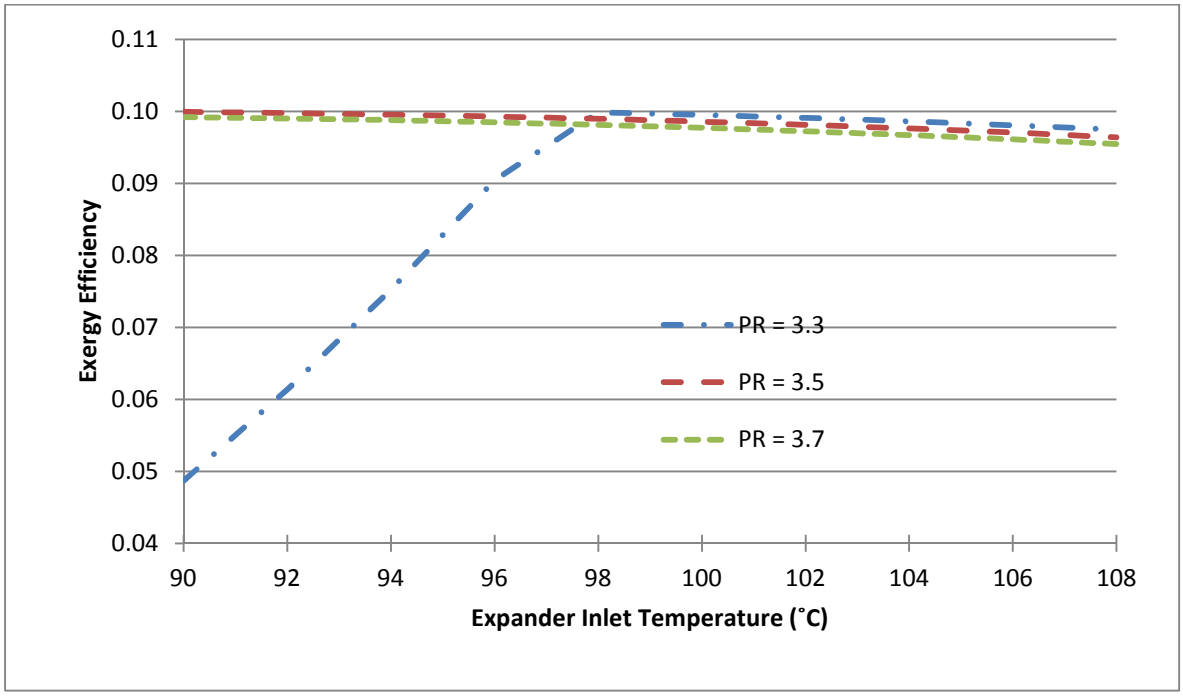

Figure 6.12: System exergy efficiency for R245fa

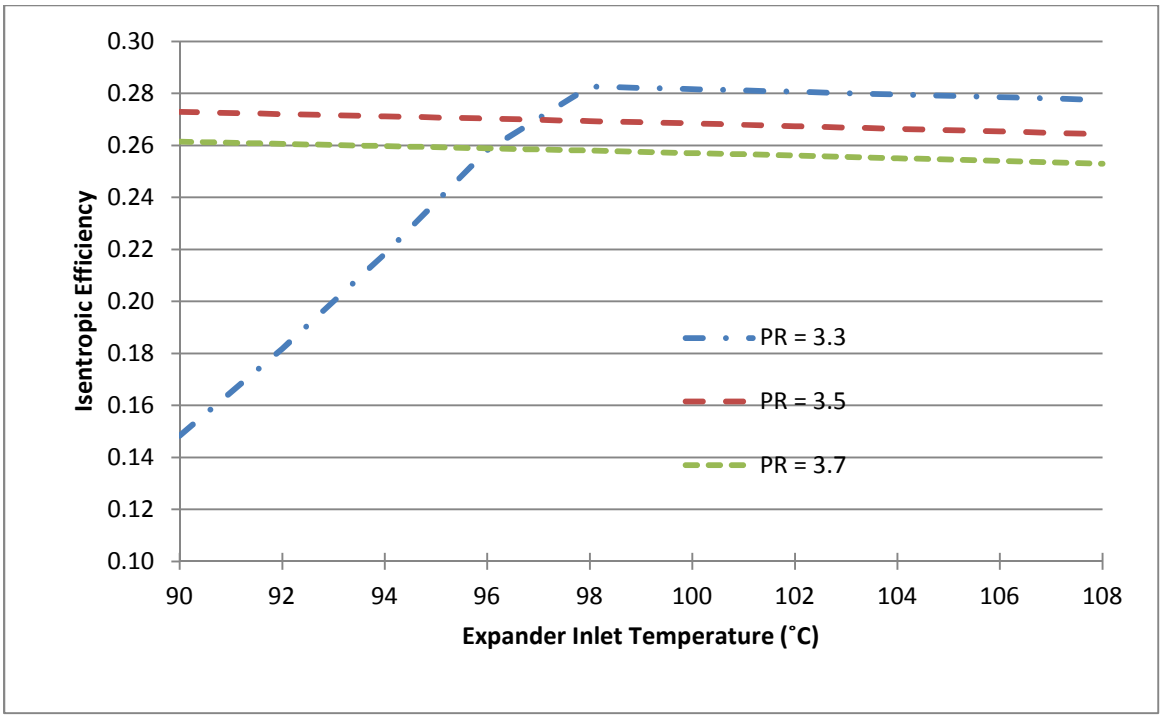

Figure 6.13: Expander isentropic efficiency for R245fa

Figures 6.11- 6.13 show the parametric performance of R245fa, using pressure ratios of 3.3 to 3.7, and temperatures of 90 to 108˚C. A pressure ratio of 3.3 shows under expansion behavior due to the fact that the inlet pressure up to 98˚C is lower than the optimal expansion pressure. Pressure ratios of 3.5 to 3.7 are in a under expansion condition and do not show the same behavior as pressure ratio 3.3. Power output is increasing at the expense of exergy and isentropic efficiency due to the increase in temperature and pressure. Once the temperature is high enough for the inlet for pressure ratio 3.3 the isentropic efficiency is higher due to the conditions being closer to optimal expansion. R245fa is showing consistent results in comparison to other dry fluids with regards to power output, exergy efficiency and isentropic efficiency.

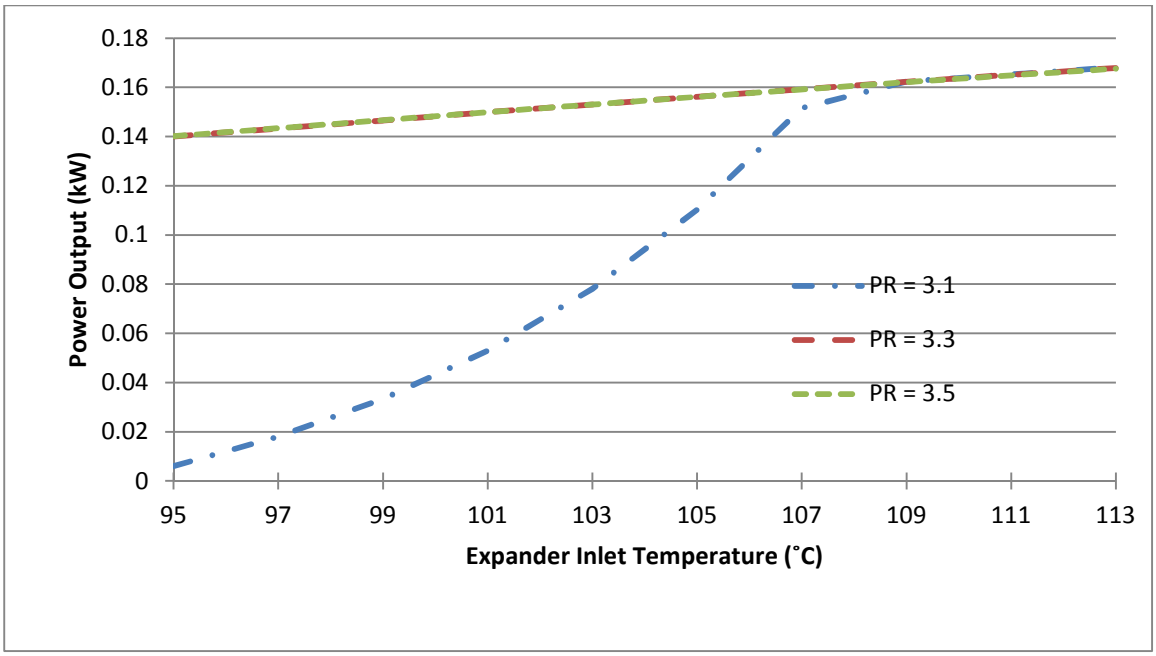

Figure 6.14: Electrical power output for iso-butane

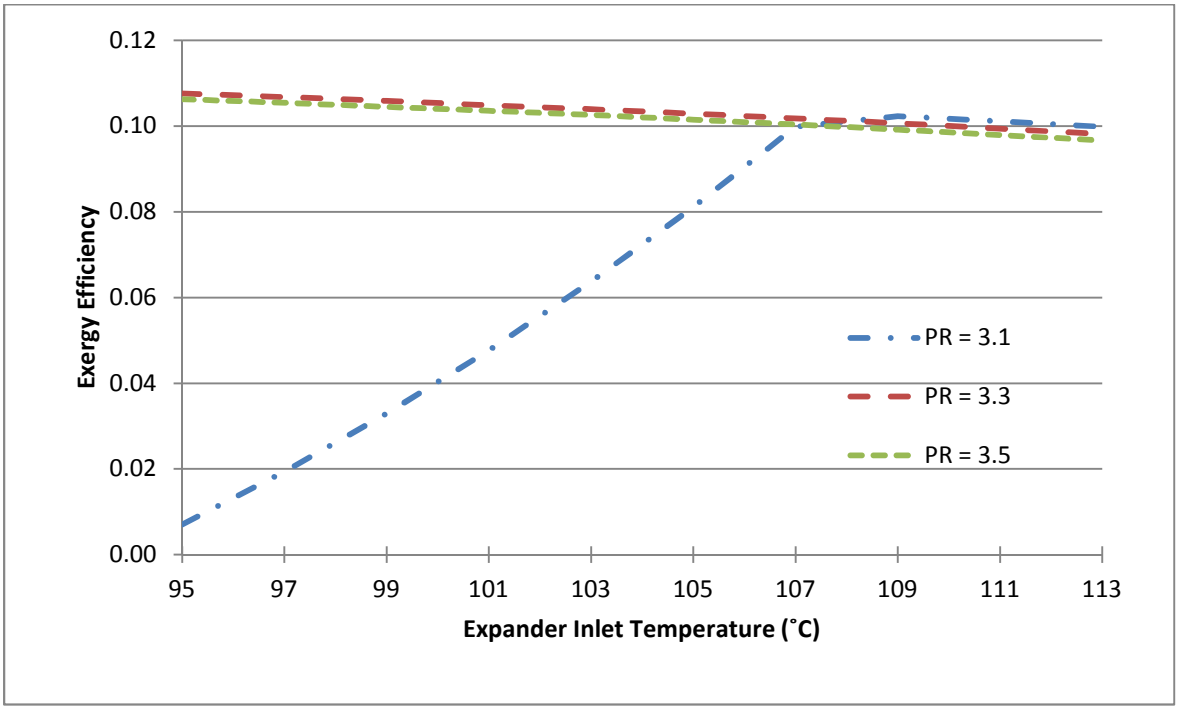

Figure 6.15: System exergy efficiency for iso-butane

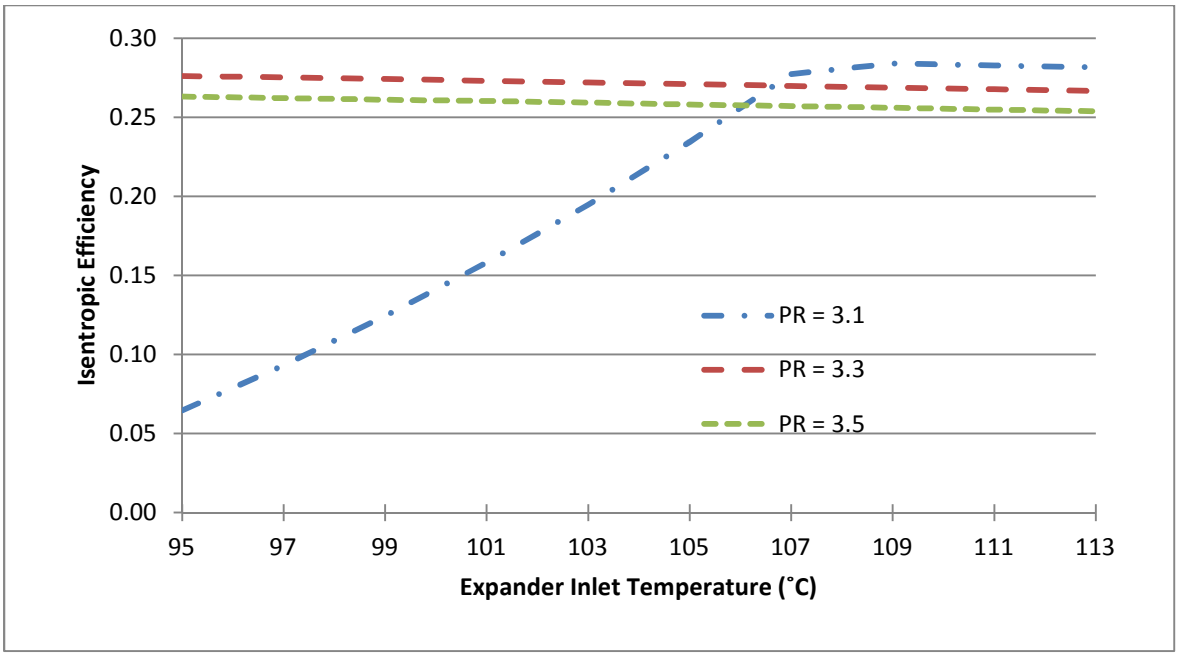

Figure 6.16: Expander isentropci efficiency for iso-butane

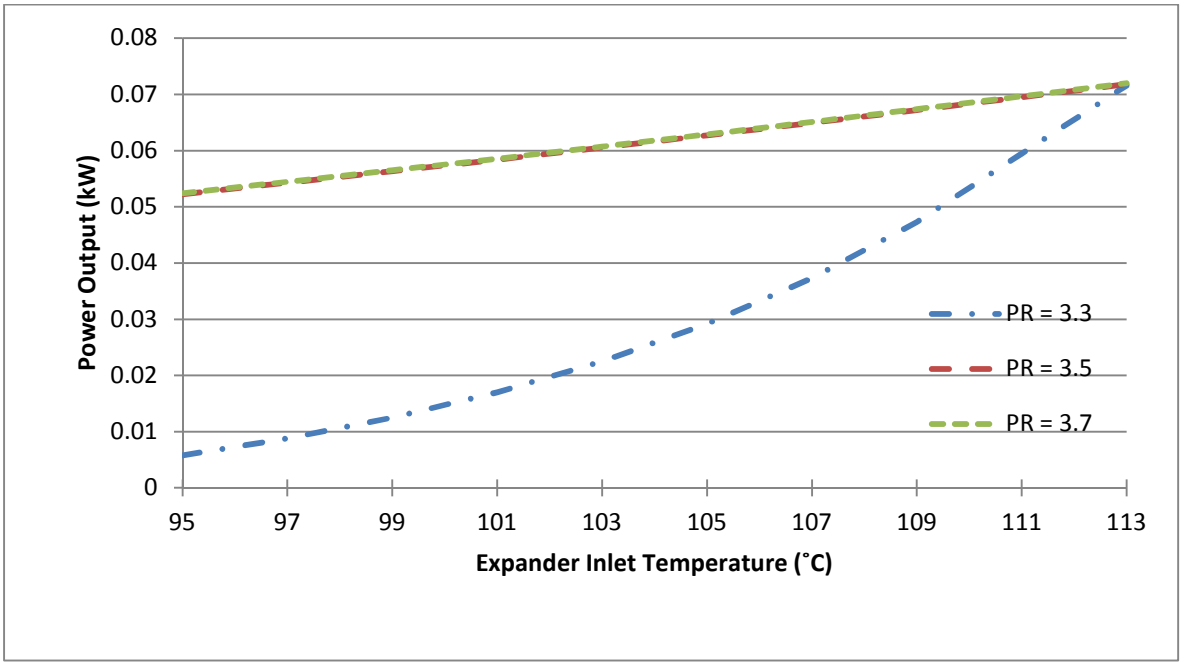

Figure 6.17: Electrical power output for iso-pentane

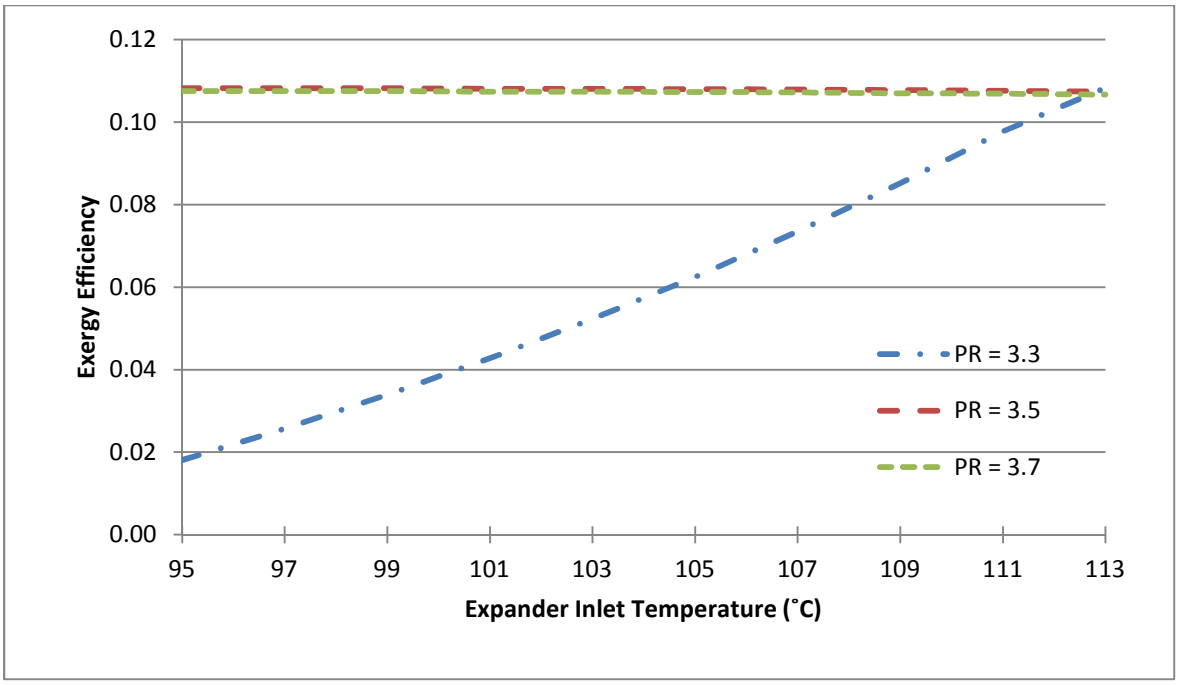

Figure 6.18: System exergy efficiency for iso-pentane

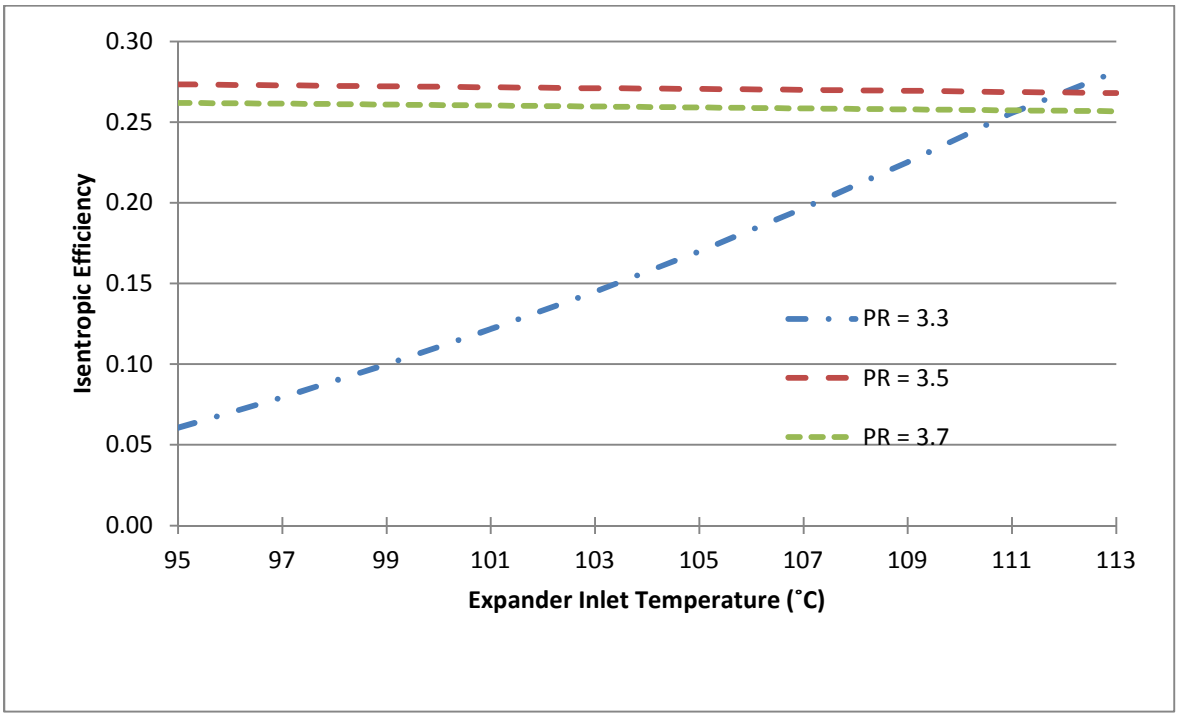

Figure 6.19: Expander isentropic efficiency for iso-pentane

Figures 6.14 to 6.19 show the parametric results for iso-butane and iso-pentane. As with the other dry fluids, these fluids exhibit similar behavior in terms of power output, exergy efficiency and isentropic efficiency. At the lowest pressure ratio for each fluid, the expander is running in an over expansion regime. As the temperature increases, the pressure increases which improves performance. Once at or near the optimal expansion point, the isentropic and exergy efficiencies are the largest compared to the other pressure ratios. Iso-pentane shows over expansion throughout the temperature range at pressure ratio 3.3. To increase efficiency, slightly increasing the pressure ratio, or decreasing the amount of superheat (which increases overall inlet pressure) will bring the expansion to the optimal point.

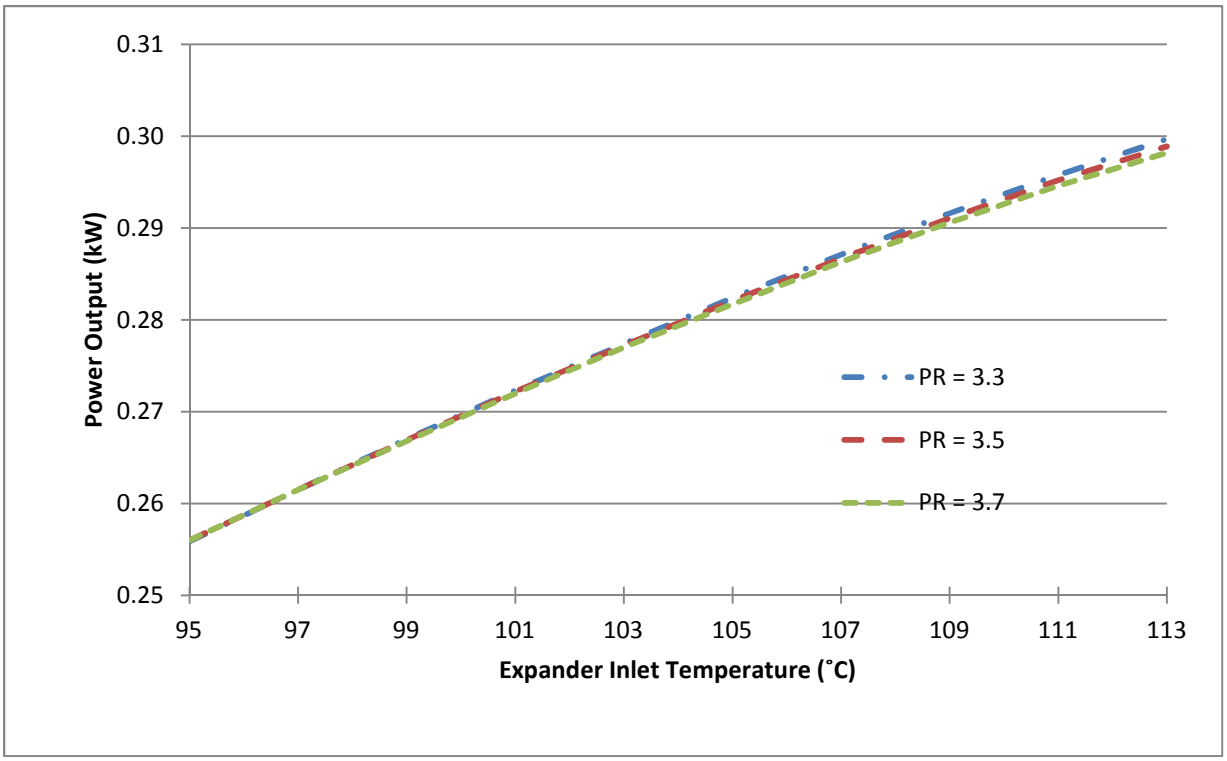

Figure 6.20: Electrical power output for dimethyl ether

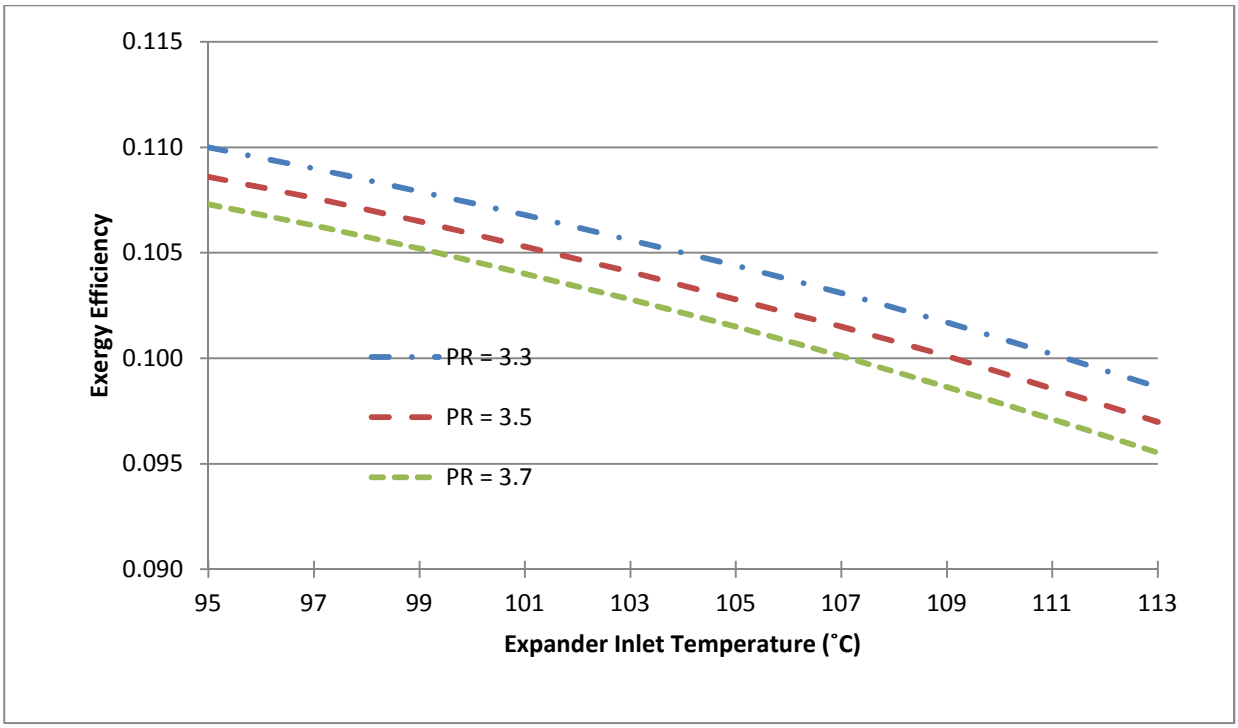

Figure 6.21: System exergy efficiency for dimethyl ether

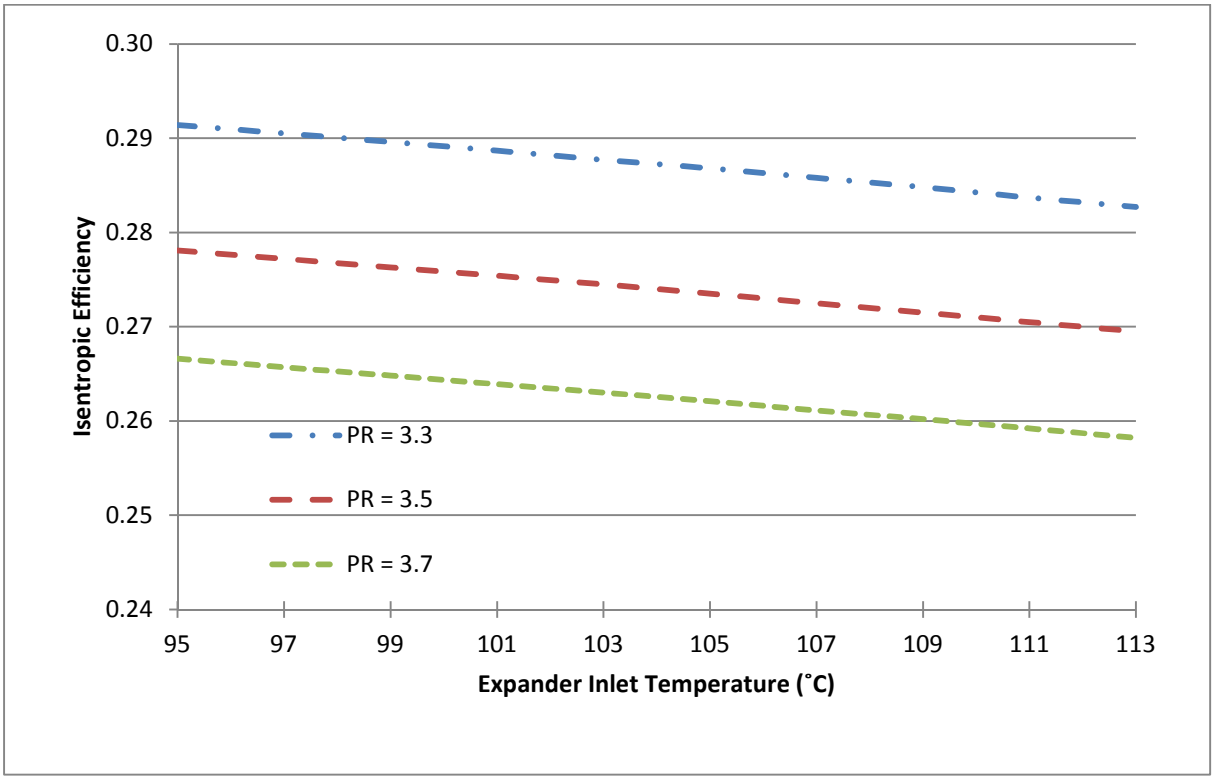

Figure 6.22: Expander isentropic efficiency for dimethyl ether

All the fluids exhibit the same behaviour for the electrical power output. The changes in pressure ratio do not have much of an effect. This is due to the fact that the expander is in the optimal or slightly under expanded area where the pressure needs to be throttled down to the condenser pressure after expansion. The only loss which makes a difference is a slight increase in leakage flow which takes away mass flow from producing useful work. R134a, R245fa, iso-butane, and iso-pentane show over expansion for certain pressure ratios resulting in additional work to raise the pressure of the fluid after expansion. The amount of pressure drop during the isentropic expansion part of the model is governed by the built in volume ratio (BVR). Because the superheat is kept constant, when temperature is dropped the saturation pressure is dropped. In some cases this results in the pressure drop during isentropic expansion to drop below the condenser pressure. This means that the expander needs to use some work to increase the pressure to the condenser pressure even after the isochoric pressure building process. This explains the low electrical power output, low exergy, and low isentropic efficiencies at certain pressure ratios. In general increasing pressure ratio results in decreased values for all the graphs. R134a and R227ea reach maximum power output at around 100˚C. Exergy and isentropic efficiencies for these fluids only decrease with increasing temperature. Overall the importance of pressure ratios and temperature is revealed with the parametric study. This is important for the optimization because guess values need to be set within range of optimal conditions to obtain proper results.

6.2 Optimization of the System

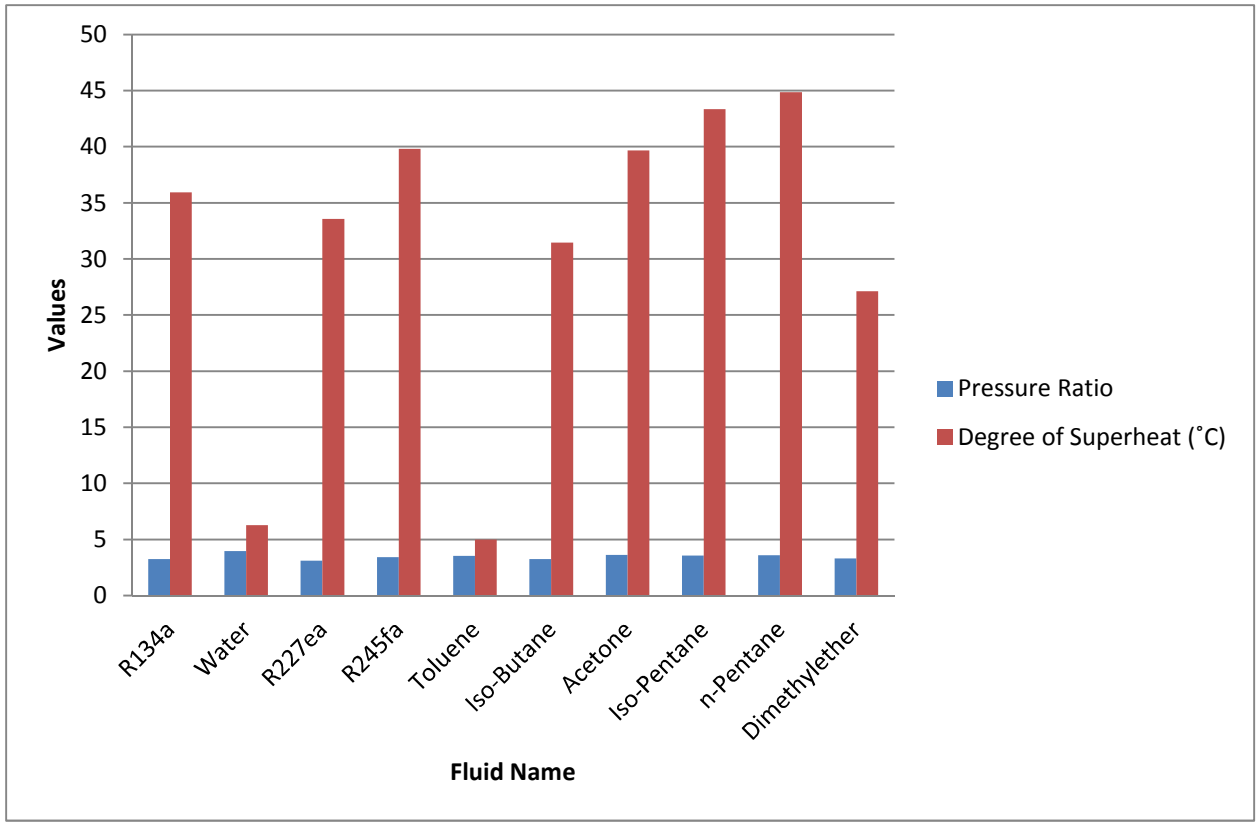

Figure 6.23: Optimized values of pressure ratio and degree of superheat for all working fluids

To optimize the system two independent variables are chosen to optimize the objective function. In this case the function to be optimized is exergy efficiency, and the two independent variables are the pressure ratio (PR) and the amount of superheat (T_{sh}). While the function of exergy efficiency may not be dependent on pressure ratio and super heat directly, these two variables influence the work output and the amount of heat input needed. These two characteristics are what influence the exergy efficiency equation since it is dependant both on electrical work output and amount of heat input.

Figure 6.23 shows the values of PR and T_{sh} that are optimized for each working fluid tested. All the dry fluids such as R227ea, R134a and n-pentane need high degrees of super

heat which approach the limit set for the analysis. The reason these values are not at the limit of 45 ˚C superheat is due to the condenser temperature being set for 25˚C. N-pentane has the highest degree of superheat with a value of 44.85˚C while Toluene has the lowest value of super heat at 5˚C. Pressure ratio varies from 3.108 for R227ea to 3.974 for water. The pressure ratio values can be considered to be optimal values as this is when the maximum isentropic efficiency occurs. Higher isentropic efficiencies produce more work output which will increase exergy efficiency. Depending on the fluid, higher superheat will increase isentropic efficiency as well. When superheat is increased, pressure ratio slightly increases for most fluids.

The values of system exergy efficiency are shown in Figure 6.24; the values range from 8.42% for water to 11.76% for dimethyl ether. This is a 39.7% increase due to the change in working fluid between water and dimethyl ether. Table 6.1 shows the percent difference for the various fluids compared to Iso-butane which has the highest system exergy efficiency of 11.81%.

Table 6.1: Percent change of system exergy efficiency between iso-butane and respective working fluids

Fluid	% Difference Exergy Efficiency
R134a	11.00
Water	40.26
R227ea	23.11
R245fa	8.55
Toluene	28.73
Iso-Butane	0.00
Acetone	10.68
Iso-Pentane	2.16
N-Pentane	5.54
Dimethyl Ether	0.43

From the table, fluids which are considered appropriate for use in systems are iso-butane, iso-pentane, n-pentane, and dimethyl ether. System exergy efficiency depends on the amount heat input that is necessary and the electrical work output. The source and environment temperature stay constant and therefore do not have an effect on exergy efficiency.

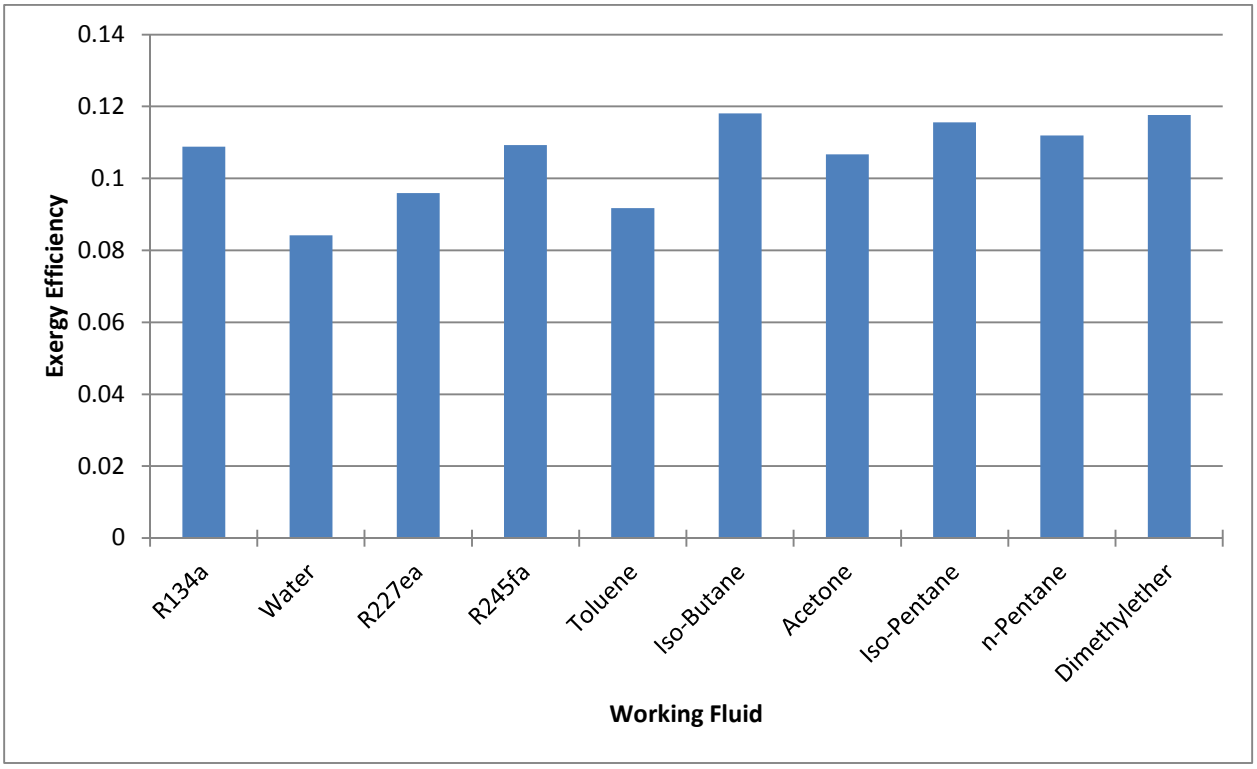

Figure 6.24: System exergy efficiency for various working fluids

Since exergy efficiency is a function of electrical work output and heat input, energy efficiency can be considered to be maximized as it depends on the same variables. Figure 6.25 shows the energy efficiency of the system taking into account the efficiency of the electrical generator. The lowest energy efficiency occurs with water, which has a value of 2.04% while iso-butane has a maximum energy efficiency of 2.86%.

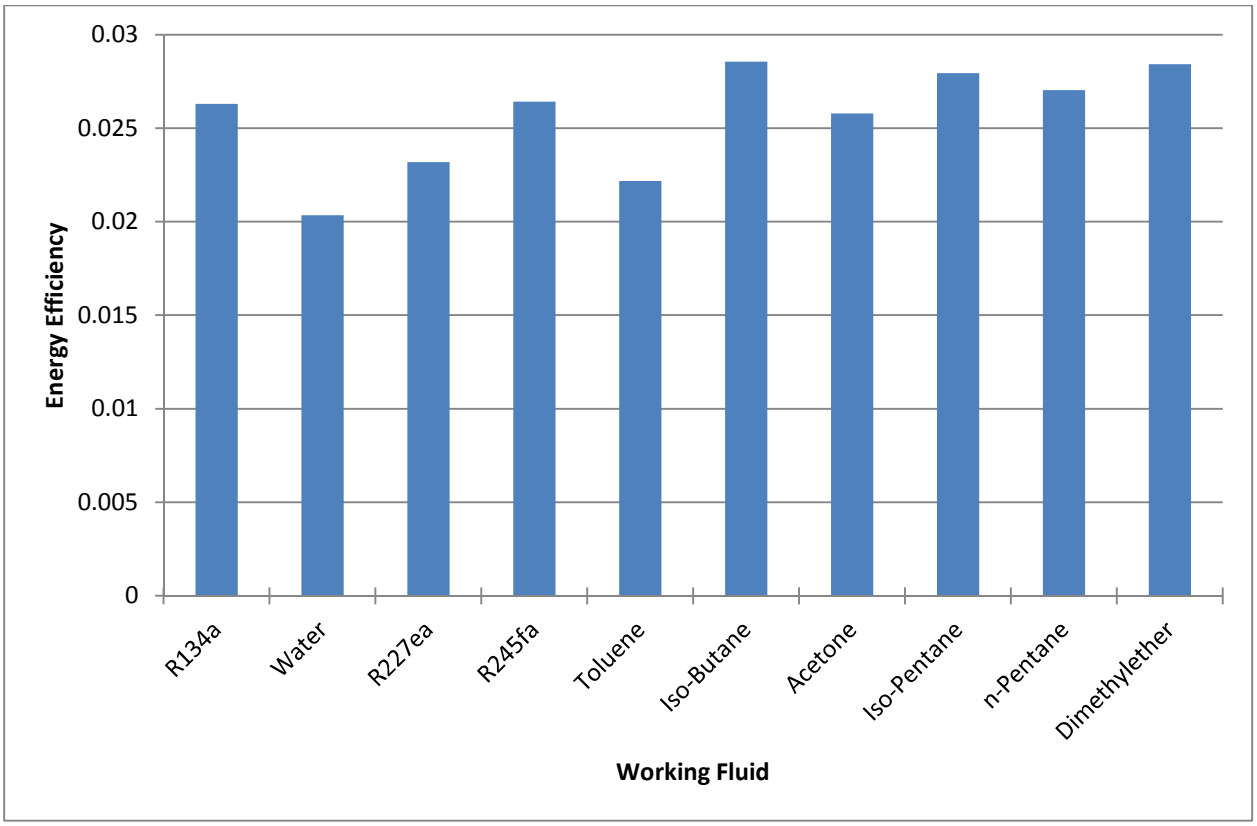

Figure 6.25: System energy efficiency for various working fluids

Dimethyl ether shows promising results with an energy efficiency of 2.84%, while iso-pentane has an efficiency of 2.79%. Comparatively R245fa has an energy efficiency of 2.64%. These four working fluids prove to be suitable for use in an organic Rankine cycle providing the best efficiency for the conditions analyzed.

Isentropic efficiency of the expander is important in determining the amount of useful work it will produce. Lower isentropic efficiencies mean that there are significant losses internally that require additional work to overcome. While the fluid is expanded, the possible work output goes towards overcoming friction and leakage losses.

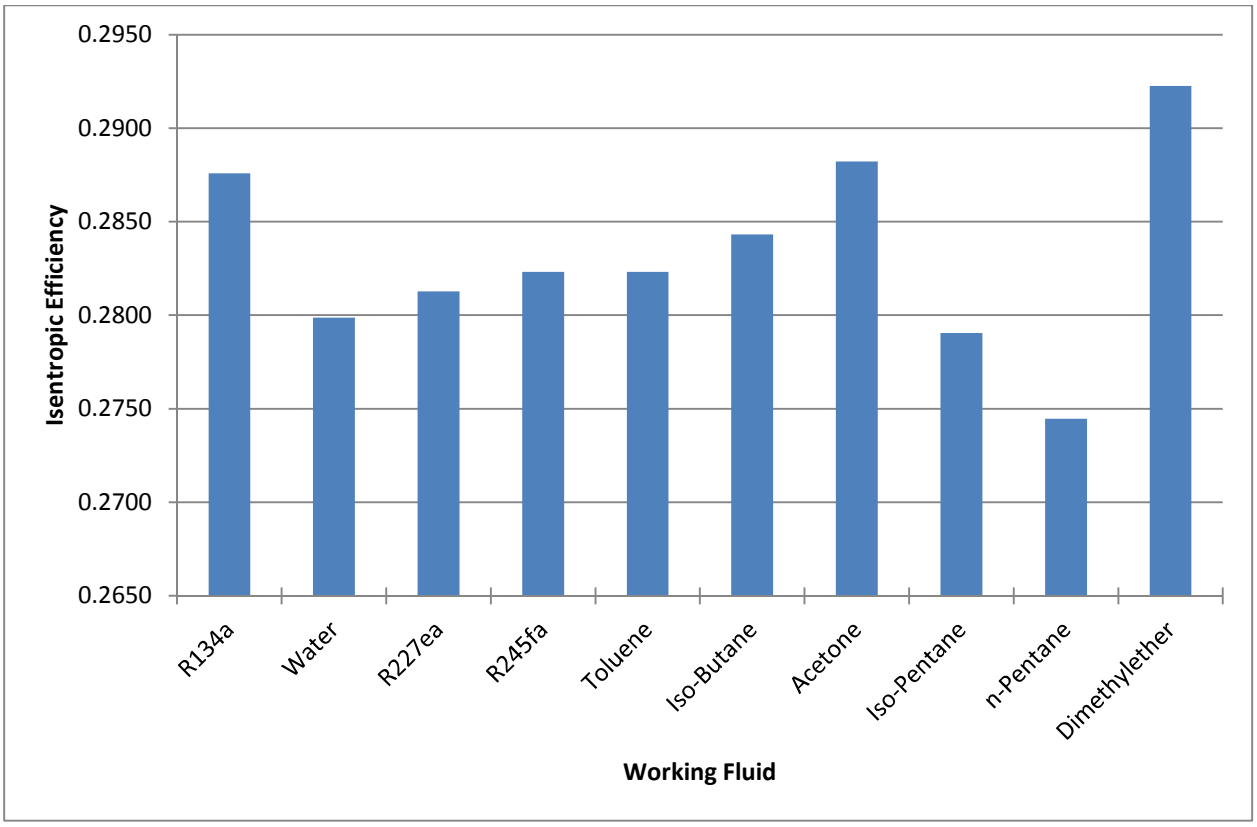

Figure 6.26: Expander isentropic efficiency for various working fluids

Figure 6.26 shows the isentropic efficiency of the expander at the optimized conditions. For most fluids this is the maximum or near maximum value at the given conditions. Isentropic efficiency is considered to be at a maximum if the pressure after the isochoric pressure building section is the same as the condenser pressure. If the pressure is higher or lower, throttling or additional work are needed. These additional processes are considered irreversibility's since they do not contribute to useful work output and waste potential work output. High pressure ratios introduce additional leakage since leakage mass flow rate is a function of input and output pressures. Dimethyl ether has the highest value of isentropic efficiency of 29.22% while n-pentane has the lowest with 27.45%. These values are very low and show that this expander has significant losses due to friction and leakage.

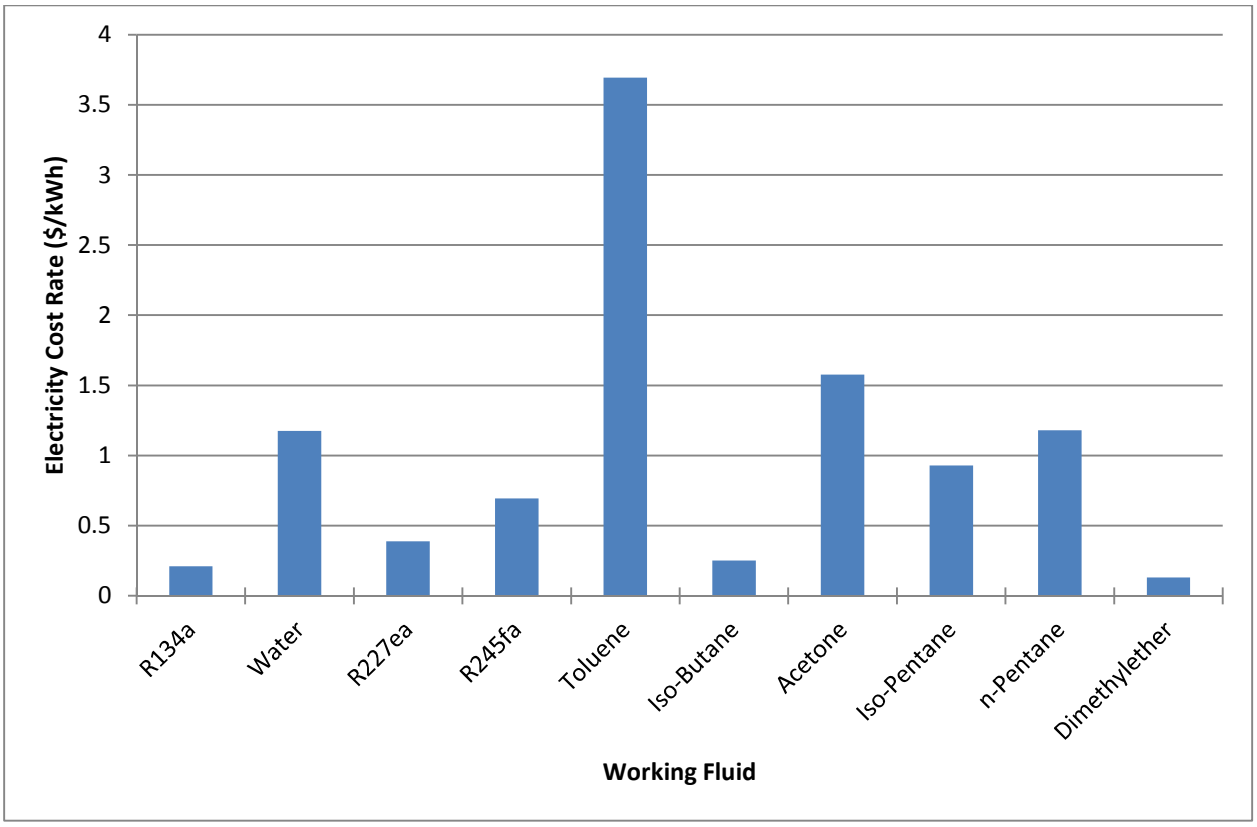

Figure 6.27: Electricity cost rate for various working fluids

Since an exergoeconomic analysis is performed, the cost of electricity in $/kWh is calculated with the optimized results. This is useful in identifying which fluid has the lowest cost for electrical output. From Figure 6.27, toluene, water, and acetone have values of 3.69 $/kWh, 1.18 $/kWh and 1.58 $/kWh which are the highest out of all the fluids. Dimethyl ether, isobutane and R134a have the lowest cost of electricity produced, with values of 0.13 $/kWh, 0.25 $/kWh and 0.21 $/kWh. These prices reflect the minimum cost that needs to be paid for the electricity produced in order to pay for the amortized cost of all the equipment plus the operating and maintenance fees. These values are not necessarily optimized values, since the capital and operating costs of the system don't change to suit each fluid. These values depended heavily on the amount of work output which is shown in Figure 6.28.

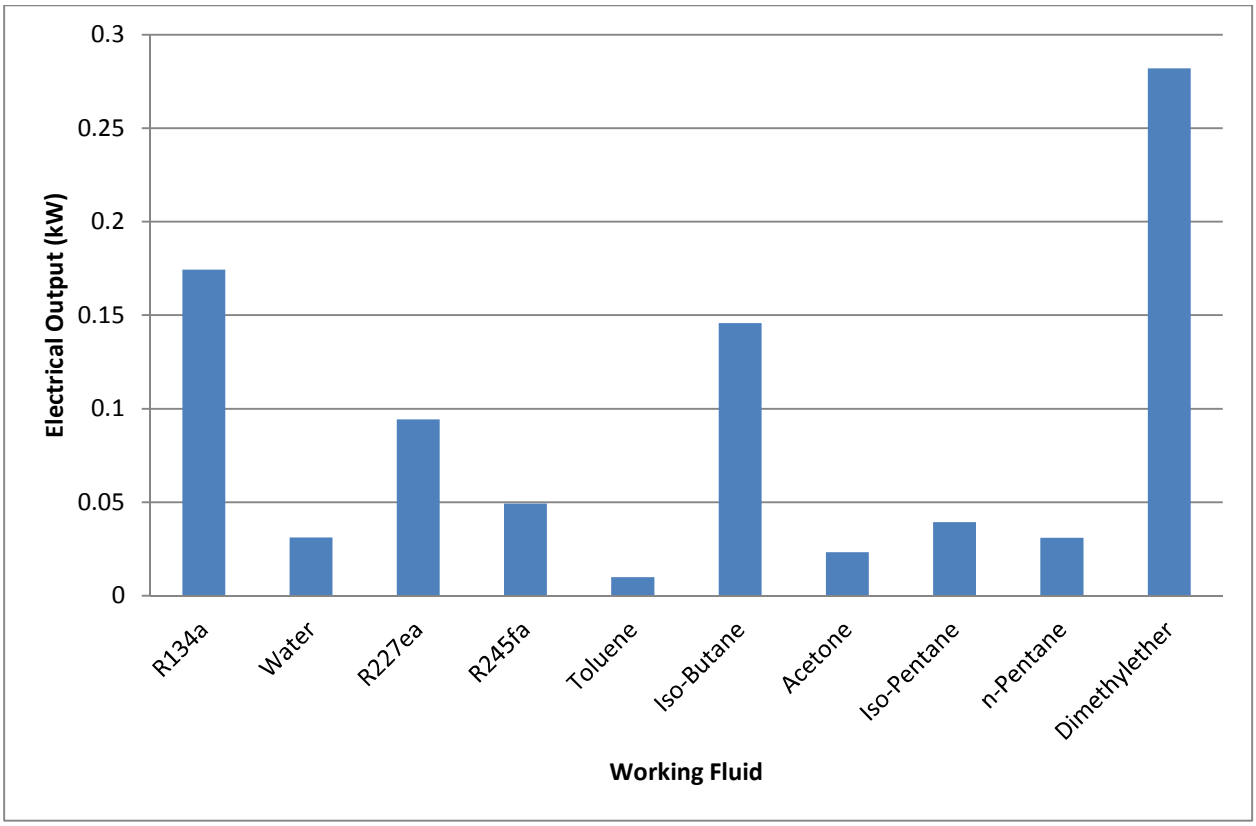

Figure 6.28: Electrical output for various working fluids

As it can be seen the fluids with the highest price for electricity have the lowest electrical work output. The opposite is true, as the fluids with the highest electrical work output have the lowest electricity rate. Dimethyl ether, iso-butane and R134a have values of 282, 146 and 174 watts. Water, toluene and acetone have electrical outputs of 31.1, 9.9 and 23.2 watts. Looking at the T-s diagrams for dimethyl ether (Figure 6.28) and toluene (Figure 6.29) it is apparent that the path of state 1 to state 2 (expansion process) is steeper for dimethyl ether than it is for toluene. Looking at the difference in pressure as well shows significant difference. A steeper drop represents more work extracted from the fluid as this represents less entropy generation (as well as less exergy destroyed).

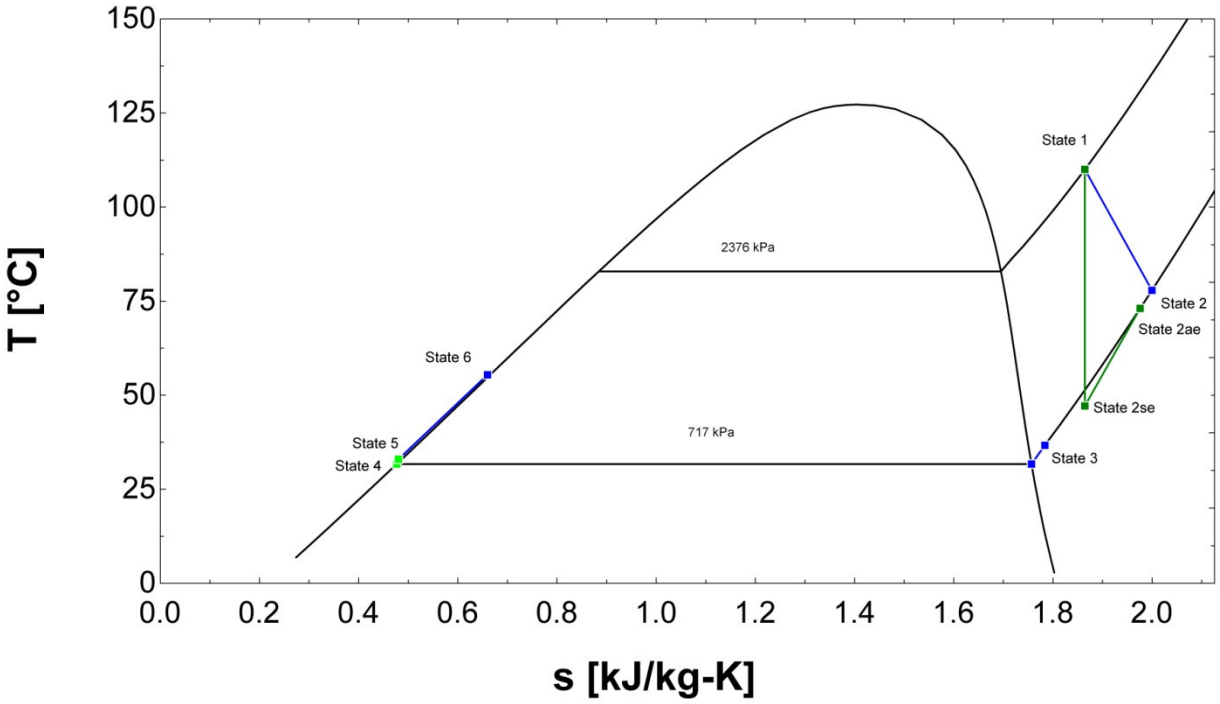

Figure 6.29: T-s diagram for dimethyl ether at optimal operating conditions

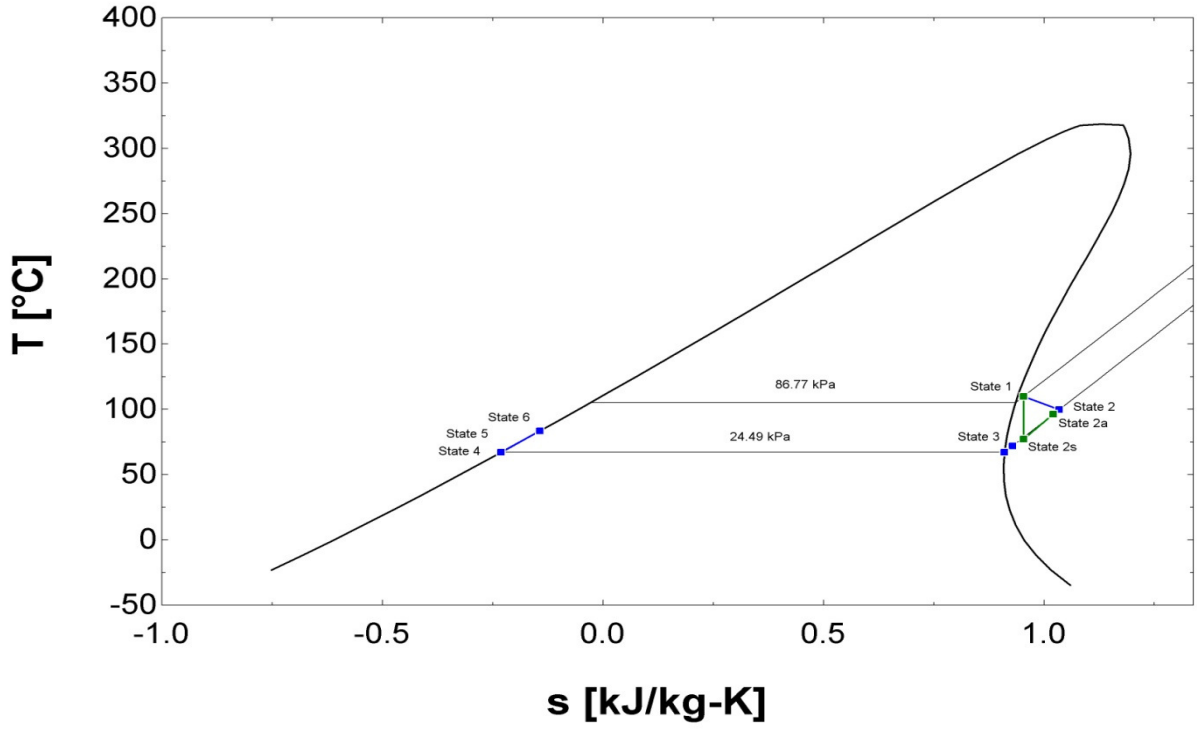

Figure 6.30: T-s diagram for toluene at optimal operating conditions

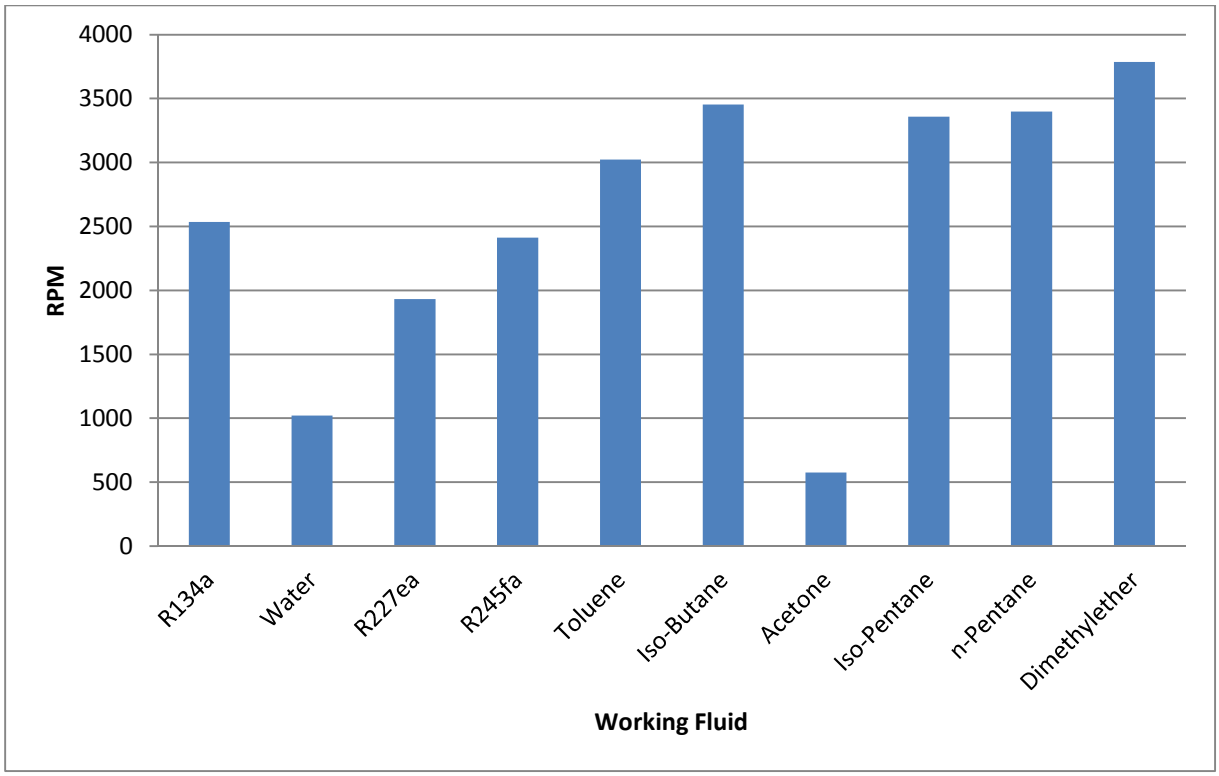

Figure 6.31: RPM for various working fluids at optimized conditions

The difference in pressure from inlet to outlet plays a large role in determining the amount of work output from the expander. Since the amount of torque produced by the expander is directly related to the difference in pressure, analyzing this across the different working fluids can explain the work outputs of each of the fluids. Figure 6.32 shows the pressure difference of the various working fluids analyzed. Dimethyl ether has the highest pressure difference with a value of 1659 kPa. The lowest is pressure difference is seen with toluene with a value of 62.28 kPa. Evidently these two fluids have the highest and lowest electrical work outputs respectively. Other fluids like iso-pentane and n-pentane have a low pressure difference which corresponds to low electrical power output.

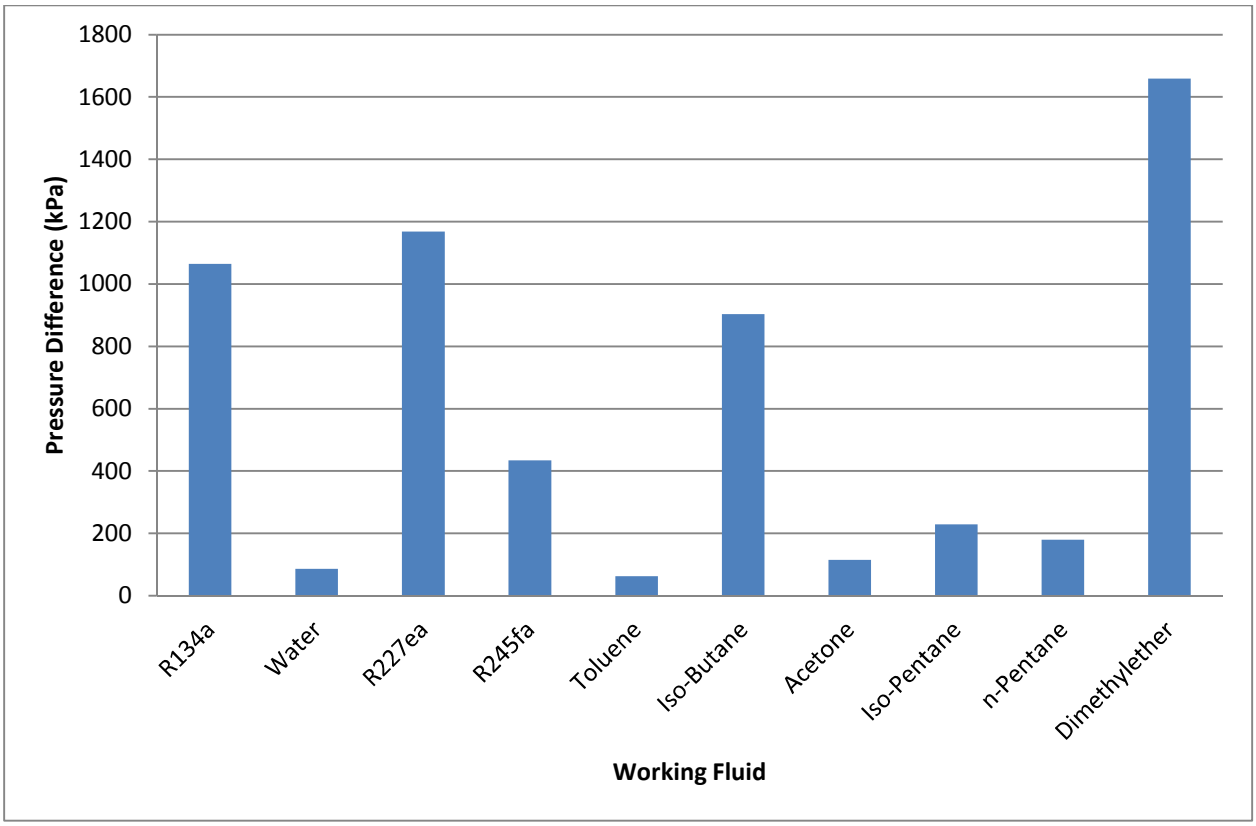

Figure 6.32: Pressure difference between Input and output of expander at optimized conditions

The amount of work output also corresponds to the amount of heat input needed to the system. Figure 6.34 shows the heat input necessary at optimal conditions for each of the working fluids. Fluids which have high work output such as dimethyl ether and R134a have high values of heat input. Dimethyl ether requires almost 10 kilowatts of heat to produce 282 Watts of electrical power. The lowest heat input needed is for toluene which requires 447.2 watts to produce 9.9 watts of electricity. These figures are important when increasing the size of the system to produce more electricity. Working fluids which have low power output make the system much larger than a working fluid with higher power output.

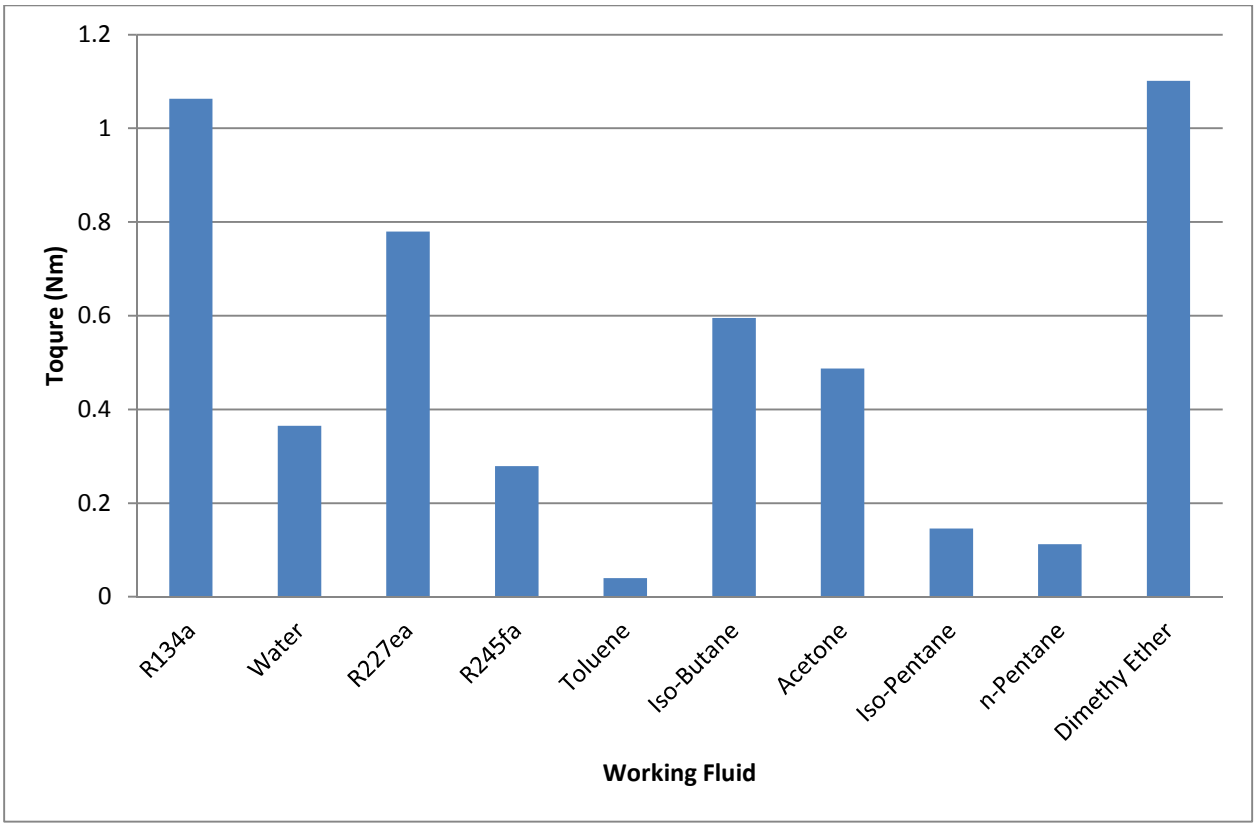

Figure 6.33: Output torque for various working fluids at optimized conditions

The idea that that low pressure difference results in reduced work can be confirmed by looking at the torque output for the various fluids. Figure 6.33 is the optimized torque output for the various working fluids. Dimethyl ether and R134a have the highest torque output which coincides with the fact that they also have the highest pressure differences. Toluene which has the lowest pressure difference also has the lowest torque. Fluids like n-pentane and iso-pentane cause the expander to have high RPM (Figure 6.31) but due to the low torque the power output is very low. This can also be explained by the low pressure difference between input and output of the expander.

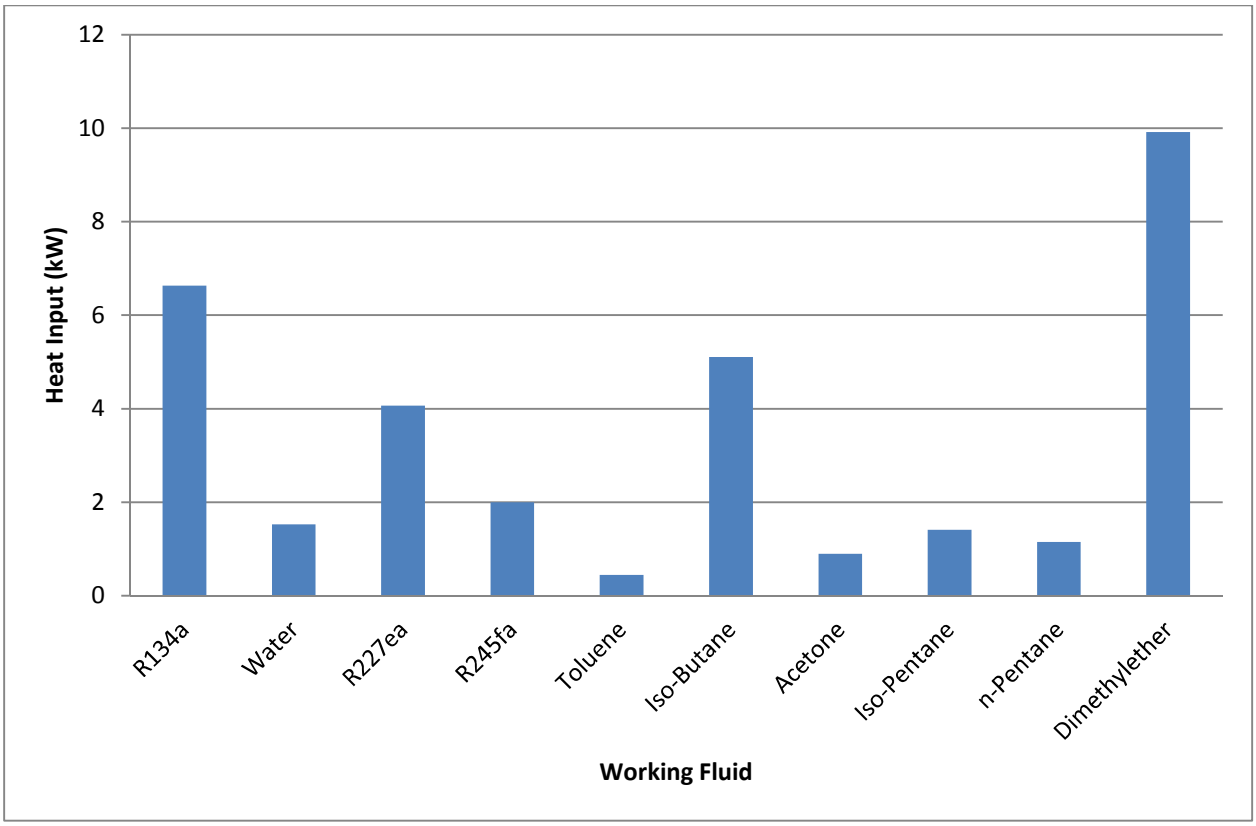

Figure 6.34: Heat input for various working fluids at optimized conditions

These results explain the performance of the system at optimized conditions for a given set of states and assumptions. In order to further improve the system, exergy analysis on each of the components should be done to see how much exergy is destroyed by each component in the system. The next subsection deals with the exergy destructions of the system for each working fluid at optimized conditions.

6.3 Exergy Analysis and Destruction

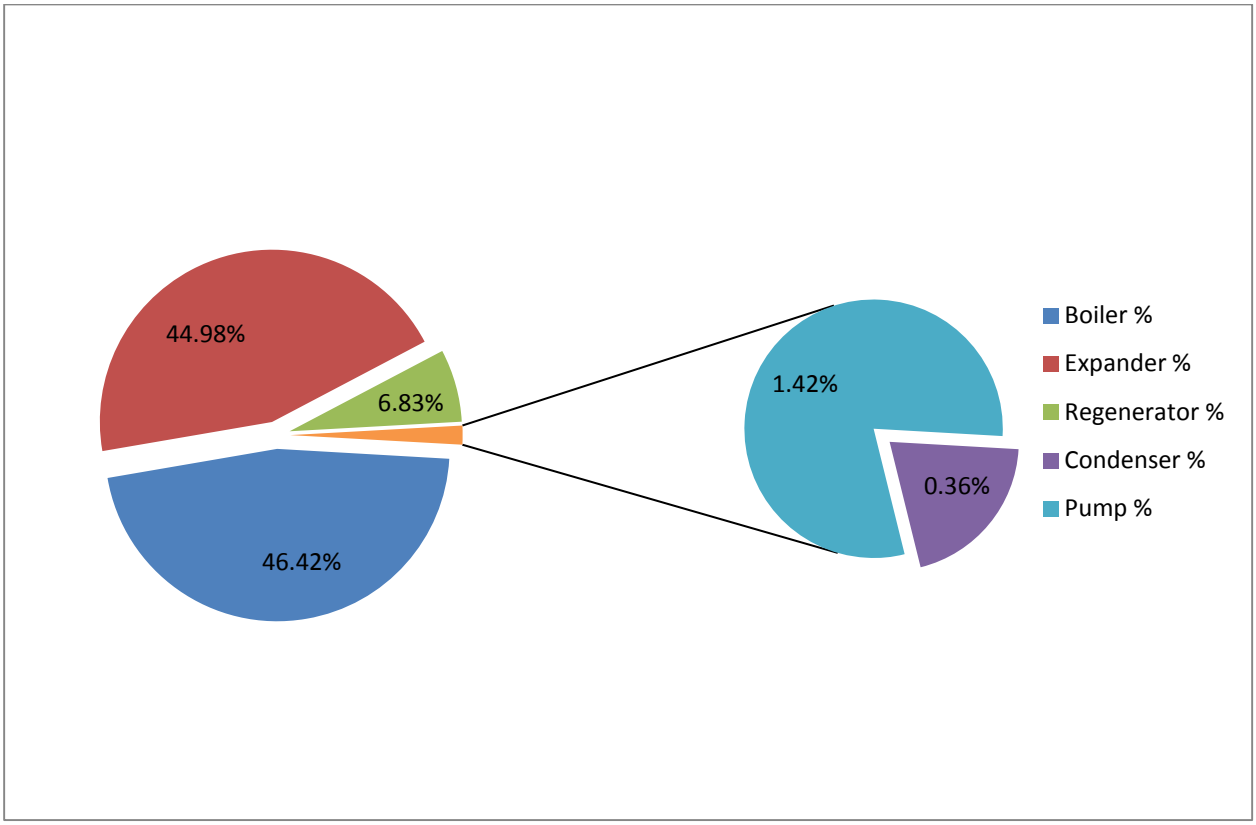

Figure 6.35: Exergy destruction of each component for R134a at optimized conditions

The first fluid analyzed is R134a (Figure 6.35) at optimized conditions. The total exergy destruction for the whole system is 1.34 kW for this case. The largest exergy destruction is in the boiler at 46.42% which is expected due to the heat transfer process involved in that component. The expander has almost 45% of the exergy destruction share which shows that there is potential for large improvement in this component. This large share of exergy destruction in the expander can be explained by the low isentropic efficiency which is 28.76%. Many larger scale systems have much higher isentropic

efficiencies approaching 80 to 90%. Therefore, in order for these systems to be competitive isentropic efficiency needs to improve.

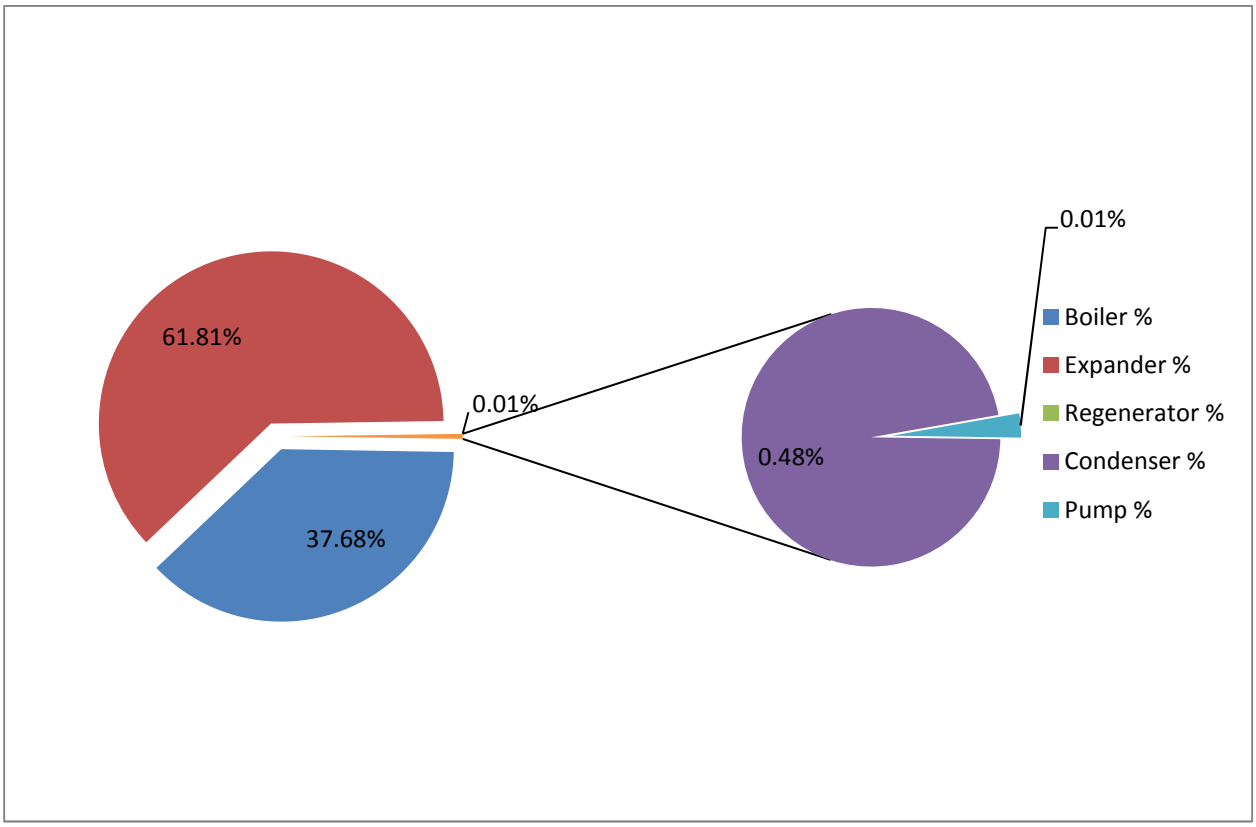

Figure 6.36: Exergy destruction of each component for water at optimized conditions

In Figure 6.36 the opposite is true; the expander has the largest share of exergy destruction. This is due to the fact that water has a low power output during expansion and therefore is not using all the available exergy from state 1. Exergy destroyed in the pump is very low compared to R134a, due to the fact that the temperature and specific volume do not change as much during pumping with water. Regenerator exergy destroyed is also low with a value of 0.01% due to the very small temperature differences involved in the component. With R227ea (Figure 6.37), boiler and expander have similar exergy destruction shares. Due to the larger amount of regeneration needed for this fluid (due to

the fact that it is a dry fluid), there is more exergy destruction in the regenerator. Condenser exergy destruction is also low and this can be attributed to the low temperature differences between the environment and the fluid at input state. There is large improvement possible from the boiler and the expander especially.

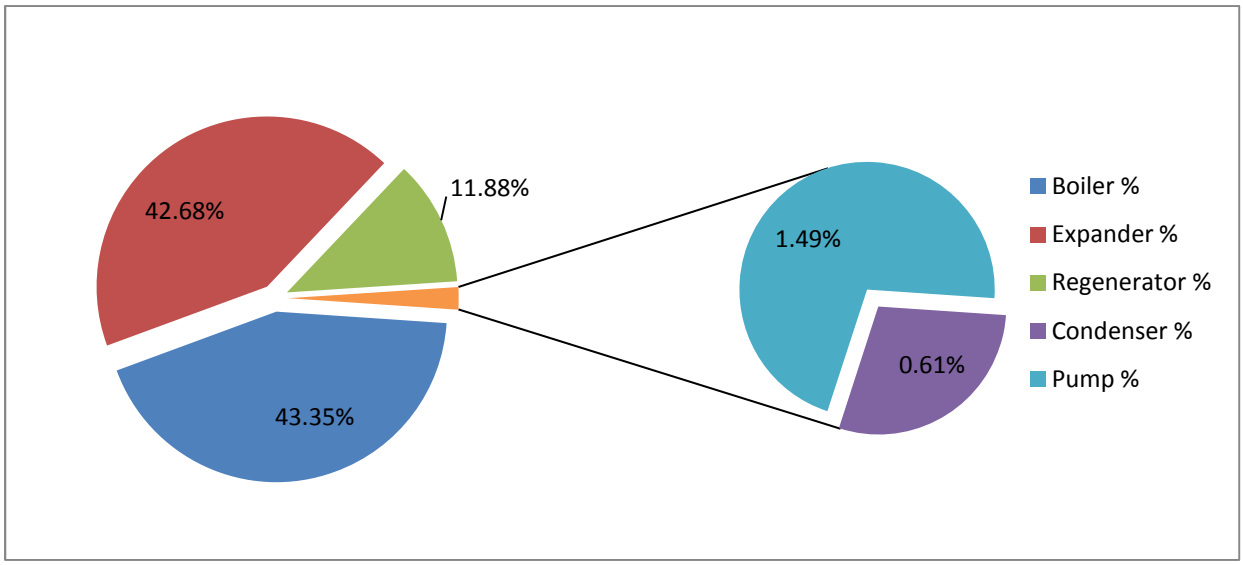

Figure 6.37: Exergy destruction of each component for R227ea at optimized conditions

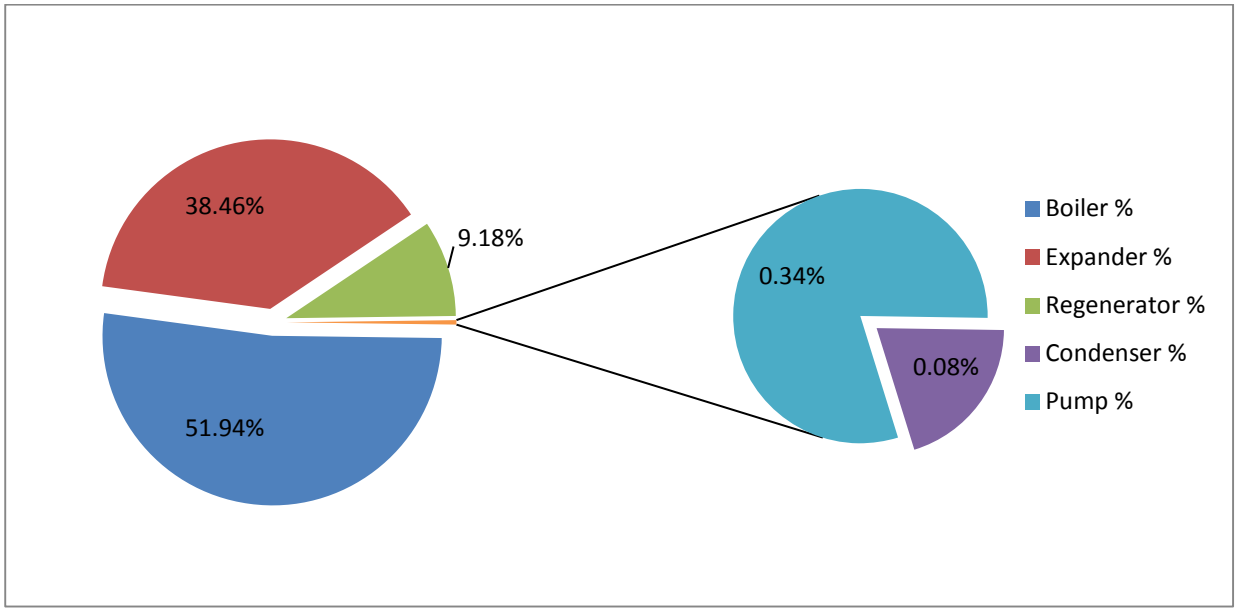

Figure 6.38: Exergy destruction of each component for R245fa at optimized conditions

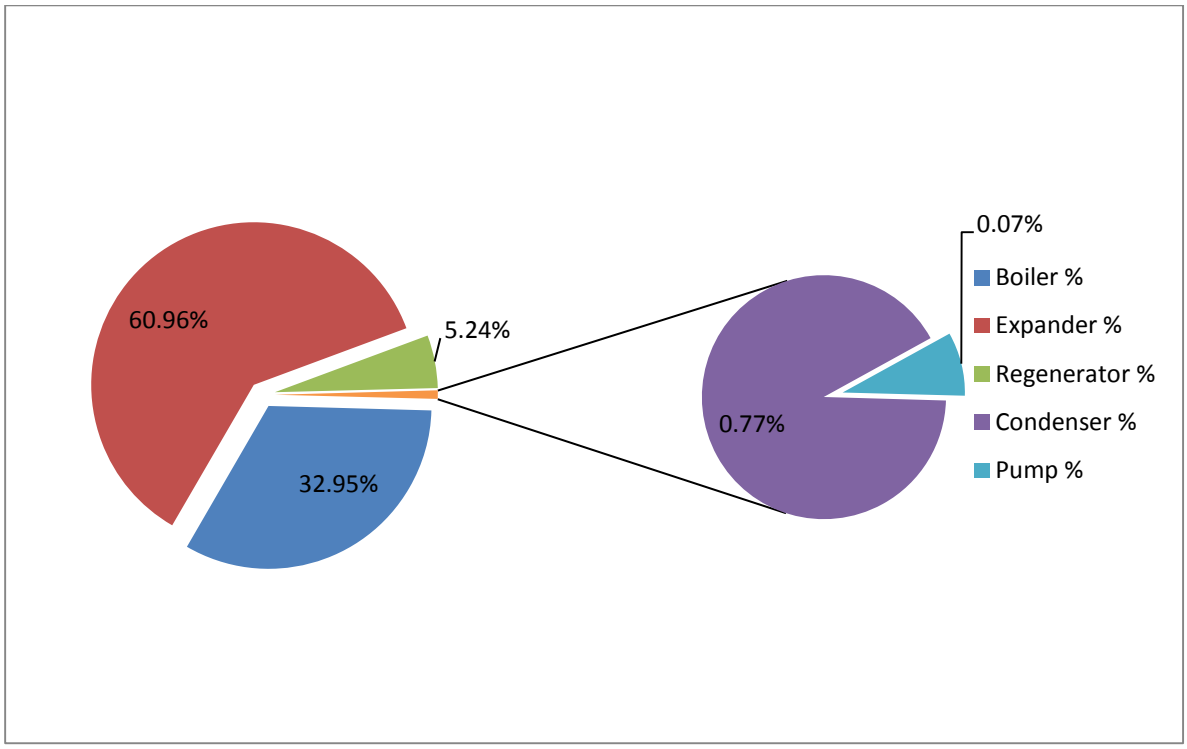

Figure 6.39: Exergy destruction of each component for toluene at optimized conditions

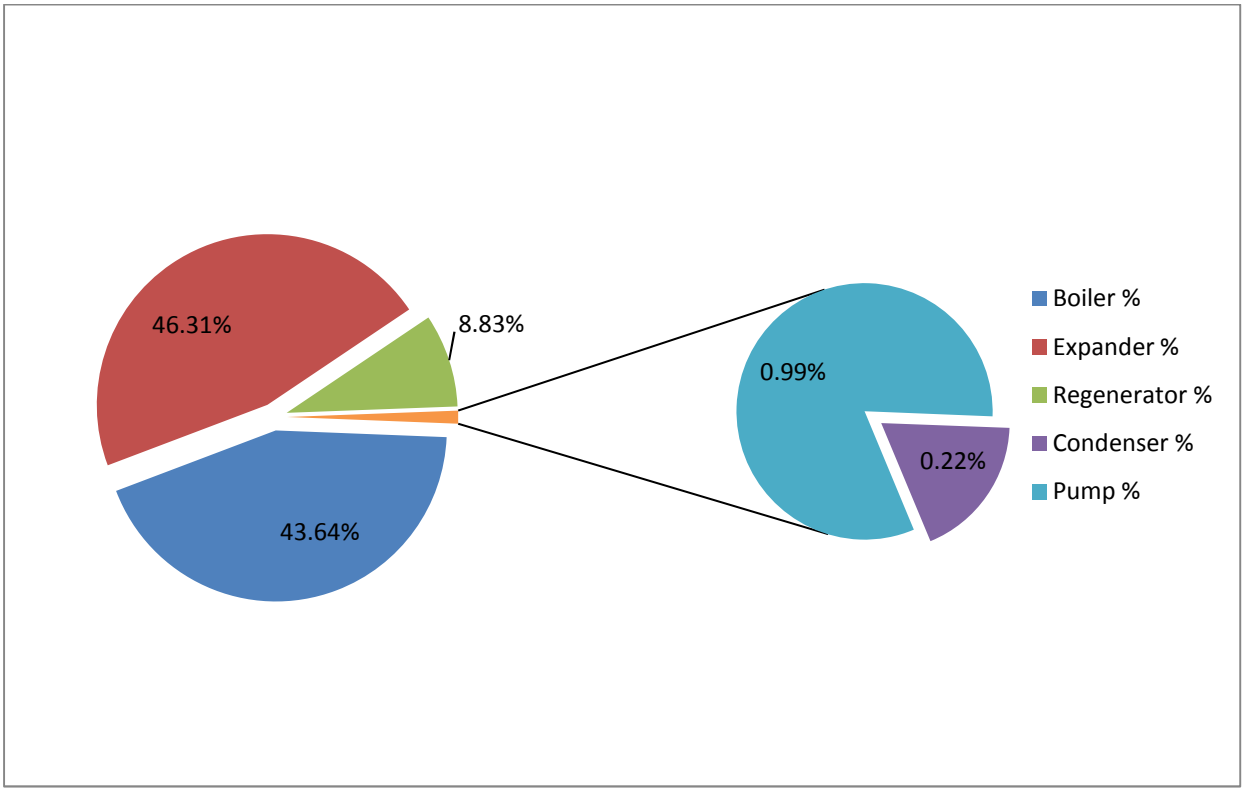

Figure 6.40: Exergy destruction of each component for iso-butane at optimized conditions

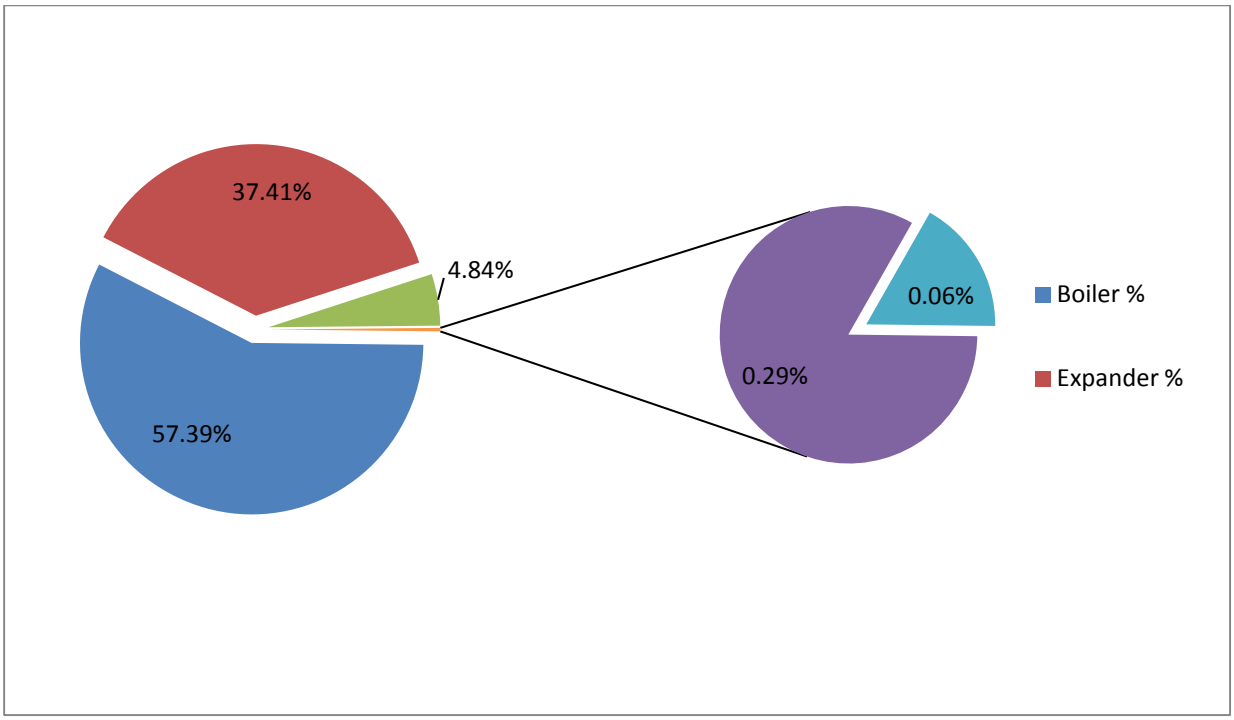

Figure 6.41: Exergy destruction of each component for acetone at optimized conditions

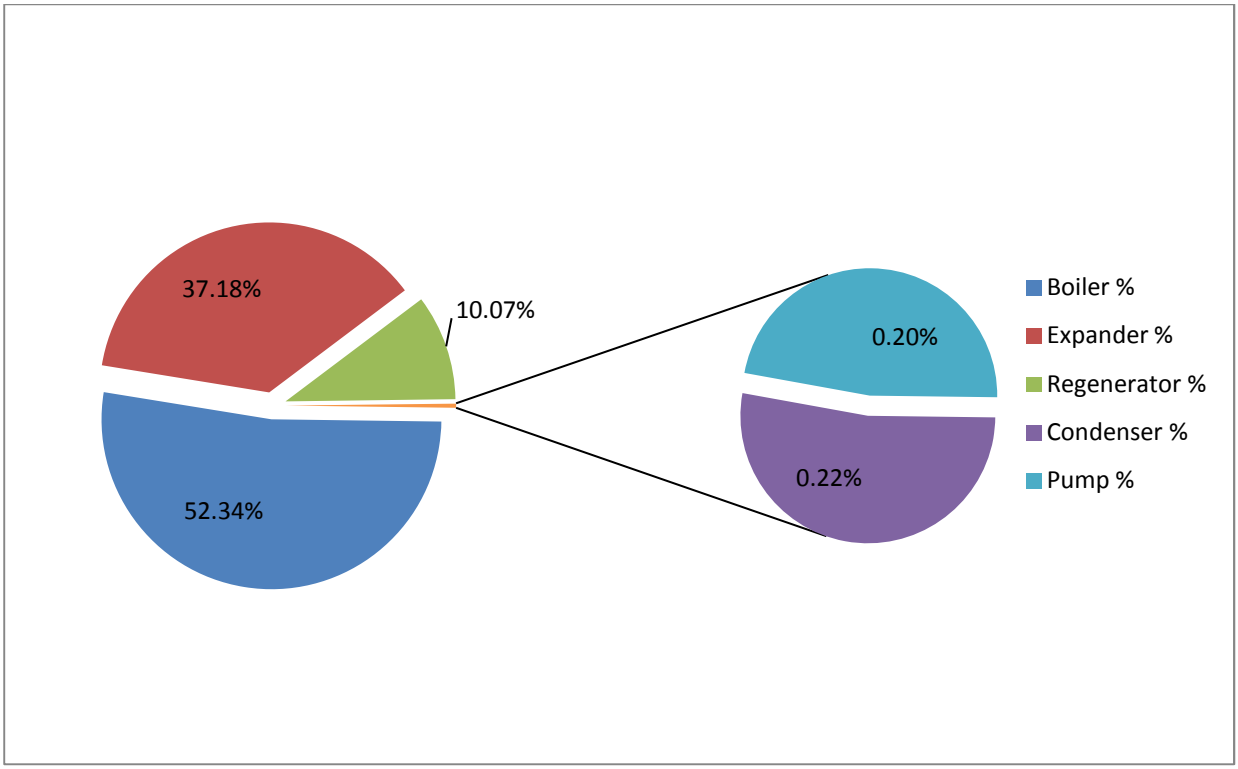

Figure 6.42: Exergy destruction of each component for iso-pentane at optimized conditions

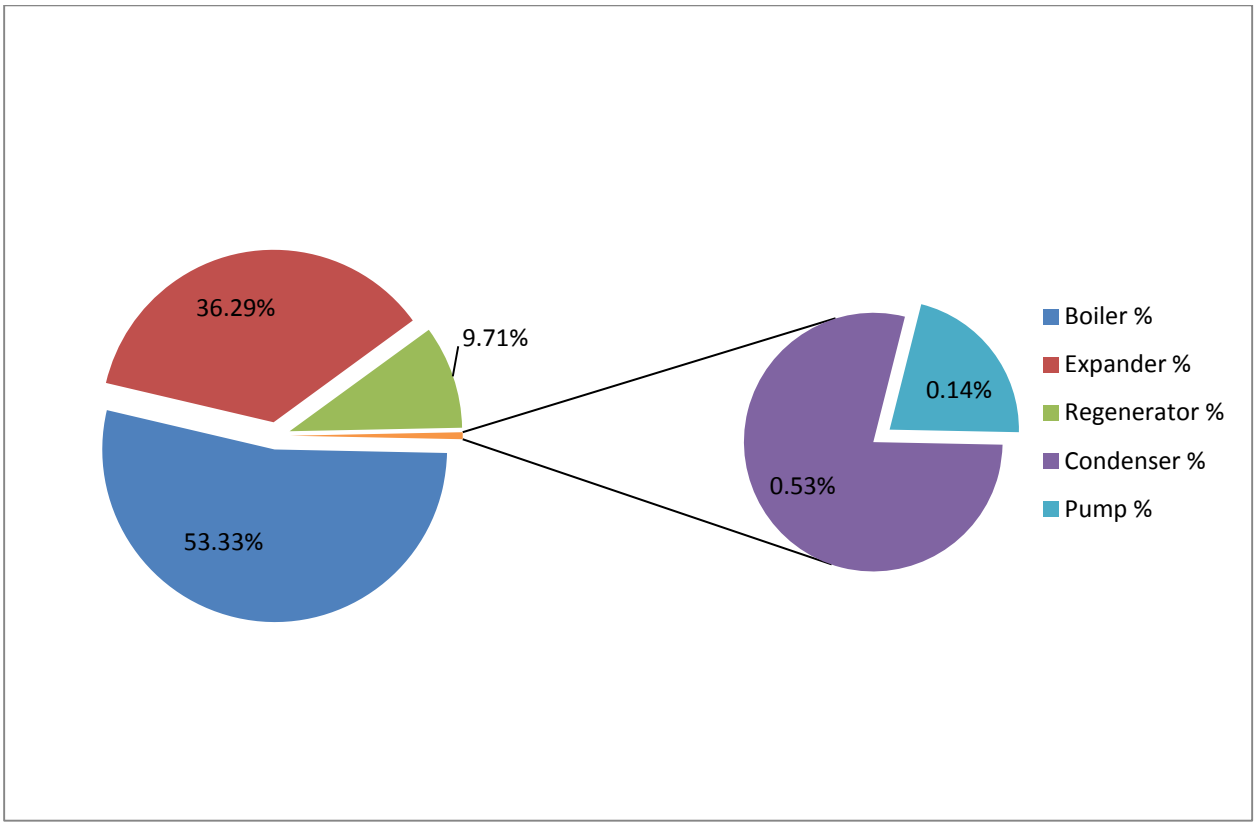

Figure 6.43: Exergy destruction of each component for n-pentane at optimized conditions

Toluene (Figure 6.39) which has the lowest power production shows a large amount of exergy destruction in the expander. As mentioned before the T-s diagram (Figure 6.30) shows that the slope for toluene is not very steep compared to the isentropic line, meaning a lot of irreversibility's are occurring during expansion. This is similar to water which has low power output and high expander irreversibility.

Iso-pentane (Figure 6.42 and Figure 6.43) and n-pentane have very similar exergy destruction rates for the expander and the boiler. This is due to their similar chemical makeup; one difference is that exergy destroyed in the condenser is higher for n-pentane than iso-pentane. A large improvement to reduce boiler exergy destruction would increase overall system exergy efficiency which should help with increasing power output and

reducing energy input. Dimethyl either (Figure 6.44) shows very good results for system energy and exergy efficiencies as well as highest electrical output. Analyzing the results for exergy destruction can help improve this fluid further. The expander has the highest share of exergy destruction, which is surprising considering the fluid has the best electrical output out of all the fluids. This fluid will benefit greatly from reduced exergy destruction in the expander by reducing losses such as leakage and friction.

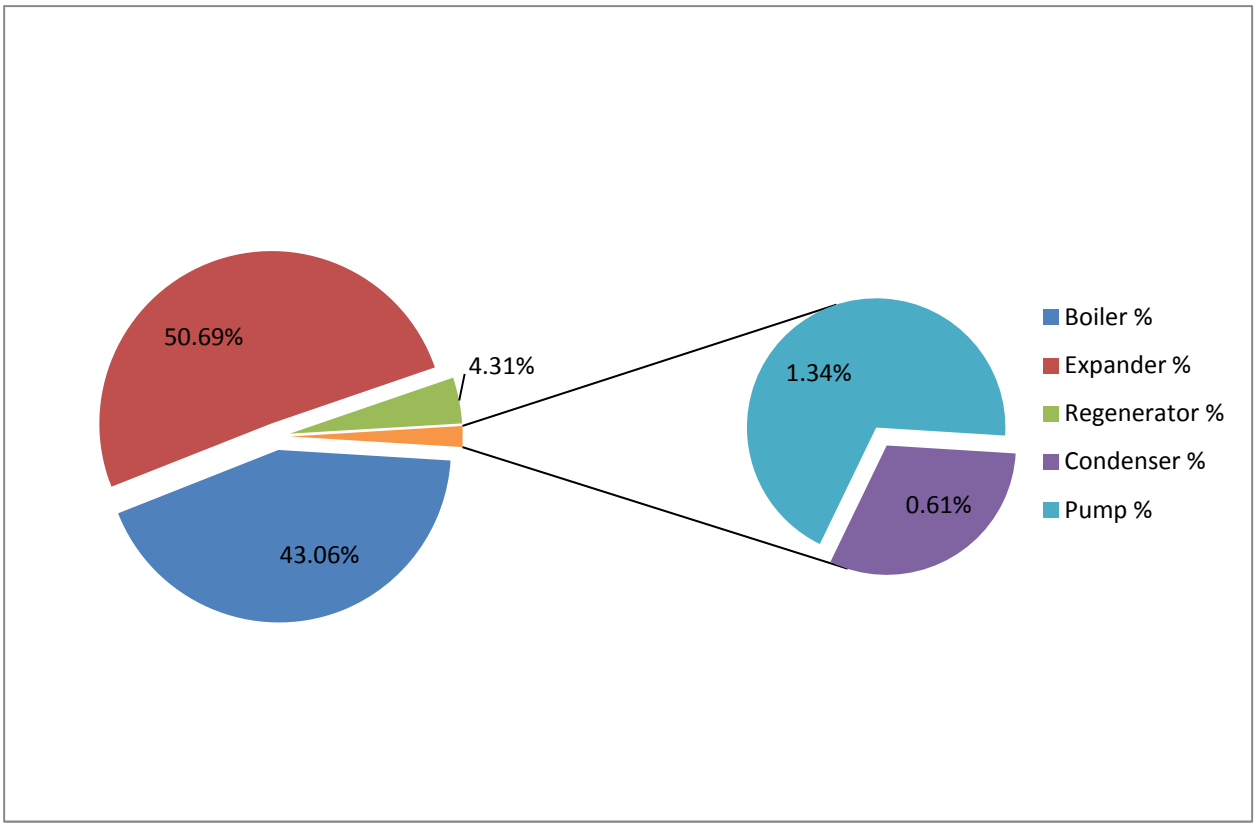

Figure 6.44: Exergy destruction of each component for dimethyl ether at optimized conditions

It's difficult to directly correlate the exergy destructions between the fluids, since the mass flow rates and the states are different for each case. Exergy destruction helps with identifying which component in the system can be improved to increase overall exergy efficiency. On average exergy efficiencies for these fluids ranges from 9 to 12% which is

very low considering that these systems need to compete with other sources of low temperature power generation. One large improvement can be made in the expander, considering isentropic efficiency is never close to the 70-80% achieved in the literature. Observations from disassembled scroll compressors show that many machine finishes on the scrolls could be improved greatly. One example is that the ends (top of the scroll height) of the involutes are very rough. When these mesh with the other scroll disk, there is a large amount of leakage (axial leakage especially) and friction produced which explains the overall drop in isentropic efficiency. Also some fluid is purposely bleed from the scroll assembly to keep the meshed scrolls from rubbing against the bearing seat that they sit on. This is a loss that should be avoided when manufacturing an expander for larger scale purpose. Even with oil lubrication available to reduce friction there is still considerable loss due to poor machining finishes. Improvements can be made with better finishing of mating surfaces, low friction coatings and better bearings.

6.4 Exergoeconomic Analysis

The exergoeconomic cost balance equations were used in the analysis above to arrive at a cost rate of electricity for optimized exergy efficiency. The equation for exergy efficiency depends on the electrical power output and the amount of heat input. The maximized value of exergy efficiency does not necessarily represent the maximum power output for the system at that particular pressure ratio. When looking at Figure 6.45 it is apparent that the maximum power output occurs with a superheat of around 15˚C. This also corresponds to the lowest cost rate for electricity. Therefore applying the optimization techniques can be useful to find the lowest cost rate of electricity for the system.

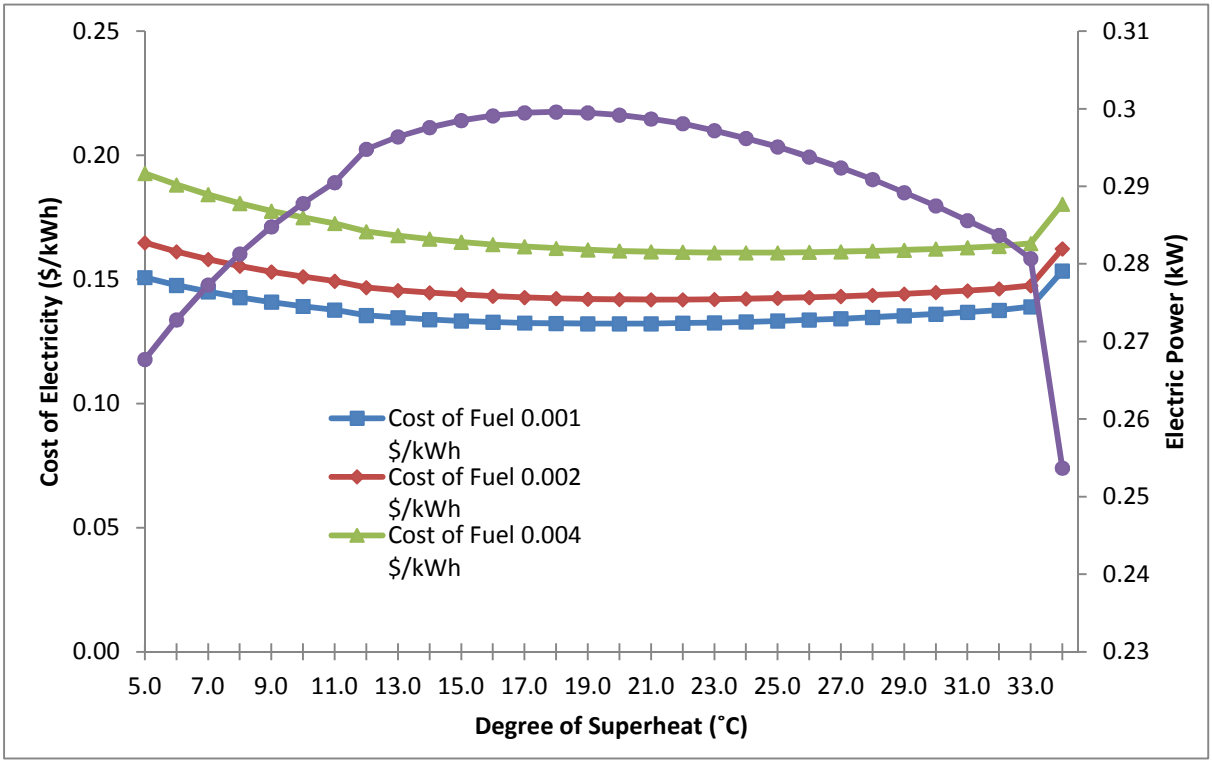

Figure 6.45: Electricity cost rate and electric power output with varying superheat at optimal pressure ratio and three different fuel costs (dimethyl ether)

Since dimethyl ether and iso-butane are the fluids which have the highest power output and the lowest cost for electricity at optimized system exergy efficiency, they are chosen for this analysis. Fuel cost is also taken into account for this analysis and 5 different fuel cost are assigned to the heat input at the boiler. Since the analysis does not take into account the combustion of biomass products, heat input is used to represent the energy from the various sources. For comparison water is run to see if the same trend occurred. Figure 6.46 shows power output and electricity cost rate for water run at the optimal pressure ratio found in the previous optimization for various superheats from 6 to 25. It is found that as the degree of superheat increases, the electrical output decreases causing the cost rate for electricity to increase. There is no "optimal" superheat as is found for dimethyl

ether. Even if the cost of electricity is minimized the power output will not be sufficient to bring the cost of electricity as close as dimethyl ether.

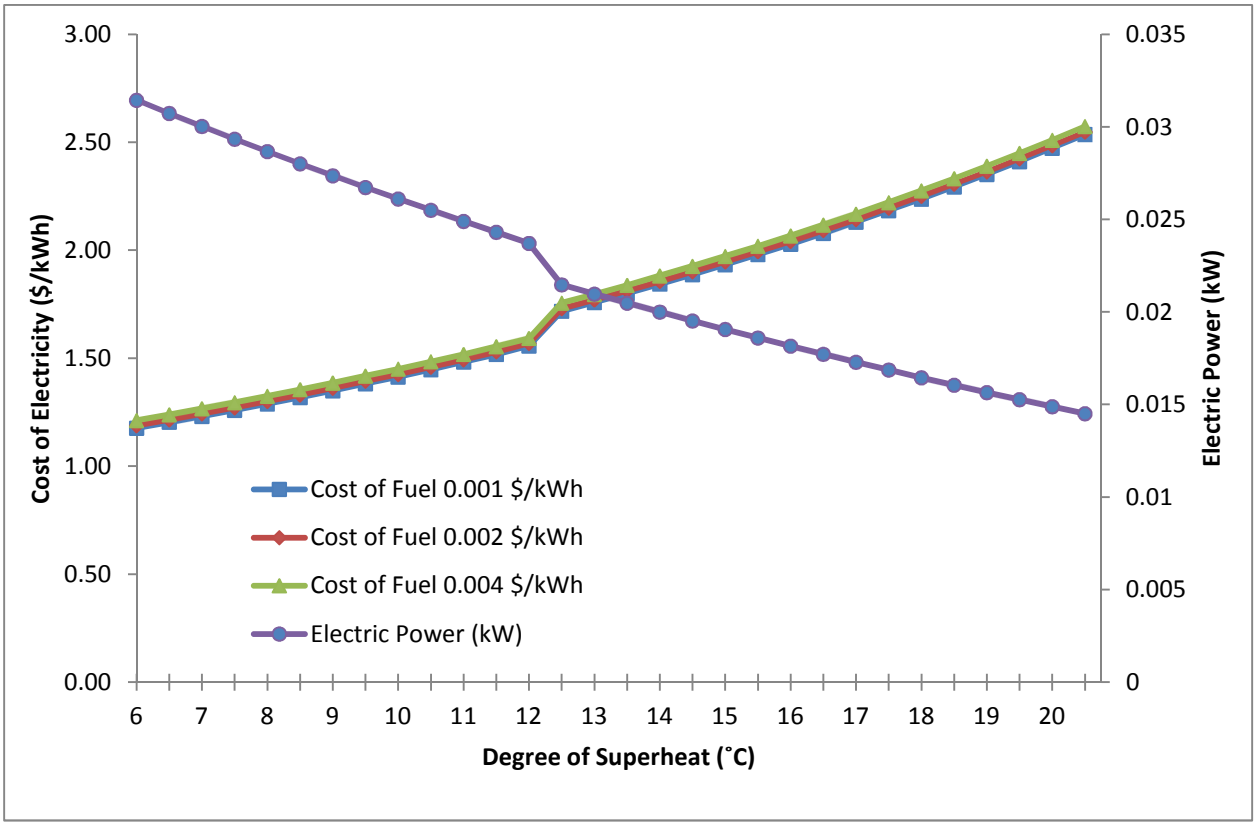

Figure 6.46: Electricity cost rate and electrical power output with varying superheat at optimal pressure ratio and three different fuel costs (water)

Optimizing the cost of electricity for dimethyl ether and iso-butane requires setting EES to minimize the function for c_e (electricity cost rate) which is found in the cost rate balance for the expander. The same two independent variables, pressure ratio and superheat are used. The bounds for the analysis do not change. Five different exergy heat input prices are used, 0.001 $/kWh, 0.002 $/kWh, 0.004 $/kWh, 0.006 $/kWh and 0.008 $/kWh. These costs are used for comparison to see how the system will react to each change. The same assumptions are used as outlined in the exergoeconomic analysis section.

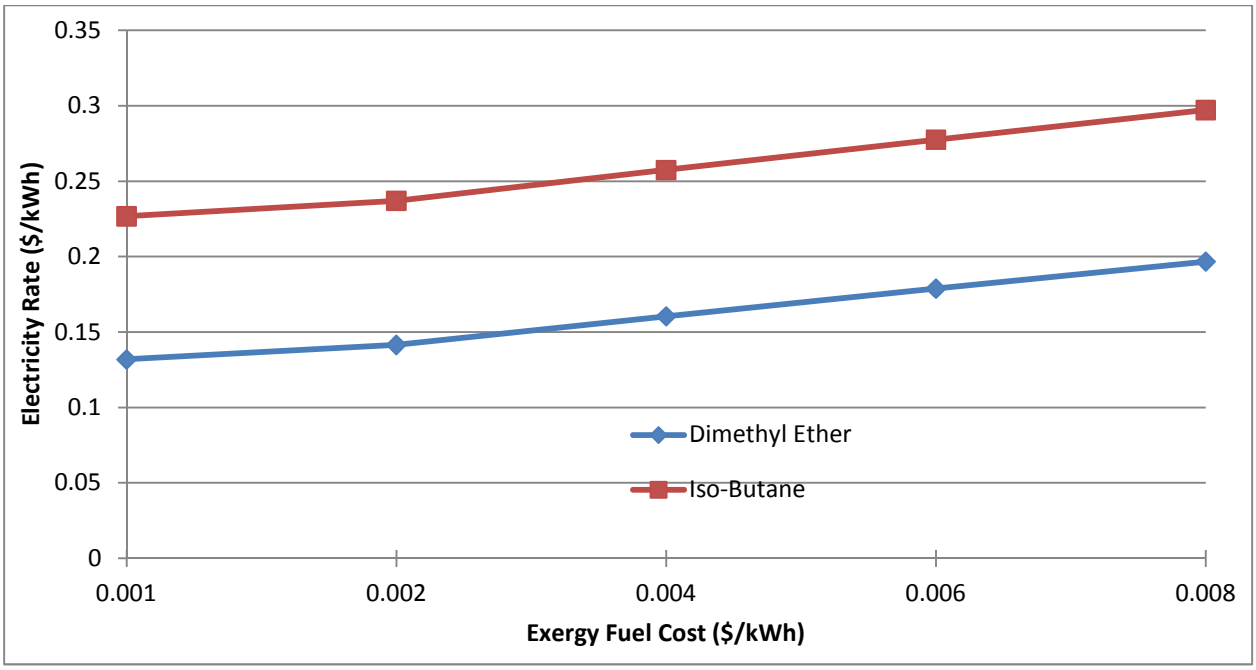

Figure 6.47: Optimized values of electricity rate for dimethyl ether and iso-butane

Figure 6.47 shows the minimized values for electricity rate for dimethyl ether and iso-butane. The highest values of 0.1968$/kWh and 0.2972 $/kWh occurred at maximum fuel cost. The lowest value of 0.1319 $/kWh and 0.2268 $/kWh occurred when the fuel cost was 0.001 $/kWh.

Ideally there are relations for cost for each component based on the calculated capacity of the system. In this case the component costs are based off the cost of the actual component costs of the current experimental system. This is done for comparison purposes and because at this size of system there are no set costs for components. There has to be some custom work done due to the size and type of experimental system. Comparing the electricity rate costs to the microFIT program offered by the Ontario Power Authority shows how competitive the system is if actually implemented. The price rate for biomass and biogas is 0.138 $/kWh and 0.16 $/kWh respectively (Ontario Power

Authority, 2010). These prices are guaranteed for 20 years. With the system running dimethyl ether, it is able to run economically considering the fuel costs up to 0.004 $/kWh. Although this is enough to pay just above the required rate of electricity calculated, it would not leave room to make a decent return on investment. Improvements with the expander would greatly increase the return on investment with this system at these guaranteed prices. Other improvements with the boiler and regenerator would also increase work output and reduce heat input which would also increase the economical viability of the system.

Chapter 7: Conclusions and Recommendations

7.1 Conclusions

Energy, exergy, optimization, and exergoeconomic analysis are performed on a scroll based organic Rankine cycle to improve performance within physical constraints. Various fluids are tested to identify the best performing fluid for the application investigated. Fluids such as water and toluene show very poor performance in this system due to the low pressure drop through the expander. This causes the power output to be very minimal compared to other fluids. Dimethyl ether and iso-butane show promising results for use as working fluids in organic Rankine cycles with high power output. It is found power output is important because the cost rate to produce electricity is directly correlated to it.

- For the dimethyl ether based system the system exergy efficiency is 11.76%.
- An Iso-butane based system has a system exergy efficiency of 11.81%.
- Power output is 0.28 kW for dimethyl ether.
- Power output for iso-butane is 0.15 kW.
- System energy efficiency for dimethyl ether and iso-butane is 2.84% and 2.86%.
- Isentropic efficiency of the chosen expander is very low (fewer than 30% for all fluids) which results in most of the exergy losses to be in this component regardless of the fluid.
- Exergy destruction in the expander for dimethyl ether is 50% of the total exergy destruction in the system.
- Iso-butane has an exergy destruction of 46.3% of the total.

- N-pentane has the lowest exergy destruction with 36.3% of the total exergy destruction in the system.
- Dimethyl ether has the lowest electricity rates with 0.1319 $/kWh at the lowest fuel input cost and 0.1968 $/kWh at the highest fuel input cost.
- Iso-butane has higher rates due to lower power output with 0.2268 $/kWh and 0.2972 $/kWh at the lowest and highest fuel input rates.

It is noticed that the optimized values from the first optimization (system exergy efficiency maximized) do not correspond to the maximum work output possible from the system. This is because system exergy efficiency depends both on input exergy and power output. Comparing these prices with the microFIT price schedule (for biomass) from the Ontario Power Authority shows that the system is economically viable. The system needs to be improved if a proper rate of return is to be realized since the price calculated is close to the price paid by the 20 year contract. Overall this shows that the system has merit to be a reliable method to convert renewable energy sources into useful electricity. This will help with lowering CO_2 emissions and air pollutants which are given off by fossil fuel energy sources.

7.2 Recommendations

Further investigation of the expander is necessary to improve the performance of the system. With the low isentropic efficiencies, this expander has high internal losses which reduce the power output greatly. Further study into modifying or custom designing an expander which can reduce internal losses greatly will be beneficial to the study of organic Rankine cycles. Designing a complete system, including improved expander,

system pump, properly designed regenerator, condenser and boiler with dimethyl ether as a working fluid will be beneficial in proving the concept of a viable organic Rankine cycle. Further study into the costs associated with components of the organic Raknine cycle system would be beneficial. Investigating multistage expanders to take advantage of high pressure drops as seen in fluids such as dimethyl ether has possible merit. A cost rate which depends on sizing of component can be beneficial in determining the optimal cost vs. efficiency point for the system. Further investigation into exergy fuel input costs is beneficial especially when taking into account solar thermal sources. This will improve accuracy of the exergoeconomic analysis. This can be considered for further work on the subject.

References

Antoniou A., Wu-Sheng L.. 2007. Practical Optimization Algorithms and Engineering Applications. Springer, New York.

Badr O., Probert D., O'Callaghan P. 2007. Performances of Multi-vane Expanders. Applied Energy 20: 207-234.

Bong T. Y., Ng K. C., Lim T.B. 1990. A Thermodynamic Model For The Analysis of Screw Expander Performance. Heat Recovery Systems & CHP 10: 119-133.

Bruno J.C., Lopez-Vllada J., Letelier E., Romera S., Coronas A. 2008. Modelling and Optimisation of Solar Organic Rankine Cycle Engines For Reverse Osmosis Deslination. Applied Thermal Engineering 28: 2212-2226.

Cengel Y.A., Boles M.A. 2008. Thermodynamics An Engineering Approach. McGraw Gill, New York.

Dai Y., Jiangfeng W., Lin G.. 2009. Parametric Optimization and Comparative Study of Organic Rankine Cycle for Low Grade Waste Heat Recovery. Energy Conversion and Management 50: 576-582.

Dincer I, Rosen M. 2007. Exergy: Energy, Environment and Sustainable Development. Elsevier Science, London.

ElectraTherm Inc. 2011. www.electratherm.com (accessed February 20, 2012).

Eneftech Innovation SA. enefcogen green, performances, Electrical power, Cogeneration efficiency. http://www.eneftech.com/en/enefcogen_green.php (accessed February 25, 2012).

Fernandez F. J., Prieto M. M., Suarez I. 2011. Thermodynamic Analysis of High-Temperature Regenerative Organic Rankine Cycles Using Siloxanes as Working Fluids. Energy 36: 5239-5249.

Gullien-Gosalbez G., Jimenez L., Boer D., Antipova E., Salcedo R. 2012. Multi-objective Optimization of Solar Rankine Cycles Coupled with Reverse Osmosis Desalination Considering Economic and Life Cycle Environmental Concerns. Desalination 286: 258-271.

Heberle F, Bruggemann D. 2010. Exergy Based Fluid Selection for a Geothermal Organic Rankine Cycle for Combined Heat and Power Generation. Applied Thermal Engineering 30: 1326-1332

Intergovernmetnal Panel on Climate Change. 2007. Changes in Atmospheric Consituents and Radiative Forcing. Cambridge University Press, cambridge, United Kingdom and New York, NY, USA .

International Energy Agency. 2011. Key Graphs. World Energy Outlook 2011. November 9, 2011.

Jie J., Pei G, and Jing L. 2010. Analysis of Low Temperature Solar Thermal Electric Generation Using Regnerative Organic Rankine Cycle. Applied Thermal Energy 30: 988-1004.

Kaushik S. C., Dubey A., Singh N.. 1994. Thermal Modeling and Energy Conservation Studies on Freon Rankine Cycle Cooling System with Renerative Heat Exchanger. Heat Recovery Systems & CHP 14: 67-77.

Kosmadakis G., Manolakos D., Papadakis G. 2011. Simulation and Economic Analysis of a CPV/Thermal System Coupled with an Organic Rankine Cycle for Increased Power Generation. Solar Energy 85: 208-324.

Kuo C., Hsu S., Chang K., Wang C. 2011. Analysis of a 50kW Organic Rankine Cycle System. Energy 36: 5877-5885.

Liu B., Chien K., Chien C. 2004. Effect of Working Fluids on Organic Rankine Cycle for Waste Heat Recovery. Energy 29: 1207-1217.

Mago P.J., Chamra L.M., Srinivasan K., Somayaji C. 2008. An Examination of Regnerative Organic Rankine Cycles Using Dry Fluids. Applied Thermal Engineering 28: 998-1007.

Maizza V., Maizza A. 2001. Unconventional Working Fluids in Organic Rankine Cycles for Waste Energy Recovery Systems. Applied Thermal Engineering 21: 381-390.

Manolakos D, Papdakis G, Kyritsis S, Bouzainas K. 2007. Experimental Evaluation of an Autonomous Low-Temperature Solar Rankine Cycle System for Reverse Osmosis Desalination. Desalination 203: 366-374.

Mathias J. A., Johnston J. R., Cao J., Priedeman D. K., Christensen R. N.. 2009. Experimental Testing of Gerotor and Scroll Expanders Used in, and Energetic and Exergetix Modeling of, an Organic Rankine Cycle. Journal of Energy Resources Technology 131/012201:1-9

Nafey A.S., Sharaf M.A., Garcia-Rodriguez Lourdes. 2010. Thermo-Economic Analysis of a Combined Solar Organic Rankine Cycle-Reverse Osmosis Desalination Process with Different Energy Recovery Configurations. Desalination 261: 138-147.

Ontario Power Authority. 2010. MicroFIT Price Schedule- revised August 13, 2010. http://microfit.powerauthority.on.ca/pdf/microFIT-Program-price-schedule.pdf (accessed February 20, 2012).

Oralli E., Ali Tarique Md., Zamfirescu C., Dincer I. 2011. A Study on Scroll Compressor Conversion Into Expander for Rankine Cycles." International Journal of Low-Carbon Technologies 6: 200-206.

Pei Gang, Li J., Wang D., Jie J. 2011. Construction and Dynamic Test of a Small-Scale Organic Rankine Cycle. Energy 36: 3215-3223.

Qiu G., Liu H., Riffat S.. 2011. Expanders for Micro-CHP Systems With Organic Rankine Cycles. Applied Thermal Engineering 31: 3301-3307.

Quoilin S., Declaye S., Tchanche B.F., Lemort V. 2011. Thermo-Economic Optimization of Waste Heat Recovery Organic Rankine Cycles. Applied Thermal Engineering 31: 2885-2893.

Quoilin Sylvain, Lemort, V., Lebrun J. 2010. Experimental Study and Modeling of an Organic Rankine Cycle using Scroll Expander. Applied Energy 87: 1260-1268.

Rayegan R., Lebrun Y.X. R. 2011. A procedure to Select Working Fluids for Solar Organic Rankine Cycles (ORCs). Renewable Energy 36: 659-670.

Roy J. P., Misra A. 2012. Parametric Optimization and Performance Analysis of a Regenerative Organic Rankine Cycle Using R-123 for Waste Heat Recovery. Energy 39: 227-235.

Schuster A., Karellas S., Kakaras E., Spliethoff H. 2009. Energetic and Economic Investigation of Organic Rankine Cycle Applications. Applied Tehermal Engineering 29:1809-1817.

Statistics Canada. 2011. Table 128-0018 - Consumption of Solid Wood Waste and Spent Pulping Liquor for Energy Production, Annual.

Sun Jian, Li W. 2011. Operation Optimization of an Organic Rankine Cycle (ORC) Heat Recovery Power Plant. Applied Thermal Energy 31: 2031-2041.

Tarique Md. Ali. April 2011. Experimental Investigation of Scroll Based Organic Rankine Systems. UOIT.

Tchanche B.F., Papadakis G, Lambrinos G, Frangoudakis A. 2009. Fluid Selection for a Low Temperature Solar Organic Rankine Cycle. Applied Thermal Engineering 29: 2468-2476

Wang B., Li X., Shi W. 2005. A General Geometrical Model of Scroll Compressors Based on Discretional Initial Angles of Involute." International Journal of Refrigeration 28: 958-966

Wang W, Wu Y., Ma C., Liu L., Jian Y. 2011. Preliminary Experimental Study of a Single Screw Expander Prototype. Applied Thermal Energy 31: 3684-3688.

Wei D., Lu X., Lu Z., Gu Jianming. 2007. Perofrmance Analysis and Optimization of Organic Rankine Cycle (ORC) for Waste Heat Recovery. Energy Conversion and Management 48:1113-1119.

Yamamoto T., Furuhata T., Aria N., Mori K. 2001. Design and testin gof the Organic Rankine Cycle. Energy 26: 239-251.

Appendix

EES example code for R134a

```
"Blitzer Expander Modeling"
"Functions"

Procedure State2ae(P_2ve,P_2ae,v_2ve,h_2ve:v_2ae,h_2ae,T_2ae,s_2ae)
$common R$

if P_2ve <= P_2ae then

v_2ae:=v_2ve

T_2ae:=Temperature(R$,P=P_2ae,v=v_2ae)
s_2ae:=Entropy(R$,P=P_2ae,v=v_2ae)
h_2ae:=Enthalpy(R$,P=P_2ae,v=v_2ae)
x_2ae:=1

Else

h_2ae=h_2ve
T_2ae:=Temperature(R$,P=P_2ae,h=h_2ae)
s_2ae:=Entropy(R$,P=P_2ae,h=h_2ae)
v_2ae:=Volume(R$,P=P_2ae,h=h_2ae)
x_2ae:=1
endif
end


"Blitzer Expander Constants"

BVR = 3.5

Pie = 0.61

zeta = 7.23E-7

K_omega = 0.0593

K_p = 4.3E-6

V_dot = 6.21"m^3/h""@2000rpm"

v_d = V_dot*(1/3600)*(1/2000)*(60) "m^3/rev"

"Working Fluid Parameters"

R$ = 'R134a'

//T_sh = 12

//T_sat = 100

T_in = 110
```

```
T_sat = T_in - T_sh
x_in = 1
P_in=Pressure(R$,T=T_sat,x=x_in)
//PR =5
P_out = P_in/PR
"State 1e"
T_1e = T_in
P_1e=P_in
h_1e=Enthalpy(R$,T=T_1e,P=P_1e)
s_1e=Entropy(R$,T=T_1e,P=P_1e)
v_1e=Volume(R$,T=T_1e,P=P_1e)
"State 2se"
s_2se = s_1e
v_2se = BVR*v_1e
T_2se=Temperature(R$,s=s_2se,v=v_2se)
P_2se=Pressure(R$,s=s_2se,v=v_2se)
h_2se=Enthalpy(R$,v=v_2se,s=s_2se)
h_2s2e = Enthalpy(R$,P=P_out,s=s_2se)
x_2se = Quality(R$,v=v_2se,s=s_2se)
T_sat_2se=T_sat(R$,P=P_2se)
"State 2ve"
v_2ve= v_2se
h_2ve = Pie*(h_1e-h_2se)+h_2se
P_2ve=Pressure(R$,v=v_2ve,h=h_2ve)
s_2ve=Entropy(R$,h=h_2ve,v=v_2ve)
T_2ve=Temperature(R$,h=h_2ve,v=v_2ve)
"State 2ae"
P_2ae = P_out
```

```
call State2ae(P_2ve,P_2ae,v_2ve,h_2ve:v_2ae,h_2ae,T_2ae,s_2ae)

"State 3e"

h_3e = h_1e

P_3e = P_1e

v_3e = v_1e

s_3e = s_1e

"State 4e"

P_4e = P_out

h_4e = h_3e

T_4e=Temperature(R$,P=P_4e,h=h_4e)

s_4e=Entropy(R$,P=P_4e,h=h_4e)

v_4e=Volume(R$,P=P_4e,h=h_4e)

"Leak Calculation"

m_dot_leak = zeta*(((P_1e/v_1e)-(P_4e/v_4e))*10^3)^0.5

"State 2e"

P_2e = P_out

m_dot = m_dot_leak+m_dot_exp

m_dot_leak*h_4e +m_dot_exp*h_2ae = h_2e*m_dot

T_2e=Temperature(R$,P=P_2e,h=h_2e)

v_2e=Volume(R$,P=P_2e,h=h_2e)

s_2e=Entropy(R$,P=P_2e,h=h_2e)

//_____________________________________________________

"Expander Calculations"

w_exp = h_1e-h_2ae

w_s = h_1e-h_2se

w_loss = h_2ae-h_2se

V_dot_2s = V_d*RPS

m_pocket = V_d/v_2se
```

m_dot = m_dot_leak*2*((h_1e-h_2se)/(h_2ae-h_2se))

W_dot_out = m_dot_exp*w_exp*1000

delta_P = P_1e-P_4e

tau_pf = K_p*delta_P*1000

tau_acc = k_omega*omega^2*m_pocket

tau_out = tau_pf-tau_acc

W_dot_out = tau_out*omega

omega = 2*pi#*RPS

RPM = RPS*60

eta_s = (h_1e-h_2e)/(h_1e-h_2s2e)

//_____

"System Calculations"

T_o = 25

P_o = 101.325

h_o = Enthalpy(R$,T=T_o,P=P_o)

s_o = Entropy(R$,T=T_o,P=P_o)

"State 1"

T_1 = T_in

P_1 = P_in

h_1=Enthalpy(R$,T=T_1,P=P_1)

s_1=Entropy(R$,T=T_1,P=P_1)

ex_1 = (h_1-h_o)-(T_o+273)*(s_1-s_o)

"State 2"

T_2 = T_2e

P_2 = P_2e

h_2 = h_2e

```
s_2 = s_2e
ex_2 = (h_2-h_o)-(T_o+273)*(s_2-s_o)

"State 3"
T_3 = T_4+5
P_3 = P_2
h_3=Enthalpy(R$,T=T_3,P=P_3)
s_3=Entropy(R$,h=h_3,P=P_3)
ex_3 = (h_3-h_o)-(T_o+273)*(s_3-s_o)

"State 4"
x_4 = 0
P_4 = P_2
h_4=Enthalpy(R$,x=x_4,P=P_4)
s_4=Entropy(R$,x=x_4,P=P_4)
T_4=Temperature(R$,P=P_4,x=x_4)
ex_4 = (h_4-h_o)-(T_o+273)*(s_4-s_o)

"State 5"
P_5 = P_in
s_5 = s_4
h_5s=Enthalpy(R$,s=s_5,P=P_5)
eta_pump = 0.7
h_5 = (h_5s-h_4)*(1/eta_pump)+h_4
T_5 = Temperature(R$,h=h_5,P=P_5)
s_5a=Entropy(R$,h=h_5,P=P_5)
ex_5 = (h_5-h_o)-(T_o+273)*(s_5a-s_o)
```

```
"State 6"
//T_6 = T_2-8
T_6 = Temperature(R$,h=h_6,P=P_6)
P_6 = P_5
//h_6=Enthalpy(R$,T=T_6,P=P_6)
s_6=Entropy(R$,h=h_6,P=P_6)
ex_6 = (h_6-h_o)-(T_o+273)*(s_6-s_o)

//_____________________________________
"System Parameters"

q_in = h_1-h_6
q_regen_out = h_6-h_5
q_regen_in = h_2-h_3
epsilon_regen = 0.8
epsilon_regen = q_regen_out/q_regen_in
q_out = h_3-h_4
w_pump = h_5-h_4
W_dot_pump = m_dot*w_pump
W_dot_net = (W_dot_out/1000) -W_dot_pump
w_turb = h_1-h_2
eta_th = W_dot_net/Q_dot_in
T_s = T_in+10
Ex_dot_in = (1-(T_o+273)/(T_s+273))*Q_dot_in
eta_ex = W_dot_elec/(Ex_dot_in)
eta_elec = W_dot_elec/Q_dot_in
W_dot_elec = W_dot_net*0.8
eta_carnot = 1 - ((T_o+273)/(T_s+273))
```

```
Q_dot_in = m_dot*q_in

Q_dot_out = m_dot*q_out

//_____________________________________________________

" Exergy Analysis"

" Boiler"

Ex_dot_6 + Ex_dot_in = Ex_dot_1 + Ex_dot_db

"Expander"

Ex_dot_1 = Ex_dot_2 + W_dot_out/1000 + EX_dot_dexp

"Regenerator"

EX_dot_3 = m_dot*ex_3

Ex_dot_5 = m_dot*ex_5

Ex_dot_2 + Ex_dot_5 = Ex_dot_3 + Ex_Dot_6 + Ex_dot_dregen

"Condenser"

h_3sv = Enthalpy(R$, x =1, P=P_3)

Q_dot_out_sv = m_dot*(h_3-h_3sv)

T_condavg = ((T_3+273)+(T_4+273))/2

Ex_dot_out_1 = (1-((T_o+273)/(T_condavg)))*Q_dot_out_sv

Ex_dot_out = (1-((T_o+273)/(T_4+273)))*(Q_dot_out-Q_dot_out_sv)

Ex_dot_4 = m_dot*ex_4

Ex_dot_3  = Ex_dot_4 + Ex_dot_out +Ex_dot_out_1  + Ex_dot_dcond

"Pump"

Ex_dot_4 + W_dot_pump = Ex_dot_5 + Ex_dot_dpump

//_____________________________________________________

"Exergoeconomic Analysis"

n_sys = 20

i = 0.05

Am = (i*(1+i)^n_sys)/((1+i)^(n_sys-1))
```

"Expander Costs"

OM% = 0.25

ICC_exp = 1000

OM_exp = ICC_exp*OM%

TCC_exp = Am*(ICC_exp+OM_exp)

t_exp = 365*24

Z_dot_exp = (TCC_exp+TCC_cond+TCC_p)/t_exp

"Boiler/Heat Exchanger Costs"

ICC_b = 1200

OM%_b = 0.15

OM_b = OM%_b*ICC_b

TCC_b = Am*(ICC_b+OM_b)

t_b = t_exp

Z_dot_b = TCC_b/t_b

"Regenerator Costs"

t_regen = t_b

ICC_regen = 1500

OM%_regen = 0.15

OM_regen = OM%_regen*ICC_regen

TCC_regen = Am*(ICC_regen+OM_regen)

Z_dot_regen = TCC_regen/t_regen

"Condesor Costs"

t_cond = t_b

ICC_cond = 1200

OM%_cond = 0.15

OM_cond = OM%_cond*ICC_cond

TCC_cond = Am*(ICC_cond+OM_cond)

Z_dot_cond = TCC_cond/t_cond

"Pump Costs"

t_p = t_b

ICC_p = 300

OM%_p = 0.25

OM_p = OM%_p*ICC_p

TCC_p = Am*(ICC_p+OM_p)

Z_dot_p = TCC_p/t_p

"Boiler Exergy Cost Rate balance"

EX_dot_1 = m_dot*ex_1

c_f = 0.001

Ex_dot_in*c_f + EX_dot_6*c_6 +Z_dot_b = EX_dot_1*c_1

"Expander Exergy Cost Rate Balance"

c_2 = c_1*0.5

EX_dot_2 = m_dot*ex_2

EX_dot_1*c_1+Z_dot_exp = W_dot_elec*c_e + c_2*EX_dot_2

C_dot_e = c_e*W_dot_elec

"Regenerator Exergy Cost Rate Balance"

EX_dot_6 = ex_6*m_dot

c_2*EX_dot_2 + Z_dot_regen = EX_dot_6*c_6